THE DEVELOPMENT OF SECONDARY ION MASS SPECTROMETRY FOR TWO-DIMENSIONAL IMPURITY PROFILING IN SEMICONDUCTORS

Graham Alan Cooke BSc(Hons)

Thesis for the degree of

Doctor of Philosophy

submitted to

The University Of Warwick

Department of Physics

July 1992

NUMEROUS ORIGINALS IN COLOUR

TABLE OF CONTENTS

This thesis was compiled using guidelines PHYS/PG/3

LIST OF FIGURES

LIST OF PLATES

ACKNOWLEDGEMENTS

I would like to acknowledge the help of the following people during the course of this project and in the preparation of this thesis.

Firstly I would like to thank Professor Chris Hill[1], not only for the original idea of profiling implants using the method described in this thesis, but also, together with Peter Pearson[1], for fabricating the samples at Caswell. I would expressly like to thank them for their commitment to the project during the reorganisation period at Caswell, when they seemingly achieved the impossible and produced the third generation of samples in the final weeks of silicon fabrication at the site.

I would especially like to thank my supervisor, Mark Dowsett, for his guidence and patience and without whom this work would not have been possible.

To all the members of the SIMS group (especially Bob Barlow for instructing me on the use of the EVA 2000 instrument) and the technical support staff of the department (especially Barrie Sheffield and Adrian Lovejoy) go my sincere thanks for all their help over the lifetime of the project.

I would like to than my parents for all their support, moral, financial, and otherwise, throughout the whole of my student career.

Finally I would like to thank my wife, Louise, for putting up with me working odd hours and for her encouragement during the preparation of this thesis.

I acknowledge the SERC for their studentship award and thank Plessey[1] for their generous financial support. The work was initiated with support from the UK Alvey Program (005 and 029) and continued under the Silicon towards 2000 Programme (IED 1540 and 1559).

[1] GEC-Marconi Materials Technology (Caswell), GEC-Plessey Semiconductors. Formally, Plessey Research (Caswell), The Plessey Company plc of Ilford, Essex

DECLARATION

This thesis is submitted to the University of Warwick in support of my application for the degree of Doctor of Philosophy. It contains an account of my work in the Department of Physics at the University of Warwick during the period October 1988 to June 1992, under the supervision of Dr. M G Dowsett.

No part of this thesis has been used previously in a degree thesis submitted to this or any other university. The work described is the result of my own research except where specifically acknowledged in the text.

G A Cooke

July 1992.

PUBLICATIONS

During the period of research covered by this thesis, the following publications of the work were made by the author.

TWO DIMENSIONAL ANALYSIS OF SEMICONDUCTORS AT DOPANT SENSITIVITY USING SIMS

G A Cooke, M G Dowsett, C Hill, E A Clark, P Pearson, I Snowden and B Lewis

SIMS VII, Proceedings of the seventh international conference on secondary ion mass spectrometry (3-8 Sept 1989), John Wiley and Sons (1990), pages 667-670.

TWO DIMENSIONAL PROFILING USING SECONDARY ION MASS SPECTROMETRY

M G Dowsett and G A Cooke

J. Vac. Sci Technol **B10(1)** (1992) 353

HIGH RESOLUTION HIGH SENSITIVITY TWO DIMENSIONAL PROFILING OF BORON AND ARSENIC IMPLANTS IN SILICON

G A Cooke, M G Dowsett, C Hill and P Pearson

SIMS VIII, Proceedings of the eighth international conference on secondary ion mass spectrometry (15-20 Sept 1991), John Wiley and Sons (1992), pages 861-864.

The work was presented by the author at both SIMS VII (Monterey California, 1989) and SIMS VIII (Amsterdam, Netherlands, 1991)

ABSTRACT

As the dimensions of devices on integrated circuits are reduced, the importance of lateral spreading of implanted impurities increases. To maintain inter-device isolation and predictable performance, knowledge of the extent and concentration of these regions is necessary. A number of computer models have been produced to predict this information, however there is a serious lack of experimental data with which to verify their results.

Secondary Ion Mass Spectrometry (SIMS) has been used for many years to provide depth profiles with high sensitivity and depth resolution, however, direct application of SIMS will not yield multi-dimensional results with enough spatial resolution and sensitivity to be useful. This is because the analyte volume is very limited.

This thesis describe the development of a technique that increases the volume available for analysis by means of a special sample. The sample geometry introduces an inherent magnification that permits the use of a relatively large, low energy, reactive ion probe. This in turn provides high sensitivity - due to enhanced secondary ion yields - and good depth resolution - due to the low range of the probe.

Using a quadrupole SIMS instrument, and a 50 μm FWHM oxygen probe, spatial resolutions of less than 70 nm have been demonstrated with a sensitivity of better than 10^{17} atoms cm^{-3} for boron implants in silicon.

1.0 INTRODUCTION

1.1 INTRODUCTION TO THE PROBLEM

Since the invention of the transistor (Bardeen and Brattain, 1948) reduction in the size of the device has been an important factor in its development. The first bipolar devices had critical dimensions of the order of one half of a millimetre - current transistors, incorporated into integrated circuits, have critical dimensions over one thousand times smaller. By reducing the size of individual devices, the capacitance is reduced. This leads to less power being required for operation, as the time constant is smaller, and thus permits faster switching. Similarly, smaller devices permit higher packing densities to be achieved, with the consequent reduction in inter-device connection lead lengths and communication times. This trend shows no sign of slowing down.

The method most often used for the introduction of dopant material into the substrate is ion implantation. The required impurity is ionised and accelerated, typically by a 10 kV to 100 kV potential, then directed at the substrate surface. The regions to receive the implant are defined by windows in a masking material - commonly photoresist or silicon dioxide. Ions are implanted at an angle to the surface, often 7° to the normal, to prevent channelling by the lattice. Figure 1.1 shows a typical arrangement.

The implanted ions are not confined to the region directly beneath the window but, because of scattering during implantation, spread under the mask edge. The implant process also causes damage to the crystal lattice that must be annealed out if the implant is to become electrically active. This thermal process causes some diffusion of the implant leading to further spreading.

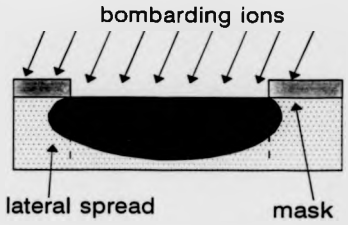

Figure 1.1 Diagram of a typical implant process

When devices were large, of the order of 10 μm, this lateral diffusion represented only a minor part of the active region and, as the distance between devices was similarly large, a spread of 0.5 μm would not compromise inter-device isolation. The reduction in device size and the increase in packing density has, however, raised the importance of the lateral spread. Now, the lateral spread may represent over 30% of the active region and, when closely packed, may easily provide a conductive path between adjacent devices. Knowledge of the extent and concentration profile of the implant side lobes is therefore an important requirement when designing modern integrated circuits.

A number of models have been proposed for simulating the lateral profile of implants. However, little experimental data is available with which to verify their results or refine their algorithms.

1.2 OVERVIEW OF THE THESIS

This thesis begins by surveying the many ingenious ways that have been, or are currently being, used to obtain information about the lateral profile of implanted material. Making a distinction between carrier (electrically active) and dopant (total impurity concentration) profiling techniques shows that the latter are trailing the former by orders of magnitude, in both sensitivity and spatial resolution. Knowledge of the distribution of impurity material is vitally important if implants are to be efficient and predictable; as inactive material may give rise to scattering and lattice distortions that degrade device performance.

SIMS has been used, for many years, to provide accurate chemical depth profiles with good sensitivity and resolution. In chapter 3, the SIMS technique is introduced and the features of the EVA 2000 instrument are reviewed. A technique is then proposed, using a specially fabricated sample, that will permit lateral information to be extracted with both high sensitivity and spatial resolution (chapter 4). The following two chapters then deal with the experimental development of the technique and the reconstruction of complete two dimensional profiles respectively.

After presenting modifications made by the author to the Penning source of the instrument, the thesis concludes with a brief summary of the advances made together with some ideas for future development.

2.0 TWO DIMENSIONAL PROFILING

2.1 INTRODUCTION

The quest for high speed, low power, integrated circuits has driven the rapid reduction in device dimensions and consequent increase of their packing density on the substrate. Early devices were large by today's standards and routine determination of the impurity profile was usually restricted to the depth dimension only, using techniques such as anodic sectioning (E. Tannenbaum, 1961), bevel and stain (C. P. Wu et. al., 1979) (R. Subrahmanyan et al, 1988a), capacitance-voltage profiling (C.P.Wu, 1975) and SIMS (Magee and Honig, 1982). However, the reduction in device dimensions, especially in the lateral direction, has forced the development of techniques capable of showing detail in both depth and lateral dimensions. It is of great importance that both electrically active and inactive impurities be mapped, especially as newer devices (ie NMOSFETS) contain very highly doped regions. Thus comparison between the two profiles is essential for optimum circuit fabrication and performance.

This chapter reviews past and current methods of mapping the impurity distribution typical of VLSI devices. Techniques are categorized broadly into two groups; those measuring the electrically active impurities, carrier mapping, and those measuring the physical distribution of impurities, dopant mapping. Where obtainable, sensitivity and resolution are discussed, together with the practicalities of each technique, such as sample preparation and the major causes of errors.

2.2 CARRIER PROFILING TECHNIQUES

2.2.1 Chemical techniques

2.2.1.1 Staining Techniques

The staining of sectioned samples is one of the oldest characterization techniques used for semiconductors. In general, a sample is sectioned at an angle, to magnify the region of interest, then immersed in a solution containing metal ions, typically copper or silver. By an electrochemical displacement reaction, metal is deposited on areas of one carrier type, thus delineating the junction. The specimen may then be observed and the junction details recorded by a microscopical technique.

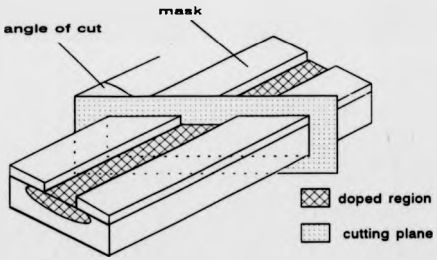

Figure 2.1 The sample used by Akasaka et. al. to gain lateral magnification.

2.2.1.2 Etching Techniques

As early as 1972, this technique was applied to the investigation of lateral profiles. Akasaka and co-workers (1972) reported the measurement of the lateral spread of thermally activated implanted boron atoms. A long, implanted, stripe was vertically sectioned, as in figure 2.1, so as to magnify the lateral dimension, and the p-type region stained with copper solution. The extent of the stained area was then measured by optical microscopy.

A similar sample, though this time implanted with phosphorus, was used by Sakurai (1979) in an investigation into the effects of mask edge topography. The specimens were observed by SEM, permitting lateral spreads of down to 0.24 μm to be measured, with a reported resolution of 50 nm. By using a carrier depth profile for calibration, obtained by anodic sectioning (see section 2.2.2.1), the delineated contour was determined to have a concentration of $2x10^{17}$ atoms cm^{-3}.

Subrahmanyan et. al. (1988b)(1990) was able to prepare specimens, with enough inherent magnification to be measured by optical microscopy, by bevelling a sample in a combination of both vertical and lateral directions. A number of similar implants and anneals were made into substrates of different background doping concentration, resulting in the junction appearing at different parts of the implant. The samples were sectioned and the junction delineated by staining. The position of the junction in each sample was recorded and these were later combined to produce a complete two dimensional map. Although the mechanical magnification technique enlarges the profile in each direction, the combination of the two bevels does not result in a simple enlargement. The final map must undergo a deconvolution, based on the two bevelling angles, to return to a linear scaling. Subrahmanyan reports a resolution of 50 nm for the

technique, with an additional 50 nm possibility for error, in the lateral direction, caused by alignment inaccuracies of the overlaid contours. The technique is very sensitive, as the stain finishes abruptly at the junction, and contours as low as $2x10^{14}$ atoms cm^{-3} have been produced.

Etching techniques provide one of the highest resolutions available for two dimensional analysis. An implanted stripe is sectioned and treated with an etching solution, whose effect is sensitive to carrier concentration, thus revealing isoconcentration contours.

Sheng and Marcus (1981) used an $HF:HNO_3$ solution to selectively etch a concentration contour at $1x10^{19}$ atoms cm^{-3} in an n^+p junction. The specimen was subsequently imaged by TEM and a resolution of better than 5 nm reported. The calibration was made by comparison with a depth profile obtained from a process simulator.

The etching technique of Sheng and Marcus was subsequently refined by Roberts et. al. (1985) to allow a number of isoconcentration contours to be presented from one sample. Initially, by etching uniformly doped n and p-type silicon substrates, under very carefully controlled conditions, the etch rate was calibrated with respect to concentration. Cross sectional samples were then prepared for TEM and etched in the solution. This resulted in the sample taking on a wedge shaped cross section, as regions of high concentration are etched more quickly than lesser doped areas. The doped region was examined using a multiple beam TEM technique that projects several fringes, the separation of which allows determination of the sample thickness, which is concentration dependent, at different locations. A sensitivity of $2x10^{17}$ atoms cm^{-3} for n-type and $6x10^{17}$ atoms cm^{-3} for p-type was reported. The resolution of the technique was estimated to be around 10 nm.

A similar approach has recently been used by Cerva (1992) for the examination of shallow junctions in silicon devices. Cerva used samples of similar cross section to production lightly doped drain (LDD) MOS transistors and shallow junction bipolar devices. The calibration was provided by comparison with SIMS profiles through larger areas and the results compared favourably with those obtained from two dimensional process simulation software and STM measurements. He reports that concentrations as low as $4x10^{17}$ atoms cm^{-3} can be observed for arsenic and $1x10^{18}$ atoms cm^{-3} for boron, with a spatial resolution of better than 10 nm.

An etching technique based on SEM observation was developed by Gong et. al. (1989)(1990) and has the advantage that up to three independent isoconcentration contours may be delineated on each sample. The sample, an implanted stripe, was carefully cross sectioned by sawing from the reverse side, to within 50 μm of the surface, then cleaving. As a precautionary measure, to reduce edge effects, the implant window was filled with deposited polysilicon before sectioning. The isoconcentration contours were then delineated by etching in an $HF:HNO_3$ solution, buffered with acetic acid, for 4-7 seconds. During etching they were illuminated with UV light. The rapid changes in etch rate, that occur at specific impurity concentrations, cause the formation of "terraces", the divisions of which represent isoconcentrations. Up to three contours were delineated in this way on a single sample and then measured by SEM. Calibration was obtained by comparison of the central 1D region, the depth profile, with a SIMS depth profile. The concentrations at which the contours appear may be varied by changing, the etch buffer concentration, temperature, immersion time and illumination. The resolution of the technique is that attributed to the observation, combined with the uncertainty of the calibration profile. The sensitivity of the technique was reported to be as low as

$6x10^{16}$ atoms cm^{-3} and the useful range allowed contours up to 10^{20} atoms cm^{-3} to be observed.

2.2.1.3 Sources of error in chemical etching techniques

Both staining and etching methods are highly environmentally sensitive and most workers report this as a major source of error. To obtain reproducible results, etch chemistry, illumination and temperature must all be carefully controlled. Junction delineation by staining has the advantage over isoconcentration etching in that it reveals a physical entity, the metallurgical junction, rather than a point on a continuum. Thus the technique may be more readily verified and therefore optimized. If the substrate doping conditions are known, then the junction concentration may be found, thus staining methods do not need further calibration. With the exception of the method due to Roberts et. al. (1985) that makes use of a calibrated etch rate, all of the etching techniques require external calibration for each profile measured.

The procedure of calibrating an etched 2-D profile with a depth profile, obtained from a technique such as SIMS, may also introduce errors unassociated with the resolution of either technique.

SIMS, and most other 1-D techniques, analyse a large area window, so any process which causes the depth dependent concentration to vary as a function of implant window size will invalidate direct comparison. Okada et. al. (1990) has identified just such a mechanism whereby the diffusion involves point defect injection from the damage in the implant window. The diffusion is thus dependent on the window size and different sized widows will cause different amounts of horizontal and vertical diffusion.

Subrahmanyan et.al. (1990) made a preliminary investigation as to the effect of stress on the delineation process. It was proposed that the stress caused by the masking oxide may affect the reaction rate and thus distort the profile. A single sample with a very thick mask was compared with one of a standard thickness; no difference was detected within the uncertainty of the experiment.

It must be noted that care should be taken when comparing SIMS, or other dopant profile, with a carrier profile, as the dopant may not be fully activated in the SIMS profile and thus the carrier profile will be incorrectly calibrated. This is especially true for high concentrations (above 10^{20} atoms cm^{-3}) where large amounts of inactivated dopant may occur, such as with high dose boron implants in silicon (Schwettmann, 1974).

2.2.2. Electrical Profiling Techniques

2.2.2.1 Anodic sectioning

Anodic sectioning is a well establish technique for the determination of carrier depth profiles in silicon (Tannenbaum, 1961). The doped sample is immersed in an electrolyte and a current passed. The anodic action causes the conversion of the surface layers to a uniform oxide. The amount of material consumed has been very well characterized (Heywood 1979) and is approximately 0.2 nm per volt applied for an amyl-phosphate:HF electrolyte. The oxide is then removed by etching in HF and the conductivity of the sample measured. Thus, after a number of anodisation and etch cycles, a conductivity versus depth profile may be produced. This may subsequently be converted into a carrier profile by comparison with published carrier concentration - conductivity tables.

A technique for applying anodic profiling methods to two dimensional analysis was first proposed by Hill and Butler in 1983 (published 1984). This was developed by Hill and Pearson (1988a), (Hill et al, 1987) to investigate boron distributions in silicon.

The method requires a specially fabricated sample, as shown in figure 2.2. Initially, three resistors, with polysilicon interconnects to standard bond pads, are formed in close proximity by implantation through an oxide mask. These are then processed to activate the dopant and introduce diffusion, following a similar schedule to that used for commercial devices. Two resistors are then anisotropically plasma etched to remove the planar portion of the implant (2.2b), the remaining one being left (2.2a). The final structure (2.2c) has the mask removed to expose the sample surface. The sample is analysed in an automated instrument, built around a commercial prober, that makes electrical contact to the bond pads. An "O" ring sealed etching cell is lowered onto the sample, covering all three resistors, and is used to contain the process chemicals. The cell remains in contact with the sample throughout the analysis. The conductivity of each resistor is measured and then electrolyte, amyl-phosphate and 15:1 buffered HF, is introduced into the cell. A voltage is applied, between the sample and a platinum probe within the cell, to form the anodic oxide. Care has to be taken to increase the potential slowly so as to allow a pin-hole free layer to form. The electrolyte is then flushed out and HF used to remove the oxide. The HF is expelled and the sample washed and dried thoroughly to enable another conductivity measurement to be made. The complete cycle takes about 12 minutes and measurements are typically made at 20 nm intervals. The arrows of figure 2.2 show how the surface recedes as the analysis progresses. By combining the three data sets thus obtained, the carrier profile may be deconvolved. Care must be taken at this stage as the profile may

be significantly distorted especially as the junction is neared and carriers of opposite sign spill across it. To obtain a correct result the Poisson equation must be solved in two dimensions for each stage of the analysis to permit calculation of the true carrier distribution. This requires knowledge of the topography at each stage, which is provided by TEM cross sections of a number of control samples. Hill and Pearson (1988b) and Pearson and Hill (1988) report a resolution of 20 nm, with an added error in mask edge location of a further 50 nm. Hill has also reported a sensitivity of 10^{18} atoms cm^{-3} for the technique (1990).

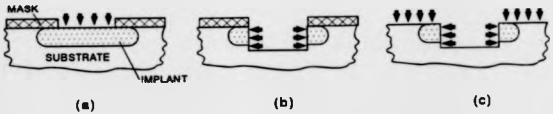

Figure 2.2 Anodic profiling technique due to Hill et al.

Another anodic technique was described by Kyung et. al. (1985). The method considers the two dimensional dopant region as a matrix of resistors connected in series parallel combinations. The measured conductivity of the complete matrix is therefore the sum of its components. The sample is sectioned anodically and the conductivity measured in a similar way to that of Hill. From the experimental data the equivalent resistor matrix may be constructed and from this the carrier concentration may be deduced. No experimental results have been presented for this method, but the resolution and sensitivity are likely to be similar to those achieved by Hill.

2.2.2.2 Capacitance-Voltage Profiling

Capacitance Voltage (CV) profiling, in the depth dimension only, is a very well established characterisation technique (C.P.Wu et. al. 1975). The method relies on the fact that in a p-n junction the space-charge capacitance is a function of the reverse bias voltage. If the reverse bias voltage is varied, and the capacitance measured, the carrier profile may be deduced (Sze, 1984a). This is most often accomplished by depositing a metallic layer on the implant surface, to form a Schottky diode, then applying a dc bias across the diode to modify the depletion region. A high frequency signal is superimposed on the dc bias to enable the capacitance to be measured as part of a bridge network. The resolution to which the profile may be determined is limited by the Debye length, the distance over which the carrier concentration rises from that in the depletion region (zero) to that in the material bulk. The Debye length is inversely proportional to the substrate doping concentration, thus it is greatest in low doped regions. To enable accurate deep profiles to be produced, the schottky may be formed using an electrolyte that also etches the substrate. The doping profile may then be determined as a function of time as the surface is eroded (P.Blood, 1986). A forward method, using the CV technique, was proposed by Ouwerling (1989) and requires three deposited metal plates to be placed near a non-uniform doping region, see figure 2.3. CV data is acquired for each plate as a function of the bias voltage on the other two. The data from each plate thus contains information about the whole of the doped region. Ouwerling then uses a forward method to produce a carrier profile. Firstly, a general active dopant distribution is assumed, and, using a fast Poisson solver, theoretical CV data for the distribution is created. The artificial data is then compared to that obtained experimentally and the assumed distribution modified.

This process is continued until the data predicted from the assumed distribution matches that obtained experimentally. The method was

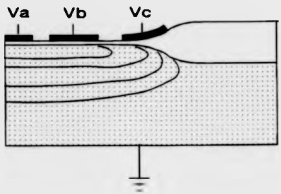

Figure 2.3 the CV arrangement due to Ouwerling

used to determine the carrier distribution around the junction of a CCD structure and a sensitivity of 10^{14} atoms cm^{-3} was achieved on both sides of the junction, with a resolution equivalent to a mesh spacing of 100 nm (Ouwerling 1990).

As carrier diffusion is modelled in the Poisson solver, this technique yields the active dopant distribution directly, thus avoiding the need for later adjustments to the distribution. In a similar way to the problems experienced in CV depth profiling, the resolution is limited by the Debye length, especially in low doped regions (Johnson and Panousis 1971). This technique is unique in that it does not require the sample to be sectioned and thus avoids the problems of carrier diffusion and profile distortion at an exposed interface.

2.2.2.3 Spreading Resistance Techniques

The measurement of depth dependent carrier distributions using spreading resistance is a routine and widespread procedure (Sze, 1984b). Samples to be analysed are bevelled at a very small angle to the substrate surface, typically 15-60', so as to effectively magnify the depth dimension. The measurement is made using a pair of metal probes typically a few hundred microns apart, with a tip radius of 1-5 μm. The probes are aligned parallel to the bevel and are then tracked down it in a series of closely spaced (1-5 μm) steps. At each point the resistance between the probes is measured. Using knowledge about the volume sampled by each measurement the effects of measurement superposition may be removed and the resulting resistance profile converted to a carrier profile; a Poisson solving routine may also be included to eliminate the effects of carrier spilling and surface effects. In many applications this deconvolution is not made and the "raw" profile is compared directly with one obtained from a known sample. Also in certain cases, such as comparison of different processing schedules, the true profile does not need to be known and the uncorrected spreading resistance profiles may be directly compared. The reason for this approach is that to obtain useful quantitative data the radius of the probe tips must be measured, and even then, any roughness of the tip will cause greater penetration into the sample leading to an erroneous result. Pawlik (1992) describes the elaborate procedure which must be undertaken to condition the probes before quantitative sample analysis can be attempted.

Vandervorst et. al. (1992) have modified the basic technique to enable two dimensional data to be collected. The sample, a long implanted stripe, is initially bevelled in the normal horizontal fashion, so as to magnify the depth scale. A second bevel is then produced across the first in a vertical direction, at

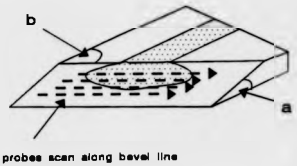

Figure 2.4 View of the sample used by Vandervorst et. al. for spreading resistance measurements

a small angle to the implant window, thus magnifying the lateral dimension (figure 2.4). The probes are tracked along the direction of the resultant edge and a spreading resistance matrix constructed. Unlike the one dimensional technique the pair of probes are not always in regions of equal concentration and may at times even be either side of the junction. This can lead to erroneous results. Vandervorst proposes that this effect may be corrected for by application of a suitable superposition scheme, however, great care must be exercised as multiple solutions may exist.

Vandervorst reports that concentrations down to junction level may be discerned by this method with a resolution of 10-20 nm in both depth and lateral directions, although no final profiles are presented. It is also suggested that a three dimensional sample could possibly be analysed using a modified version of this technique.

2.2.2.4 Scanning Tunnelling Microscopy Techniques

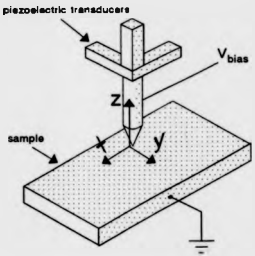

Figure 2.5 Diagram showing arrangement of the components in the STM

The scanning tunnelling microscope (STM) has generated a great deal of interest for the determination of impurity profiles, as it is capable of making measurements with atomic resolution. This instrument, shown diagrammatically in figure 2.5, comprises a very finely tipped probe, a typical tip radius being 50 nm, mounted on a three dimensional (X, Y, Z) piezo-electric translation system with very high precision. In operation, a bias of a few volts is applied across the sample and the probe, the two are then brought together until a current, due to tunnelling between the electron clouds of each, is detected. The tip is then scanned in a raster pattern across the surface using a feedback system to maintain a constant tunnelling current, or other electrical quantity such as capacitance. The output from this system is therefore representative of the

sample topography. If the sample is flat, tunnelling will occur from only one point on the tip and a resolution of atomic order may be achieved.

STM measurements may be made in air or vacuum. However, the latter is preferable for high resolution analysis as, in air, measurements are subject to surface chemistry changes, such as the adsorption of impurities. The use of STM at UHV, together with in situ sample preparation, ie cleaving or epitaxy, allows the investigation to be made without effects being introduced by oxide growth. As the STM is sensitive to the electron density of the surface, anything affecting this will be recorded, thus impurity atoms, junctions and charged defects can be observed under the right conditions. A variation of the basic STM concept was used by Muralt et. al. (1987) to study the electrical potential distribution across a vertical cleave through a GaAs double heterojunction device. Their technique, described as scanning tunnelling potentiometry, allowed a resolution of nanometre order in the lateral dimension.

The first reported use of STM for junction delineation was made a year later by Hosaka et. al. (1988). The junctions studied were made on the surface of silicon substrates by implantation and subsequent anneal. Although this geometry is very rarely used in devices, the substrate surface provides an ideal sample for STM as it is highly flat and crystalline. Care was taken during the processing so as to maintain this flatness. The native oxide was removed prior to analysis by wet etching, this also removed any adsorbed impurities, and the sample was placed in the instrument under vacuum. The tunnelling characteristic, as a function of junction bias, was recorded and distinct differences were evident on either side of the junction. The resolution reported for the delineated junction was better than 100 nm.

Kordic et. al. (1992) developed another technique for distinguishing between n and p-type material and applied it to the cleaved cross section of a

more conventional device. The STM tip is positioned using the constant current method to maintain altitude above the sample and a constant potential is applied to the p-type material. The scan is then disabled and the tip position held whilst a ramp voltage is applied to the n-type side. The tunnelling current is then recorded as a function of ramp voltage.

When the tip is positioned on the p side of the junction and the junction remains reverse biased (or only slightly forward biased with negligible current flow) the surface potential, and therefore the tunnelling current, will remain constant. If the tip is above the n-type material the surface potential will vary with the ramp voltage and the tunnelling current will likewise vary. By making a number of such measurements, in a closely spaced array, Kordic was able to delineate the junction with a resolution of 50 nm in air (Kordic et. al. 1989). The relatively poor resolution obtained (for an STM technique) is attributable to the growth of native oxide during the measurement, which took a number of hours in total. The experiment was repeated using a UHV instrument together with in situ cleaving. Here the sample was available for several days, thus a more comprehensive and accurate study could be made. Under these conditions Kordic (1992) reports a resolution of 30 nm. For similar reasons to those of staining techniques, the location of a physical position (the metallurgical junction), this technique is capable of high sensitivity, with 10^{15} atoms cm^{-3} being reported.

A further modification of the STM apparatus has been used by Williams et. al. (1989)(1990) to permit highly localised capacitance-voltage measurements (section 2.2.2.2) to be made on planar surfaces. The STM tip, of approximately 50 nm radius, was biased with respect to the sample with a dc potential, upon which was superimposed a 30 kHz ac signal. Instead of maintaining a constant tunnelling current, the tip was scanned in a constant

capacitance mode which was found to avoid problems of stray capacitance and low frequency drift. The varying tunnelling current resulting from this technique allowed mapping of the surface topography. At a number of points CV characteristics were recorded by varying the sample tip bias, thus locally depleting the material of carriers. Williams (1990) also reports that using this technique trapped charge (at interfaces) and surface defects may be detected as well as the direct measurement of a variety of device capacitances. Although full dopant distributions were not produced, a spatial resolution of 100 nm was reported together with a sensitivity of 10^{15} atoms cm^{-3}.

A development of the STM is the Atomic Force Microscope AFM (Martin, 1988), shown diagrammatically in figure 2.6. The instrument consists of a tungsten wire cantilever a few hundred microns in length whose end is bent through a right angle and etched to a fine tip, typically a few tens of nanometers in radius. A piezoelectric scan system, similar to that of the STM, is used to position the probe. The tip is brought into close proximity with the sample and vibrated at one of its resonant frequencies. Using an optical interference detection system, the motion of the cantilever is monitored. As the tip is scanned across the surface, changes of the tip-sample force cause the resonant frequency to vary. In operation, a constant force is maintained by feedback loop control of the tip altitude. O'Boyle et. al. (1992) have used the AFM to measure doping concentration. They applied a dc bias to the tip, so as to deplete the surface of carriers, and superimposed an ac signal to induce mechanical oscillation at a resonant frequency of the cantilever (a different frequency from that used for topographic control). The variation of signal oscillation amplitude then corresponds to changes in the depletion capacitance and therefore carrier concentration. Experimental measurements were again made using a planar sample, a thermally activated BF_2 implanted grating

pattern, and showed the capability to detect concentrations in the range 10^{15} - 10^{20} cm^{-3}. The resolution of the AFM capacitance probe technique is typically in the tens of nanometre range. A point of interest arising from this experiment was that lattice expansion, of the order of 0.5 nm vertically, was observed in the region of the implant due to incorporation of the dopant.

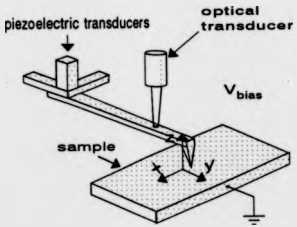

Figure 2.6 Diagram showing arrangement of the components in the AFM

The resolution of the STM and similar instruments in a surface imaging mode is possibly the greatest of all microscopical techniques and, in the short time since its inception (Binnig, 1982), has made rapid development in the field of two dimensional characterisation. At present however, many problems remain, not least of which is that to fully utilize potential resolution, the analysed surface should be very flat and clean. With the exception of Kordic (1992), most workers have not attempted to analyse real cross sections of devices, as a cleave is rarely flat enough, especially at the surface. The cross

section presented by Kordic (1992) is incomplete for this reason. The resolution of all these techniques is limited by the tip radius of the probe, not less than 10 nm, and the question has been posed as to what the term *resolution* in electrical profiles actually means when it is less than the Debye length (Subrahmanyan, 1992).

2.2.2.5 Electron Beam Induced Current (EBIC)

When the electron beam of a SEM is incident on a semiconductor device electron-hole pairs may be generated. By applying a bias to the device, the carriers may be collected and the resultant current used to modulate the image. This mode, EBIC, may be used to identify regions within the device and is of particular importance for locating failure points, as junction damage is easily visible (Sze 1984c)(Leamy, 1982).

The EBIC mode, combined with etching, has been used by Roitman et. al. (1984) to investigate implanted regions. The results where not wholly successful and junction delineation was achieved with a resolution of 100 nm. It was hoped to improve upon this by using more sophisticated data analysis methods.

Roberts et. al. (1983) imaged an NMOSFET device in cross section and were able to locate the source n^+-p junction with an accuracy similar to that of Roitman.

2.3 DOPANT PROFILING TECHNIQUES

2.3.1 TEM Techniques

The TEM has been used extensively for 2D carrier analysis using etching and staining methods (section 2.2.1.1-2.2.1.3), however there has been little work done on measuring dopant (chemical) distributions. Renteln et. al. (1989) have used scanning TEM and energy dispersive X-ray analysis (EDX) to investigate NMOSFET cross sections. They were able to profile the highly doped source region (arsenic), taking their calibration from SIMS and RBS depth profiles. The sensitivity of the method was increased by allowing the high current density probe to melt the silicon (in a region typically several nanometres in diameter) which permitted As to become concentrated in the liquid phase, thus amplifying the X-ray signal. The resolution of the technique is limited by the diameter of the beam (as small as 1 nm), however, to obtain a useful signal a greater volume must be sampled, hence, Renteln reports a resolution of typically 10 - 20 nm with a detection sensitivity of 3×10^{18} cm^{-3}.

Hill et. al. (1985) used a technique based on the concentration dependent oxidation properties of highly doped silicon. An arsenic implant was made into a silicon substrate and the mask removed. The sample was then subject to steam oxidation at 700° C. The oxide thickness thus replicated the impurity concentration and was observed by TEM. A lateral resolution of 10 nm was reported and concentrations of 10^{20} atoms cm^{-3} were detected.

2.3.2 SIMS Techniques

Secondary Ion Mass Spectrometry (SIMS) is able to provide high sensitivity depth profiles (Wittmaack, 1976) and high resolution mass resolved images (Levi-Setti 1985). However, to achieve high sensitivity, enough of the sample must be consumed to permit the detection of a statistically significant number of impurity atoms. When imaging, the small amount of analyte present in each voxel places severe restrictions on the number of atoms available for counting. Consequently operation at the required sensitivity and lateral resolution is not currently possible. This constraint is explored more fully in section 4.2.1.

Direct application of imaging SIMS has been used (Bryan et. al. 1985) to obtain a vertical section through an n-p-n bipolar device. Using a reactive probe for enhanced secondary ion yields, and the resistive anode encoder of a Cameca stigmatically imaging instrument, a spatial resolution of 500 nm was reported. This is of little practical benefit for modern devices, as features of less than this value are often produced. If SIMS is to used for two dimensional profiling using current instrumentation, indirect techniques must be sought.

A method has been devised to permit two dimensional impurity profiles to be obtained from a number of one dimensional profiles at different angles (Goodwin-Johansson et. al. 1989). The technique is similar to that used for medical imaging using X-rays. Figure 2.7 shows diagrammatically the principle involved. In the x-ray technique a collimated beam of x-rays passes through the sample and is received by the sensor. The beam and sensor are scanned across the sample, the signal received at each point being proportional to the sum of the attenuation caused in all the voxels through which the beam passes. When a complete scan has been made, the source-sensor arrangement is rotated about the

sample and another scan made. The voxels through which the beam passes this time are different to those of the previous scan, and consequently the received signal will be different. This cycle is repeated for a number of different angles. The data is deconvolved using an iterative technique,

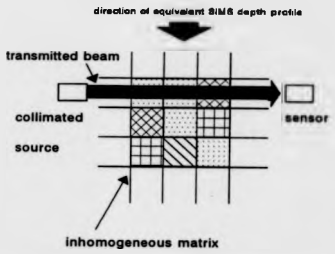

Figure 2.7 The analogy between x-ray and SIMS computed tomography

the EM (Estimation Maximisation) maximum likelihood algorithm (Lange and Carson 1984). This works by estimating the likelihood that a given set of measurements could result from an assumed distribution within the voxel array. By modifying the contents of the assumed distribution within the voxel array, so as to maximise the likelihood that the set gave rise to the measured signal, a solution is found. Care must be taken to ensure realistic solutions are found as with limited data sets the solution may not be single valued.

The data points of a SIMS depth profile may be considered as being analogous to each measurement of an x-ray scan at a single angle (figure 2.7). However, unlike the x-ray method, SIMS is a destructive technique and thus to

employ a similar methodology requires as many samples as angles to be measured.

Goodwin-Johanson et. al. (1992) prepared their specimens on silicon wafers by first depositing a boron doped polysilicon layer on a surface oxide. This was photolithographically patterned and etched to form long mesas. Parallel to the mesas long windows, 2 μm wide, were opened in the photoresist, through which boron was implanted at 20 keV with an areal dose of 10^{15} cm^{-2}. The resist was removed and the entire wafer covered with a thick silicon capping layer. After dicing the wafer, individual dies were mounted in a bevelling jig and bevelled at different angles until the doped polysilicon stripe became visible, as in figure 2.8.

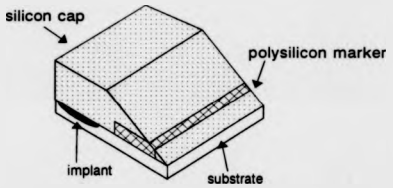

Figure 2.8 The sample used by Goodwin-Johansson for computed tomography 2d SIMS

The samples were analysed in a quadrupole SIMS instrument with the beam normally incident to the bevelled surface. Depth profiles were performed on the bevelled face of each sample, resulting in the collection of data sets for four different sectioning angles, 1°, 6°, 11° and 15°. The use of an implanted stripe, rather than a small square for instance, serves to increase the amount of

material available for analysis and thus overcome the constraint of direct analysis.

Despite the signal enhancing effect of the sample geometry, the SIMS data presented (Goodwin-Johansson 1992) show a very poor dynamic range, less than two orders of magnitude, with a high level of noise. This is in part due to the fact that the implant is still contained in a very small region, a single stripe 500 μm in length and 2 μm wide, that must be significantly overscanned by the analysed area for a full analysis. Thus the relatively low signal obtained from the stripe is subject to the addition of noise from the whole of the analysed area. The effect of a poor signal to noise ratio is demonstrated by the authors and results in corruption of the doping profile especially at the edges of the distribution where the ratio is poorest. This will remain a fundamental problem, limiting the sensitivity of this technique, as the amount of dopant in the stripe is relatively small, and the need to scan large areas of undoped material, so as to enclose the structure, has a further diluting effect. The reported sensitivity was 10^{17} cm^{-3}.

A potentially more serious problem, than lack of sensitivity, is that of inaccurate alignment of the bevel with the implanted stripe. To obtain maximum resolution the sputtered planes must be removed parallel to the long axis of the structure, any deviation will cause material from other depths to be removed too soon. This results in a smearing of the profile and thus lack of resolution. The polysilicon stripe is used to assess the misalignment, which has been reported to be in the range 20 nm to 630 nm along the full 500 μm length. The authors report that the algorithm may be compensated for this skew effect, if the misalignment is known, but admit that loss of resolution does nevertheless occur. For well prepared samples a resolution of 50 nm is attainable in both depth and lateral dimensions.

A further drawback of this method is that for all but the most trivial cases, a substantial amount of computing power is required which, coupled with the extensive sample preparation needed for precise bevelling of many samples and the need to analyse them all, makes this technique fairly time consuming.

Another SIMS based technique has been developed to measure the depth dependent lateral spreading of implanted ions (Ashworth et. al. 1988 and Oven et. al. 1988). A number of implants were made into amorphous silicon targets at different angles. These were later depth profiled using SIMS and a distribution curve fitted to the normal incidence case. Using this distribution for comparison, it was possible to derive information about the lateral spreading of the implant from the angled implant cases; as for an angled implant part of the depth profile is due to effective lateral spread, with respect to the implanting beam. The method requires that the depth profile be accurately modelled, and choosing the moments with which to describe it inevitably leads to inaccuracies.

2.4 COMPARISON OF TECHNIQUES

The wide variety of techniques that have been applied to the problem of determining the lateral spread of impurities in semiconductors, reflects the technological need of such information and the fact that no one technique is capable of yielding all of the required data. Figure 2.9 shows the typical regimes of each technique. The staining (2.2.1.1), together with the CV technique of Ouwerling (section 2.2.2.2), provide the most sensitive measurements, being capable of identifying concentrations as low as 10^{14} atoms cm^{-3}, however, their spatial resolution is relatively poor. The highest lateral resolution yet achieved is that due to Sheng and Marcus (5 nm) although this was at the expense of sensitivity (10^{19} atoms cm^{-3}). These extremes illustrate

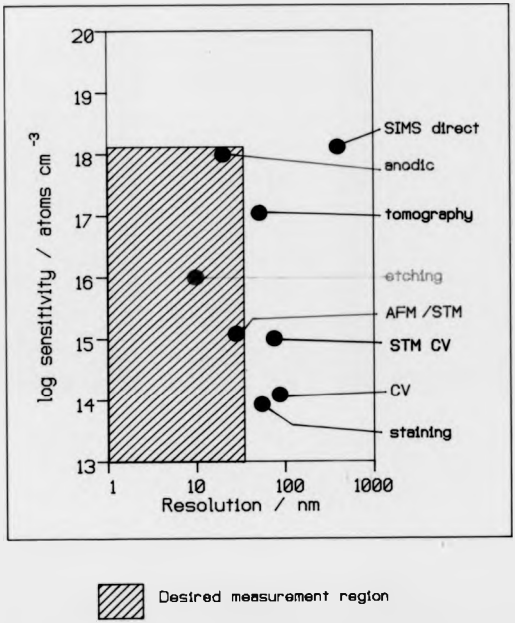

Figure 2.9 Plot showing the sensitivity and lateral resolution achieved by the techniques described in chapter 2.

that all of the measurement techniques are ultimately a compromise between lateral resolution and sensitivity, with the highest resolution being achieved where the doping is greatest, thus providing more material for analysis (for dopant profiling) and ensuring a short Debye length (for carrier profiling).

The SIMS technique of Goodwin-Johansson does attempt to break this constraint by analysing a long dopant stripe, thereby sacrificing one dimension to amplify the signal in the other. This advantage is weakened by the fact that so much undoped material must also be removed, adding to the background signal and degrading the signal to noise ratio which must be kept high if meaningful results are to obtained.

It will be immediately obvious that a greater number of techniques have been devised for carrier measurement. Rather than one method being supreme, these techniques should be regarded as complementary, as between them enough information is already available to aid in the validation of process modelling software.

No such diversity exists in the dopant profiling techniques, leaving a very important space in the data available for validation. Any technique that aims to fill this gap must overcome the constraint of finite sampling volume, so as to maximise sensitivity, but without introducing errors which will compromise resolution.

3.0 SECONDARY ION MASS SPECTROMETRY (SIMS)

3.1 Introduction

Since the construction of the first complete secondary ion mass spectrometers (Honig, 1958; Bradley, 1959) SIMS has become a routine analysis technique for both surface and in-depth measurements. Essentially, the specimen to be analysed is bombarded with a chemically clean beam of ions that sputter erode the surface. A fraction of the material leaving the analyte is in an ionised state, this permits collection and subsequent mass analysis. Thus the composition of the specimen may be determined.

This chapter reviews the fundamentals of the sputtering process and describes the typical configurations of secondary ion mass spectrometers. A full description of the EVA 2000 SIMS instrument used for the experimental work contained in this thesis is given.

3.2 THE EFFECTS OF THE PRIMARY ION BEAM

3.2.1 Sputtering

In SIMS, ions, typically having an energy in the range 500 eV to 30 keV, impact the sample surface. This causes sputtering of the surface layers and incorporation of the incident ions. The phenomenon of sputtering was first reported by Thomson in 1910 when studying "Canalstrahlen" or positive ion rays (J.J Thomson 1910). He noted that both neutral particles and positive ions were emitted from a metal surface when Canalstrahlen impinged upon it. Very

importantly, Thomson determined that these particles were ejected in all directions and that the charged fraction was small in comparison to the total flux.

The first theoretical explanation of sputtering was attempted by von Hippel (1926) who proposed that the energy from the incident ion appeared as heat about the point of impact. He suggested that the small hemispherical region heated by the ion impact was hot enough to permit evaporation of the target material. However, this explanation failed to explain quantitatively the relatively high proportion of ions produced, many more than would have been expected from an evaporation source. A more important failing of the "hot spot" theory was its inability to account for the observed reduction in the number of sputtered particles as the energy of the incident ions was increased. The hot spot explanation predicted that the spot grew hotter, thus increasing the evaporation rate. The theory was refined by other investigators (Townes 1944), however the concept of thermal emission was unable to explain quantitatively many of the observed features.

The most successful explanation of the sputtering process to date is the collision cascade model due to Sigmund. (Sigmund 1969, 1974). Sigmund uses the approximation that at energies above about 10 eV the interaction between lattice atoms and a heavy particle travelling through the lattice may be considered as a series of classical elastic binary collisions (nuclear collisions). This leads to the description of a *collision cascade*, whereby the incident ion undergoes multiple discrete collisions with target atoms that, if the energy transfer is great enough, themselves recoil and go on to collide with other target atoms. In this way a large number of target atoms are set in relatively low speed motion. The effect of this cascade in a crystalline material is the generation of defects, as atoms are displaced from their lattice sites, ultimately

leading to amorphisation of the upper layers. Where the cascade intersects the surface, and the moving atoms have energies in excess of the surface binding energy, emission may occur. Figure 3.1 shows a two dimensional representation of this process where the incident ion becomes incorporated in the target and the collision cascade it initiates results in the emission of target atoms. As the path taken by the incident ion is more or less random, the cascade may result in the emission of a greater or lesser number of particles, the average ratio of emitted to incident particles is known as the *sputter yield*.

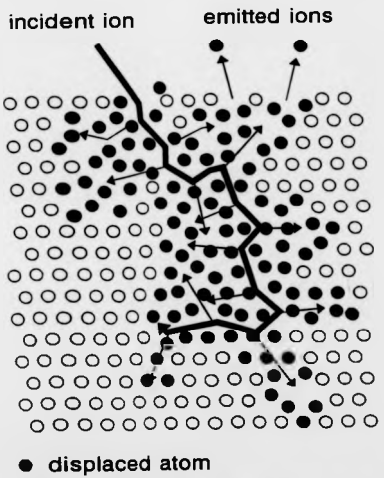

Figure 3.1 Two dimensional representation of Sigmund collision cascade.

The lifetime of typical cascade is assumed to be of the order of 10^{-11} to 10^{-12} s, with dimensions of the order of 10 nm. Thus with a current density of less than a few mA cm^{-2} cascades may be treated as discrete non-interactive events (Werner 1974).

Sigmund's theory has proved able to explain quantitatively both sputter and ion yields, as well as their energy distribution and dependence on atomic number and incident ion energy. An important consequence of the collision model is that the emitted particles originate from the uppermost surface layers. It is this type of emission that gives rise to the high surface sensitivity possessed by SIMS.

3.2.2 The effect of probe chemistry and angle of incidence

During SIMS analysis only those particles that leave the surface in an ionised state have a chance of being collected, analysed and passed to the detector. Thus, as the analyte contains only a finite amount of material, to obtain high precision, as much as possible of that sputtered must be charged. It is found that the *ion yield*, the proportion of the sputtered material that is ionised (Williams 1979), varies strongly with the surface chemistry, thus the chance of a specific atom being emitted in a charged state may vary by as much as 10^5 depending on the matrix it is in and the bombarding species. In the presence of reactive species, the emitted particles have a greater probability of being charged (Maul and Wittmaack 1975). To obtain enhanced ion yields it is therefore usual to introduce reactive elements during analysis. This is most often accomplished by using the reactive element as the bombarding species. It is found that electronegative elements, such as oxygen, greatly enhance the positive ion yield

and electropositive elements, like caesium, the negative ion yield (Wittmaack 1981).

An alternative to bombarding with a reactive species is to "flood" the sample region with reactive gas (Wittmaack 1980). This technique is especially useful when segregation effects need to be minimised and where reactive probes cannot be used, such as high resolution imaging using a gallium probe from a liquid metal ion source. For depth profiling, the flood method can be inefficient (Lang and Degrève 1985) owing to the relatively high erosion rates often employed. This may not allow sufficient time for the reactive species to combine with the surface (at a flood pressure of 10^{-4} Pa only about one monolayer is deposited each second).

The angle of incidence that the primary ion beam makes with the sample surface has a great effect on the sputter and secondary ion yields (Wilson et. al. 1985). At normal incidence, the sputter yield is low. As the angle to the normal is increased the amount of material ejected increases; at around 60° it is over an order of magnitude greater for silicon under O_2^+ bombardment. The increase in sputter yield is accompanied by a decrease in the ionised fraction, for silicon under O_2^+ bombardment at 60° the ion yield is over three orders of magnitude lower than at normal incidence.

3.2.3 Atomic mixing and the altered layer

As stated in section 3.2.1, an incident ion sets a large number of target atoms in motion about the region of the collision cascade. When the impact parameter for a collision is small, target atoms will receive a great amount of energy and be displaced from their site. A recoiling atom may be driven some distance in the direction of the received momentum. The effect of a large

number of such random collisions is to thoroughly mix the target atoms, together with incorporated probe atoms. As well as mixing by nuclear recoils, the general motion about the impacting ion causes a more isotropic mixing and a redistribution of material (Tsong et. al. 1981). Incident ions may travel some distance in the target material (Ziegler 1985) leading to a mixed region a few tens of nanometres thick. They may then diffuse further into the target. The region in which this occurs is known as the *altered layer* and contains a mixture of probe and target atoms. If a narrow feature is contained in this layer it will become diluted throughout the volume of the layer, and further diluted into lower regions as the surface recedes through sputtering, and more matrix atoms are mixed in. This leads to a broadening effect in the depth profile of such a structure with a characteristic steep leading edge, as the concentration of the feature rises sharply when it is first mixed in, and a shallower trailing edge caused as the concentration of the impurity becomes more and more dilute in the layer (Vandervost et. al. 1984) (Wittmaack 1984).

The thickness of the altered layer thus has a direct bearing on the resolution that may be attributed to a depth profile, the thicker the layer, the poorer the resolution (Barlow et. al. 1992). The layer formed by a normally incident probe is thick, as the momentum of the ions is directed deep into the target. A shallower angle of incidence thus results in a shallower altered layer, as less momentum is directed inwards, however, in general the ion yield may be orders of magnitude below that for the normal incidence case resulting in poor sensitivity. For silicon bombarded with oxygen, good depth resolution is attainable at normal incidence owing to the formation of a diffused SiO_2 layer beyond the direct range of the ions that pads the matrix out (Augustus et. al. 1988). This effect can also exclude impurities from the altered layer causing them to segregate at the interface.

When analysis commences, the altered layer builds up as the probe is incorporated. After a period of time a steady state is reached when as many probe atoms are sputtered as are being implanted (Williams 1979). Thus, until this equilibrium is reached, the composition of the altered layer is continually changing leading to large variations in both the sputter and ion yields. One effect is to cause a shift of the profile, the differential shift (Wach et. al. 1981), that may seriously affect the apparent depth at which a feature appears. This pre-equilibrium region, although relatively narrow, makes quantification in the near surface region difficult .

3.3 THE SECONDARY ION MASS SPECTROMETER

3.3.1 Overview

Secondary ion mass spectrometers may be considered as comprising a source of ions, a specimen and a means of collecting and mass analysing the sputtered material. A typical instrument may have a number of guns; one for positive and one for negative ion yield enhancement and a third for high resolution imaging. However, it is likely to be equipped with only one type of mass spectrometer, and this largely determines the performance and application of the instrument. It is therefore usual to classify instruments by the type of mass spectrometer they utilise. The following sections describe the main types of instrument, their applications and performance.

3.3.2 Magnetic sector instruments

The magnetic sector mass spectrometer, the oldest means of ionic mass separation, is based on the fact that in a uniform magnetic field heavy ions will describe a trajectory of larger radius than lighter ones possessing the same charge and energy.

As the secondary beam is not truly monochromatic, ions with greater energies will follow a larger radii and vice-versa. Thus to operate a magnetic sector at high mass resolution would necessitate very heavy energy filtering and consequent loss in overall transmission. To overcome this problem it is standard practice to place an electrostatic sector before the magnetic sector. The chromatic dispersion of the electrostatic sector causes ions of different energy to be injected into the magnetic sector along slightly different paths. The overall effect is to exactly compensate for the chromatic dispersion of the magnetic sector, thus permitting an increase in transmission. This mode of operation is termed *double focussing*. The resolution of the system is determined by the width of the inlet and exit slits; the narrower the slit separation, the narrower the portion of the mass dispersed spectrum will be passed to the detector, thus the higher the mass resolution. The angular aberations of the system limit the ultimate mass resolution when the spread of the desired ions at the detector slits becomes equal to the slit separation.

Magnetic sector instruments generally provide high mass resolution (at least 30 000) and good transmission, making them the first choice for depth profiling. They are also capable of good quality imaging. However, this class of mass spectrometer works best with ions having energies of at least a few keV, thus requiring high extraction fields and extraction optics of short working distance. This leads to a relatively small field of view (typically 400 μm

maximum) and perturbing of the primary beam, especially at lower energies, by the high extraction field.

The work presented in this thesis requires the uniform collection of data from a square sample of side 2 mm. Thus, this constraint prevents a magnetic sector instrument from being used.

3.3.3 Quadrupole instruments

The quadrupole mass filter (Paul and Steinwedel 1953) provides a very cost effective means of mass selection and was the choice of many of the early experimenters in SIMS (Wittmaack 1977a, Magee et. al. 1978). Essentially the device uses inhomogeneous oscillatory electric fields to permit a transmission path for a specific charge to mass ratio. Theoretically, setting up the field

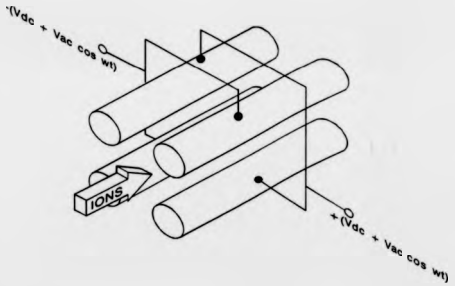

Figure 3.2 Diagram of quadrupole mass filter

requires four hyperbolic cylinders arranged about the beam axis, however, a good approximation can be made using rods of circular cross section. In operation opposite rods are paired and oscillatory voltages, superimposed on a dc component, are applied to each pair, as in figure 3.2. As ions enter the filter the fields cause them to describe a complex orbital path about the axis (Dawson 1974). The path is stable for ions of a specific charge to mass ratio, permitting them to pass to the detector. All other ions are forced into unstable trajectories, eventually leading to collision with the rods, exit aperture or vacuum vessel wall.

The pass mass and resolution of the filter is adjusted by varying the amplitude and ratio of the ac and dc voltages. Figure 3.3 shows a typical stability envelope diagram for a quadrupole filter for masses M_1 to M_4 (Dowsett 1978). Scan line (a) represents the cut off scan where the resolution has been increased to the point where transmission is zero. By changing the way the voltages are varied, the analyser may be made to filter with constant mass

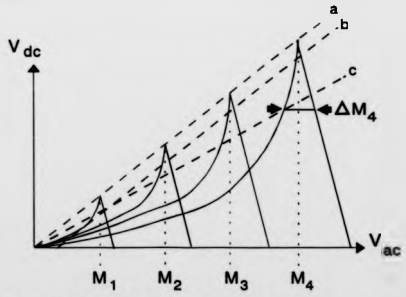

Figure 3.3 Stability diagram for quadrupole mass filter

resolution (scan line c), constant peak width (scan line b), or a combination of both. This allows the response of the quadrupole filter to be tailored to a specific requirement, such as high resolution at high masses, to permit peak separation, and lower resolution at low masses, where mass interferences are less common, to increase transmission. Similarly, the filter may be operated to compensate for the lower overall transmission of the filter at high mass (Benninghoven, 1987).

The resolution of the quadrupole analyser is dependent upon the unwanted ions spending long enough in the device for the unstable trajectories to deviate significantly from those of the required species. A particular problem occurs when high energy ions are injected as they may have enough velocity to pass through the filter virtually unperturbed by the fields. This is overcome by energy filtering the ions prior to injection, selecting only those with relatively low energies (typically up to a few tens of eV). The desired energy range of the quadrupole analyser makes it ideal for SIMS as the acceptance energy requirements coincide with the peak of the secondary ion emission energy, thus the need for high target bias, as with magnetic sector type instruments, is avoided. The lower extraction potential permits a larger more uniform field of view; this is an extremely important requirement of the technique proposed in section 4

Quadrupole instruments are now generally used for depth profiling applications, where the low extraction potential permits lower probe energies to be employed leading to enhanced depth resolution. The relatively low extraction field has a correspondingly small influence on the primary beam trajectory, thus permitting normal incidence probes to be used. Although quadrupole analysers were used for static SIMS, their relatively poor

transmission and resolution characteristics have meant they have largely been superseded by time of flight instruments.

3.3.4 Time of flight instruments

In concept the time of flight (TOF) mass spectrometer is possibly the simplest, however it is only in recent years with the availability of high speed timing that it has been realized. The ion gun is pulsed, or the ions bunched, so that they impact the sample as a group. The sputtered material then leaves the surface as a pulse and the secondary ions are extracted. After extraction, the ions pass into a drift region containing an electrostatic element, either an ESA or reflectron, that compensates for the chromatic spread of the ions by forcing higher energy ions to follow a longer path than those of lower energy. The time taken for an ion to reach the detector is thus a function of its mass, with light ions arriving first and heavier ions arriving later. The resolution of the system is therefore governed by the width of the pulse of emitted ions (this will be slightly greater than the pulse of the probe), the ability to correct for the spread in ion energy, and the performance of the detector and timer. As heavy ions may be easily detected in the TOF system a major application has been in the study of polymers and their fragments.

TOF equipped instruments are invariably used for surface studies and imaging, owing to the high transmission, typically greater than 0.1, and the fact that the system is capable of true parallel detection (the complete mass spectrum is detected for each pulse). To this end, most TOF based instruments are configured with fine focus liquid metal ion sources. To allow all ions generated to drift to the detector, the duty cycle of the gun is very low, therefore average current density is correspondingly small and little material is removed. For this

reason TOF instruments are not used for depth profiling, and whilst a separate gun may be fitted to enable quasi-dynamic sputter profiling, as used in auger, the instrument should really be regarded as specialist for static SIMS.

3.3.5 Ion Guns

The type of ion used for analysis determines the number and types of secondary ion produced. For depth profiling, where high secondary ion yields are required for good sensitivity, reactive species (oxygen and caesium) are preferable. Noble gas probes (argon and xenon) may also be used for profiling where a mass interference must be avoided or chemical segregation may distort the profile. However, the secondary ion yield from such sources may be more than a thousand times lower than with reactive species. The ions from gas sources are obtained by extraction from a plasma, commonly a Penning type arrangement or the brighter duoplasmatron (von Ardenne 1956)(Bacon 1978).

For high resolution imaging, in the ion microprobe mode (section 3.4.3), a very fine probe is needed. This is generally provided by a liquid metal ion gun (LMIG) using gallium. The LMIG source extracts ions from the high field region about the tip of a fine needle, wetted by the metal to be ionised.

Once the ions have been extracted from the source they are often filtered for mass and charge state, to ensure a non-contaminating probe is formed.

3.4 OPERATIONAL MODES OF SIMS INSTRUMENTS

3.4.1 Static SIMS

The tasks performed by SIMS instruments may be divided into two categories, static and dynamic.

Static SIMS requires that the ion dose be low enough so that the collision cascades of adjacent primary ion impacts do not overlap. Typically, this limits the ion dose to a maximum of 10^{13} ions cm^{-2}. As the emitted ions come almost entirely from the surface layers, static SIMS is used for surface chemistry studies, often involving in-situ sample preparation, such as cleaving. The amount of material available is very small and efficient analysis is essential. To this end, TOF instruments are most frequently employed.

3.4.2 Dynamic SIMS

As the ion dose is increased past the static SIMS limit sputtering causes the surface to recede. Analysis of the sputtered material as the erosion proceeds allows a profile of chemical composition with depth to be recorded. The depth resolution attainable is determined by the probe energy, and hence the resultant atomic mixing, and the evenness with which the erosion takes place, so the underlying structures are not exposed too early thus smearing the profile. To achieve this, it is vital that a similar ion dose is received by the entire analysed area. This is most often accomplished by scanning a focussed beam (of diameter 1 - 100 μm) in a raster pattern. Wittmaack (1977b) has calculated that adjacent scans should overlap by at least 66 % to ensure a flat floor to the resulting crater.

When the probe is near the crater edge some ions will fall on the crater wall and cause secondary emission. As the crater wall is essentially a section through the specimen to the depth that is currently being sampled, this will introduce a background signal onto that recorded for the crater floor. To overcome this problem it is usual to collect ions from only the central, or *gated*, region of the crater. The gated area may be defined optically, such that ions are only accepted from the required area, or electronically, by disabling the counter when the probe is outside the gate (Wittmaack 1977b).

3.4.3 Imaging

Imaging in SIMS instruments may be achieved in two ways. Firstly the whole specimen may be illuminated by the primary beam and the secondary ions extracted and analysed by a stigmatic system and then projected onto a sensitive surface (ie a microchannel plate and phosphor screen for direct viewing or a resistive anode encoder for electronic detection). This system, the *ion microscope* mode requires very carefully designed optics but has the advantage that the resolution is independent of probe size allowing high current reactive ion probes to be used for imaging. As quadrupole instruments cannot be made stigmatically imaging this mode of operation is limited to magnetic sector instruments and is a feature of those marketed by Cameca.

The second imaging mode is the *ion microprobe*. In a similar way to that used in a scanning electron microscope, a fine probe is raster scanned over the sample and the secondary ion signal related to the position of the beam. The resolution of this mode is dictated by the diameter of the probe. By use of fine spot sizes, resolutions of the order of 30 nm may be achieved (Levi-

Setti et. al. 1985). This system may be used with any mass spectrometer and the secondary ion optics require less stringent design than for the microscope mode, thereby allowing optimisation of other parameters such as transmission.

3.5 THE EVA 2000 QUADRUPOLE SIMS INSTRUMENT

3.5.1 Overview

The EVA 2000 SIMS instrument, on which all of the experimental work of this project was conducted, was originally designed and built by Dowsett some twelve years ago. Since that time it has been continually improved and modified to keep pace with technological developments. The instrument is currently configured with a 19 mm rod diameter quadrupole mass spectrometer and is equipped to bombard the sample with either oxygen (O_2^+) or noble gas (Ar^+) ions at energies in the range 500eV to 15 keV.

3.5.2 Primary ion column (Ion gun)

The primary ion column, shown diagrammatically in figure 3.4, comprises a source of ions and a means of bringing them to focus on the sample.

Ions are generated in a Penning type discharge and extracted axially through a 0.7 mm hole in the cathode (see chapter 7). The pressure within the plasma cavity is approximately 0.1 Pa and the cathode hole also serves to separate this from the lower pressure in the upper column, approximately $1x10^{-4}$ Pa. The extraction optics draw ions from the plasma and pass a converging beam to the Wien filter. The plasma potential is very close to that

of the anode in the discharge, hence the total energy of the emergent ions is approximately the sum of the discharge voltage and the potential across the extraction gap. The current version of the source, designed by the author, permits easy replacement of the components within the plasma cavity and provides the long term stability required for analysis of the samples used in this project. It is discussed further in chapter 7.

As the major purpose of SIMS analysis is to provide sensitive measurement of impurities, the probe must be chemically clean in order to prevent implantation and subsequent release of contaminants. This is achieved by the use of pure materials in the discharge cavity (oxygen and aluminium (Dowsett et. al. 1983) and by removal of unwanted species and charge states by the Wien filter. The Wien filter consists of crossed electrostatic and magnetic fields, thus only ions having a particular *velocity* continue on axis. As all of the ions fall through the same extraction field they have similar energy, thus their velocity is dependent on their mass and charge state. The Wien filter may therefore be considered as performing an e/m selection. The magnetic field is provided by a permanent magnet and a second set of condenser plates facilitate alignment in the X direction.

Ions leaving the Wien filter, on axis, next pass through the pressure step aperture. This aperture, approximately 1.5 mm in diameter, separates the upper column, pumped by a turbomolecular pump, from the lower column that projects into the main chamber where the pressure is maintained at around 10^{-7} Pa by a liquid nitrogen trapped diffusion pump. A special feature of this aperture is that it is mounted in an insulating ring and grounded through a virtual earth amplifier that allows the current falling on it to be measured. When aligning the column, a minimum in the collected current may be observed when the beam is centred in this aperture.

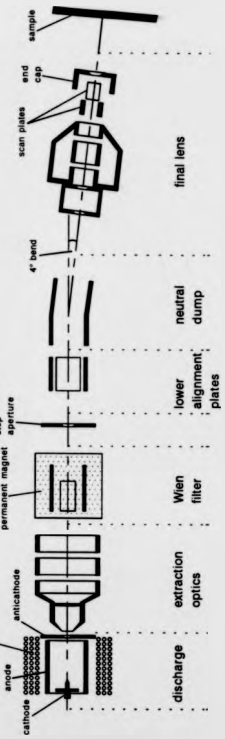

Figure 3.4 Diagram of the EVA 2000 primary ion column

Beyond the pressure step are two sets of steering plates. The first is a quadrupole set to permit alignment in both X and Y directions, and the second is dipole set that include a small bend (approximately 4°). As the ions are steered around this bend, neutral particles in the beam continue on an undeviated course and collide with the entrance aperture of the final lens. The potential applied across the plates may be reversed in order to blank the beam.

The filtered ion beam then enters the final lens, a symmetric einzel lens, and is brought to focus on the sample. Immediately after the lens are two dipole condenser plate sets, used to scan the beam in X and Y directions across the specimen.

3.5.3 Specimen stage

Samples to be analysed are mounted on a stainless steel sample holder, a little larger than a commercial microscope slide, using conductive paint or small spring clips. To enable the main chamber vacuum to be maintained at all times, the sample holder is introduced via a loadlock with a magnetically coupled arm. The specimen stage is mounted on a four axis manipulator and is electrically isolated from the rest of the instrument. This allows it to be floated at a potential to optimise secondary ion extraction (or investigate the energy spectrum of the secondary ions). A facility is also available to measure the ion current falling on the sample. This is especially useful when aligning the column, as a real time observation of the beam focus may be obtained by scanning the spot across a fine copper grid mounted on the stage and using an oscilloscope to plot current as a function of position. Using this method, independently in X and Y directions, it is easy to see astigmatism, coma and other aberrations caused by poor alignment and to observe, in real time, the

effects of corrective measures. It also allows objective estimates of probe size to be obtained immediately prior to analysis.

For accurate current measurement a Faraday cup, built by the author, is located to one side of the stage.

3.5.4 Secondary ion column

The secondary ion column comprises extraction and energy filtering optics, the mass spectrometer and the detector.

Ions are extracted and matched to the acceptance of the mass spectrometer by a modified Wittmaack "box" style energy filter (Wittmaack, 1982), figure 3.5 . Ions are drawn from the surface by the electric field applied between the sample stage and extraction electrode, approximately -200V for positive ions. This field is modified by the screening plate having the effect of concentrating the extraction field on one area of the sample. By variation of the screen potential the field of view is changed and a zoom effect is achieved. Ions passing through the electrode enter a quadrupole condenser arrangement (the"box"), where energy selection occurs. Only ions having energies in a specific range are able to describe the curved trajectory necessary to leave via the exit aperture. Others, especially the high energy ions that will contribute only to the background signal (3.3.4), collide with the plates. Variation of the potentials V_a and V_b controls the energy dispersive property of the filter and determines the vertical position on the target from where ions are extracted. The condenser set parallel to the plane of figure 3.5 permit two dimensional focussing and allow lateral positioning of the extraction area. Thus mechanical misalignment of the primary and secondary beam axes may by compensated for. A further effect of

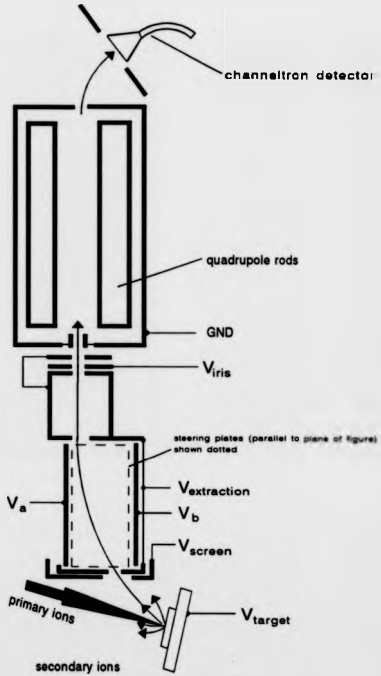

Note: all potentials with respect to ground

Figure 3.5 Secondary ion column of EVA 2000

the filter is to eliminate ions with a high take off angle (with respect to the surface normal) thus preventing them from being injected into the mass spectrometer at large off axis angles. The filter can usefully accept ions over a relatively large solid angle, typically providing a field of view up to 3 mm across at the sample surface. This is a special requirement of the 2D profiling technique discussed in this thesis. The characteristics of the filter fitted to the instrument are investigated in section 5.

Above the filter box is an electrostatic iris that is used to attenuate high secondary ion currents that may otherwise damage the detector (Dowsett 1982). The secondary ion current may also be reduced by selecting ions with energies away from the peak emission energy by changing the target potential. However, the primary ions also experience the extraction field and large changes cause displacement of the probe, especially at low energy (below 4 keV). The electrostatic iris has no displacing effect and is therefore preferable when beam displacement is unacceptable. The upper iris electrode and the quadrupole housing form a immersion lens system, decelerating the ions and injecting them into the analyser with an energy of less than 10 eV to ensure adequate mass filtering.

The quadrupole mass spectrometer (the operation of which is described in section 3.3.4) is an Extranuclear Corporation model 162-8 with 19 mm diameter rods, operating at either 1.5 or 3 MH_z. The mass range of the device is determined by the rf head used, two are available giving 0 - 200 amu and 0 - 30 amu. The work presented in this thesis employed the high range head only. The rods of the spectrometer may be biased (with respect to ground) so as to further decelerate the ions and thus improve resolution, this is the pole bias control.

The Mass filtered ions exit the quadrupole enclosure and are immediately subject to an electric field that draws them to the detector. The detector employed is of the channeltron type, a Galileo 4816, used in pulse counting mode. Ions incident on the bell shaped entrance cause secondary electron emission, these are then multiplied by a factor of $\approx 10^8$ by the continuous dynode deposited along the inner wall of the device. The resulting electron pulse is collected at the anode and fed, via a preamplifier, to the pulse counting system.

3.5.5 Charge compensation

As the ion beam impacts the target positive charge builds up at the surface. If the sample has a suitable conductivity then electrons (from earth) can travel to neutralize it. However, in insulating materials, and when profiling effectively reverse biased junctions, the surface charging leads to large changes in surface potential. This has a similar effect to varying the target bias and prevents consistent extraction of ions at a single energy. To overcome this problem the area being profiled may be bathed in low energy electrons (500 - 1000 eV) obtained from an electron gun sited to one side of the primary column.

3.5.6 Controlling electronics

The control system of the instrument is based on a Research Machines Ltd 380Z microcomputer. During profiling this has command of the mass spectrometer, target potential, raster size and pulse counter. It is also able to turn the beam on and off and issue a command to the safety interlock interface

to turn the accelerating potential off and place the instrument in a safe state when a profile is complete. This is especially useful for overnight running as it prevents the blanked beam (not steered around the final bend) from unnecessarily sputter depositing material around the region of the final lens. Thus the instrument is capable of unattended running.

The raster scan is driven by a high linearity 8-bit digital scan unit that provides exceptionally flat floored craters. The unit is also the master time keeper for the entire instrument, defining the gate and frame times. The computer is therefore a slave once a frame has been initiated.

When the collection period has ended (this may either be a single linescan or complete frame) the scan unit informs the computer which then interrogates the pulse counter. The data are stored in the computer and a hardcopy is recorded in real time on a printer and plotter to enable the progress of the task to be monitored. On completion of the profile the contents of the data array are copied to disk.

Control programs are written in the BASIC language. Machine code routines for operating the hardware are incorporated as extensions to BASIC, thus new applications may be quickly programmed without detailed knowledge of the actual interface code (Dowsett et. al. 1986). A number of "standard" programs are available for depth profiling and mass and energy spectrum collection, together with more specialised software such as that used for this project.

4.0 THEORY

4.1 INTRODUCTION

In chapter 2 it was stated that direct use of SIMS (imaging) was incapable of providing two dimensional profiles with the combination of good sensitivity and high spatial resolution. In chapter 4 the reasoning behind this statement is presented and an alternative to both the direct imaging and the computed tomography techniques described. A full description of the geometry of the specially prepared sample is given and expressions for the ultimate spatial resolution and dopant sensitivity are derived.

The specification for a SIMS instrument with which to analyse the samples is discussed and reference made to the features of EVA 2000 that make it most suitable for the purpose.

Once the data have been collected they may be processed to provide an optimum combination of spatial resolution and sensitivity as these parameters may be mutually traded, post acquisition, within the limits set by the experiment. A number of data reduction schemes have been devised, these are presented and the virtues of each discussed.

4.2 MULTIDIMENSIONAL PROFILING USING SIMS

4.2.1 Why SIMS cannot be applied directly

Detection limits of 10^{16} atoms cm^{-3} and below are regularly obtained for SIMS depth profiles in semiconductor materials and in imaging experiments lateral resolutions of 30 nm have been reported. If both of these results could be achieved simultaneously it would appear that direct mapping of the dopant distribution in two or even three dimensions should be possible. However, to obtain high lateral resolution a gallium liquid metal ion gun is used, this has little ion yield enhancement resulting in a poor detection limit. To gain the high yields produced in depth profiling a reactive bombarding species is required, however, to date, finely focussed reactive probes are unavailable.

It may be argued that this constraint can be overcome by loading the specimen surface with oxygen by thermal oxidation, or supplying a rich oxygen flood during analysis, and analysing with a liquid metal ion gun. Both of these would increase the ion yield and therefore lower the detection limit. However, the former would cause distortion of the profile and the latter would only partially increase the ion yield. This is because to obtain a fine probe high energies are required, hence the probe is highly penetrating and material from below the surface oxide (in an unoxidised state) may be ejected.

Even if a finely focussed reactive beam were available, or some other scheme to increase ion yields were employed, direct mapping still presents a problem. Suppose a spatial resolution of 30 nm is desired for determination of the dopant distribution of boron in silicon. Each voxel may therefore be represented by a cube of side 30 nm. The atomic density of silicon is 5×10^{22} atoms cm^{-3} (Sze 1981), each voxel thus contains $\approx 1.4 \times 10^{6}$ atoms. If a

very high useful yield of 1% is assumed then ≈ 14 000 ions reach the detector. For a very modest statistical precision of 33% ten impurity ions must be detected. The voxel must therefore contain at least 1000 impurity atoms, representing an atomic concentration of 3.7×10^{19} atoms cm^{-3}. Thus for a particularly favourable combination of instrument and sample the detection limit is still two orders of magnitude worse than that required for verification of process modelling software. Figure 4.1 shows the variation of sensitivity with resolution for the described conditions.

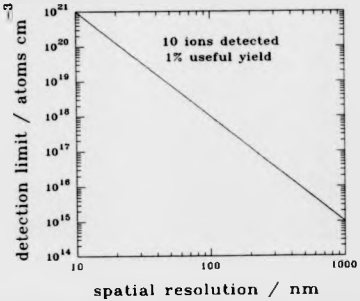

Figure 4.1 Variation of

The experiment may be modified, to increase the amount of material available, by sacrificing the third dimension and profiling only in two, in a similar way to that shown in figure 4.2. However, to recover information down to 10^{17} atoms cm^{-3} the extension factor must be at least 100. Thus each voxel is now 30 x 30 x 3000 nm. To maintain optimum spatial resolution (30 nm) the long direction of the analysed voxel must lie exactly parallel to the implanted feature. As this is not practical, some margin of error should be permitted. A

30 nm error in the alignment would degrade the lateral resolution by a factor of two (to 60 nm), as adjacent regions are being sampled in one scan, and still require an alignment accuracy of 0.5°.

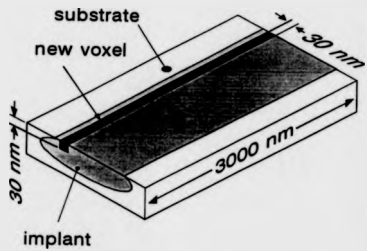

Figure 4.2 By sacrificing one dimension the voxel volume may be extended to lower the detection limit

Added to the problem of alignment is the mixing effect of the probe, as the LMIG must run at > 30 keV to provide the high resolution. This effect will distort the profile as the analysis proceeds as, unlike static imaging, the underlying layers will be extensively mixed with the emissive surface.

The above examples are highly optimistic and results obtained using currently available instrumentation are likely to be worse by at least an order of magnitude (using reactive species and stigmatic imaging, limiting the spatial resolution to 500 nm, Bryan et. al. (2.3.2) achieved a sensitivity of only 10^{18} atoms cm^{-3}).

Direct application of SIMS cannot at present provide the sensitivity with adequate resolution required for useful determination of dopant distribution in more than one dimension.

4.2.2 Indirect use of SIMS

In section 4.2.1 it was demonstrated that SIMS could not be applied directly to produce two (or more) dimensional dopant maps because there is simply not enough impurity material in each sampled element to provide reasonable statistical precision. In depth profiling applications, where *a lot* more material can be consumed, detection limits of the order of one part in 10^8 are often achieved. This is much better than can be achieved with other techniques possessing spatial resolution, eg Auger, and thus SIMS is already part way to providing the solution. To allow this potential to be realised in multidimensional profiling the analyte volume must be increased *independently* of the spatial resolution. This may be done by analysing many similar volumes simultaneously, although accurate registration between them must be maintained.

The ideal approach to solving this problem would be a specimen that may be analysed using existing instrumentation, that does not require extremely accurate registration of microscopic features (ie not on the nm scale) and that can be analysed with reactive probes to enhance the ion yield.

4.3 A SPECIAL SAMPLE DESIGN

The technique of sectioning semiconductor features at shallow angles (bevelling) has been applied to two dimensional analysis, section 2.2.1.1. Usually an implanted stripe is sectioned along its length, effectively magnifying the lateral features. The lateral magnification factor, E, of this system is given by,

$$E = 1 / \tan \Theta \qquad (4.1)$$

where Θ is the angle between the stripe and the sectioning plane. Figure 4.3 shows such a system with the lateral spread magnified many times along the bevel. However, the depth dimension remains unmagnified and extraction of the information would require high resolution imaging that would again be subject to the statistical and quantification problems previously discussed.

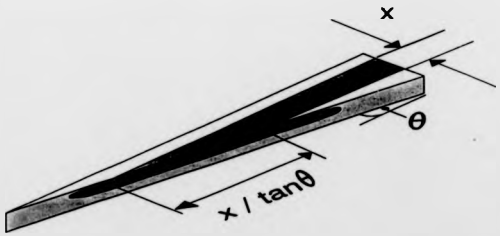

Figure 4.3 Lateral magnification may be achieved by sectioning an implanted stripe

Although the direct lateral resolution of SIMS using reactive probes is relatively poor, the depth resolution obtained whilst depth profiling may be better than 30 nm and be fully quantifiable with good sensitivity. The depth information contained in the bevelled stripe may thus be obtained by depth profiling through the structure. However, to simultaneously record the lateral information, the analysis must be performed in a linescan acquisition mode rather than the more common frame mode. For normal depth profiling the secondary ion signal is integrated over a complete frame (representative of a single depth) and recorded, however, in linescan acquisition mode the signal obtained from each linescan of each rastered frame is recorded; this is shown in figure 4.4.

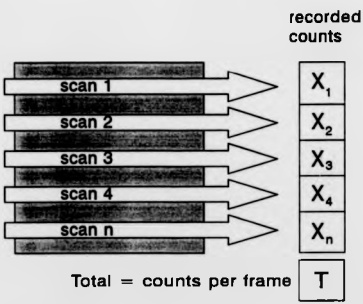

Figure 4.4 Schematic of linescan acquisition technique

A diagram showing this collection technique applied to a bevelled implanted stripe is presented in figure 4.5 and represents the basis of the analysis procedure described in this thesis.

Because of the high magnification that may be achieved with a shallow angle section, the linescans may be of much greater width than an imaging probe extracting information from a similar region, therefore larger reactive probes may be employed for similar resolution. The use of reactive probes increases the secondary ion yield thereby enhancing sensitivity, a further increase is also provided by the fact that the sampled volume is much greater than that available from a simple cross section.

Generally the rastered area is square, thus a single stripe a few microns wide represents very inefficient use of the analysed volume and includes a vast proportion of material that will contribute only to the background signal. The sample design is thus completed by arranging for many hundreds of similar bevelled stripes to be positioned in a square area. This multiplies the impurity signal from the bevelled stripes by the number used to fill the area thus reducing the contribution of the background signal. The final structure to be fabricated is shown in figure 4.6.

Figure 4.5 Diagram showing analysis of vertically sectioned implant stripe

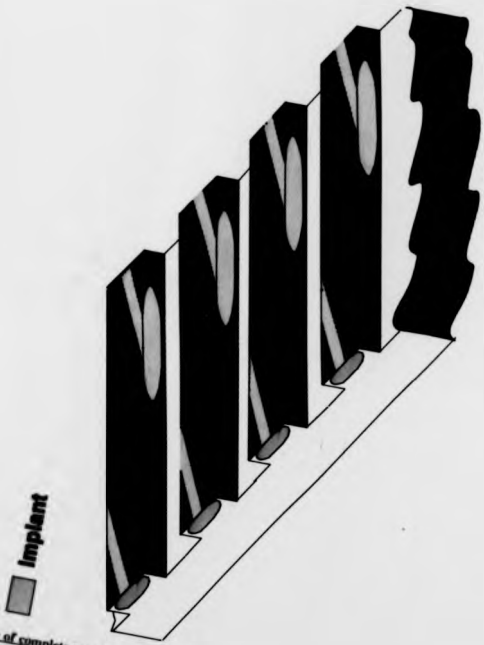

Figure 4.6 Diagram of complete sample

4.4 GENERAL CONSIDERATIONS

4.4.1 Data acquisition

The data are collected as linescan data, with successive linescans being offset from each other by approximately 0.25 of the FWHM beam diameter so as to maintain a flat bottomed crater. The maximum resolution attainable is therefore equal to the beam diameter.

Figure 4.7 shows modelled data collection from a planar distribution below the implant window, from which exponential lateral diffusion has occurred. In region I, data are collected from the laterally diffused part only, leading to an exponential increase in the detected signal. The data from region II comprise the total integrated signal from region I together with the signal arising from the planar implant. As region III is entered, data are again collected from the laterally diffused area, although this time being representative of the other side of the window. The signal finally levels off in region IV as the complete unsectioned structure is reached. An important feature of the data is the central minimum. This provides a starting point for the reconstruction.

To make efficient use of the collected data, neighbouring linescan signals are integrated up to the width of the beam. These integrated signals will be termed **BANDS** and have a minimum width equal to the FWHM of the primary beam.

In the vertical direction, the depth resolution, R_D, is much smaller than the lateral resolution, R_L, obtained after analysis; as typically only 1 nm is removed per frame and the lateral resolution at best will be 10 nm. By integrating the signal from the same band in successive frames, a larger analyte is produced

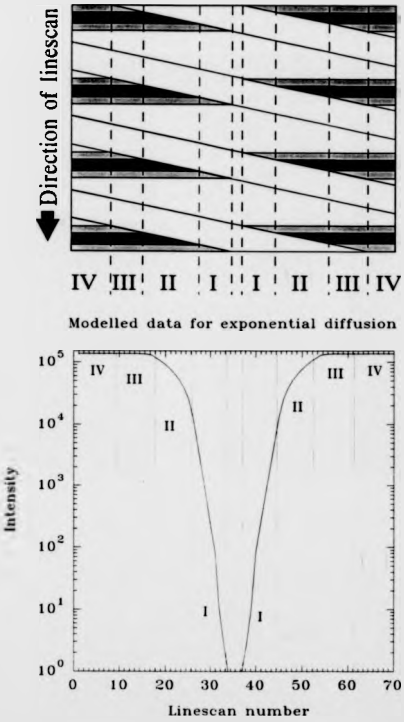

Figure 4.7 Schematic of data collection from the structure (above) and modelled data for an exponential lateral diffusion (below)

with consequent increase in sensitivity. This new depth increment will termed a **LAYER.**

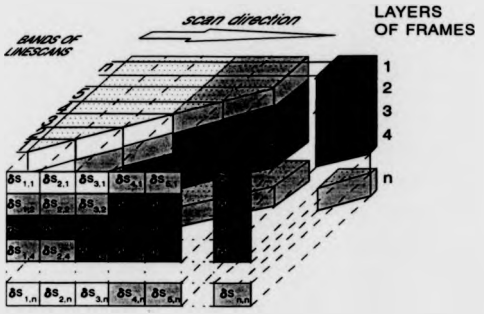

Figure 4.8 Schematic of profile reconstruction principle

Figure 4.8 shows the collection of data from a sectioned stripe, with the level of shading representing dopant concentration. Only one stripe need be considered when deducing the profile reconstruction methods as the measured signal is simply a multiple of that arising from one stripe. Each band, at a particular level, gives rise to a signal S, that is the integral of the signal from all of the voxels contained in its bounds. In general, the aim of all of the data reduction methods is to deduce the signal from each voxel, $\delta S_{i,j}$. With this information the profile may be reconstructed in two dimensions, as shown.

The data reduction techniques presented in this thesis are based on obtaining the δS values independently for each layer. Therefore only one layer need be considered when deducing a technique. When reconstructing the profile, the technique may then be applied to all other layers. The diagrams used represent a general layer containing the intersection point of the implant with the trench.

4.4.2 Calibration

It has been a criticism of many 2d analysis techniques that calibration is provided by comparing a depth profile through a narrow implanted structure with a depth profile from a planar implant, section 2.2.1.3. Although the implant window dimensions may be known very accurately, vertical and horizontal concentrations may vary as a function of window size (Okada et. al. 1990). This is shown diagrammatically in figure 4.9.

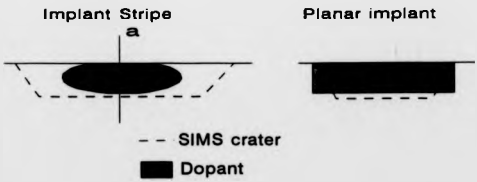

Figure 4.9 Comparison between profile of infinite planar implant and localised implant

In order to obtain a more accurate result the depth profile along the line (a) should be compared with that of the planar implant. In the technique presented, this is indeed possible. A depth profile is made through a structure implanted *at the same time* as the stripes. This structure will have received exactly the same processing and thus the vertical profile should be very similar. A slight error may occur with samples that have had a very long anneal, as a significant part of the dopant in the central region of the stripe may have been transported. However, this is unlikely for the relatively short diffusions used in modern processing.

A calibration coefficient, K, is obtained by comparison of the peak concentration of the planar implant with the signal arising from the central planar region of the stripe at a similar depth. The $\delta S_{i,j}$ values are then multiplied by K to convert them to concentration of ions cm^{-3}. A rapid check of the validity of this method is readily available by comparison of the two depth profile shapes.

4.4.3 Effect of angular misalignment

To permit correct data acquisition the beam must scan orthogonally across the direction of the original implanted stripes. If this is not the case, the lateral resolution will be degraded, as in figure 4.10.

If perfectly aligned, the structure is scanned by a band the FWHM beam diameter, d, wide. A misalignment of angle, α, results in the sampling of parts of the structure contained in width B, where

$$B = (L \tan \alpha) + d \qquad (4.2)$$

Where L is the sampled length.

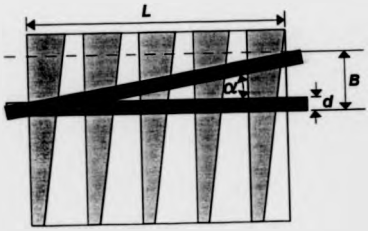

Figure 4.10 Effect of misaligned scan

The overall result of this process is to blur the resulting reconstructed profile, as the angled scan may be considered as being a band of width B, however, the step between bands is now less than one complete band. Thus wholly new information is recorded only when the start of the scan has moved distance B up the structure. This effect must be taken into account before data processing has begun, as the number of linescans, H, grouped into a band must obey the condition;

$$H > B / w \qquad (4.3)$$

Where w is the step size of the linescan data.

4.5 ALIGNMENT METHOD

As stated in the previous section, misalignment between the linescan direction and the structures results in loss of lateral resolution by effectively sampling with a larger beam. To achieve optimum sampling it is necessary to have a technique to align the sample and also a method of determining the misalignment.

The technique devised involves scanning the probe along a series of fine aluminium stripes, that are orthogonal to the original implant stripes, and monitoring the Al^+ secondary ion signal as a function of beam position. Figure 4.11 shows the technique with a misalignment of angle α. As α is reduced, so the wavelength of the signal, λ, increases.

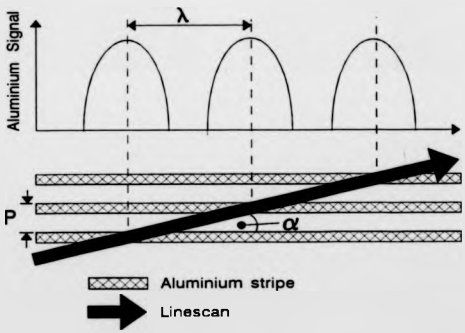

Figure 4.11 Diagram showing the alignment structure and its use

The structure also permits α to be calculated from,

$$\alpha = \tan^{-1} (P / \lambda) \qquad (4.4)$$

where P is the pitch of the structure.

The minimum measurable misalignment, α_{min}, occurs when the probe lies between the stripes, with the extinction of the Al^+ signal at both ends. Thus;

$$\alpha_{min} = \tan^{-1} \{(P - (T + d)) / L\} \qquad (4.5)$$

where L is the length of the scan

and T is the width of the aluminium stripe.

4.6 THE PARALLELOGRAM METHOD OF PROFILE RECONSTRUCTION

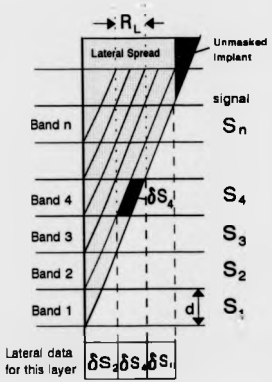

Figure 4.12 Schematic of parallelogram reconstruction technique

The parallelogram method relies on a simple construction of similar parallelograms. Figure 4.12 shows a general layer from a 2d analysis. In order to reconstruct the lateral distribution the δS values must be calculated. This is easily done as the signal arising from the voxel δS_4 may be calculated by subtracting the total signal for band 3, S_3, from the total signal for band 4, S_4. Thus the signal arising from any voxel may be found from;

$$\delta S_n = S_n - S_{(n-1)} \qquad (4.6)$$

In this case the minimum lateral resolution, R_L, is the total width of a parallelogram. Thus;

$$R_L = 2d \tan \Theta \qquad (4.7)$$

Thus data are spaced at distances of $R_L/2$

Although this method is inefficient in terms of use of the collected data, as R_L is twice the sampling distance, it provides a quick method of profile reconstruction that is very robust. The content of each voxel depends on the magnitude of the signal from two neighbouring bands only, thus there are no cumulative errors and the analysis may be started anywhere. Because of these strengths, this technique may be used as a check for the more sensitive techniques to be described.

4.7 BASIC TRIANGLE RECONSTRUCTION

This technique is an extension of the parallelogram method, with each parallelogram being subdivided into two equal area triangles. Figure 4.13 shows this method applied to a general layer.

The first scan to encounter dopant, band 1, gives rise to signal S_1. Thus, as this is the first voxel $\delta S_1 = S_1$. This signal is also detected in band 2, together with a signal from its complementary triangle. If the signal from both these triangles is assumed to be the of the same magnitude then, by subtraction of their sum from the signal arising from the whole of band 2, that due to the new voxel, δS_2, may be determined.

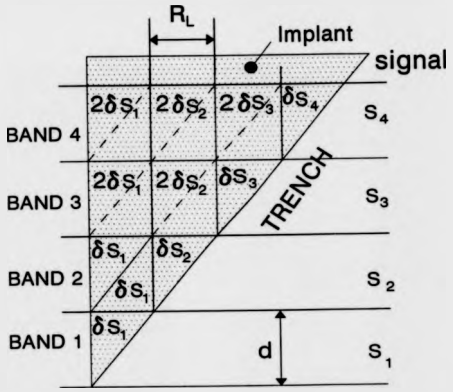

Figure 4.13 Schematic of Triangle reconstruction method

This process may be extended to calculate the signal from any voxel, δS_n, as,

$$\delta S_n = S_n - \sum_{i=1}^{n-1} 2\delta S_i \qquad (4.8)$$

The lateral resolution of this technique is double that of the parallelogram method, being,

$$R_L = d \tan\Theta \qquad (4.9)$$

4.8 ITERATIVE RECONSTRUCTION TECHNIQUE.

The basic triangle reconstruction technique assumes that there is no concentration gradient across each voxel, thus the elements containing $2\delta S_i$ may be considered. In reality, a concentration gradient exists across the element.

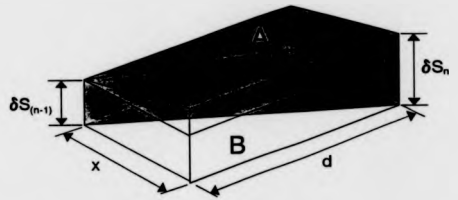

Figure 4.14 Diagram of typical triangle pair showing concentration gradient

Figure 4.14 shows a typical triangular element together with its complimentary element. The z direction is the concentration scale. Using the basic triangle technique A=B, however, this is clearly not the case. By simple geometric argument, and assuming a linear concentration gradient across each cell, the following may be found.

$$A = (\delta S_{(n-1)} xd / 2) + ((\delta S_n - \delta S_{(n-1)})\, xd / 2) / 3 \qquad (4.10)$$

and

$$B = (\delta S_{(n-1)} xd / 2) + 2\,((\delta S_n - \delta S_{(n-1)})\, xd / 2) / 3 \qquad (4.11)$$

the difference is therefore

$$((\delta S_n - \delta S_{(n-1)})\ xd\ /\ 2)\ /\ 3 \qquad (4.12)$$

The concentration gradient, g, across this element is

$$g = (\delta S_n - \delta S_{(n-1)})\ xd\ /\ 2 \qquad (4.13)$$

thus the total signal arising from the element A+B, $S_{(A+B)}$ is

$$S_{(A+B)} = 2A + g/3 \qquad (4.14)$$

For this correction factor to be applied to the complete reconstruction the gradient, g, across each element must first be determined.

An iterative method has been devised to make use of these principles. Initially, the basic triangle method is applied to enable the value of g across each element to be determined. Next, the same method is again used but this time a correction for concentration gradient is made by the addition of $g/3$ to each rectangular element pair. The new δS_n values, so obtained, permit new values of g to be calculated. These are then used to find further δS_n values. By working through this loop until convergence in the δS_n values are obtained, the inaccuracies of the original technique are removed. Thus for the jth pass equation 4.8 becomes

$$\delta S_n = S_n - \sum_{i=1}^{n-1} [2\delta S_i + (g_{i,(j-1)} / 3)] \qquad (4.15).$$

The basic triangle method of section 4.4.6 actually gives rise to oscillation about some intermediate value, as an overestimation in one band causes underestimation in the next. It must be noted that this iterative scheme makes only *positive* adjustments to the estimates of signal from each element and does not distinguish between over and under estimated cases. This results in the final values being superimposed upon a small constant signal originating from the underestimated cases. As calibration is made to a point on the distribution, and not by using a concentration per count constant directly transferred from a standard, the absolute signal level is not required, thus this offset is of no consequence to further processing.

As data from SIMS measurements are inherently noisy due to the random nature of emission, a certain amount of smoothing must be incorporated. The iterative method contains an amount of inbuilt smoothing that is sufficient for normal circumstances and is highly localised, thus rapid changes in concentration are not lost, as would be the case with a running average type of smoothing. Where a greater degree of smoothing is required, such as in regions of very low count rate, this may be added by calculating a running average through the g values. As increasing the stiffness of the distribution effectively reduces lateral resolution, the smoothing may be made selective by making it a function of signal, thereby employing it only where required.

Figure 4.15 compares both reconstruction techniques applied to an ideal linear diffusion giving noise free data. The upper plot shows the reconstructed data over its complete range. The lower plot details the deviation of the reconstructed data from the original values. It can be seen that the basic triangle method results in an oscillatory output with a peak-to-peak distance of 0.5 units. The relaxation method shows some bounce at the start but quickly settles to a steady value, at the mean level of the other technique.

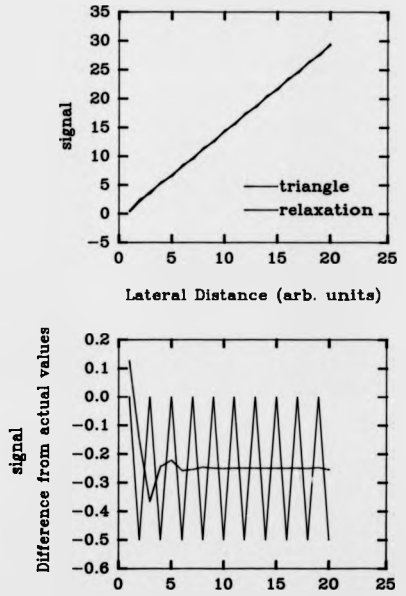

Figure 4.15 Plots showing comparison of triangle and relaxation method.

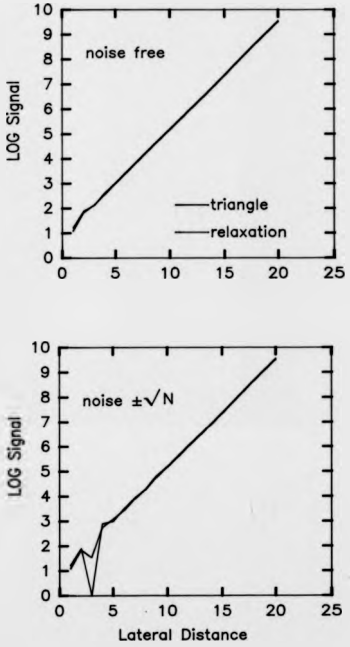

Figure 4.16 Plots showing the effect of noise on the triangle and relaxation methods.

Figure 4.16 compares the effect of the two techniques on an exponential data set. The upper plot shows a data set without noise. The relaxation method provides a slightly more accurate response than the basic triangle technique. The lower plot shows the effect of the two methods with noise added randomly as $\pm\sqrt{N}$, where N is the magnitude of the signal. Here the relaxation method displays a significant improvement over the basic method. This is most clearly seen in the reduction in magnitude of the trough near the origin where an error of two orders of magnitude has been reduced to less than half of one order. This has been accomplished *without* additional smoothing and shows the power of the technique in the regions of high noise that occur in the minima region of the 2d data.

4.9 SENSITIVITY

As previously mentioned, the sensitivity of a technique such as SIMS is a function of the amount of material in a voxel and how efficiently it can be detected.

The fractional atomic concentration F_X of an atomic species X in a measurement that consumes N sample atoms is given by:

$$F_x = n_x / N \Gamma_x \beta_x, \qquad (4.16)$$

where n_x is the number of ions of X detected,

Γ_x is the product of the collection, transmission and detection efficiencies for X.

β_x is the emission probability for the charge state ϕ detected.

Γ_x and θ_x are difficult to measure independently, however, their product τ_x, known as the useful yield, is easily measured for specific applications. Thus;

$$F_x = n_x / N\tau_x \qquad (4.17)$$

The elemental area analysed in the 2d technique is a triangle of area $(d^2 \tan\Theta)/2$. As the beam is scanned laterally, data are accumulated from m triangles, where m is the number of dopant stripes traversed. The effective analyte volume V is therefore;

$$V = m(d^2 \tan\Theta)\ \delta z\ /2, \qquad (4.18)$$

where δz is the depth of the analysed layer.

The total number of sample atoms N consumed per data point is

$$N = Dmd^2\ \delta z \tan\Theta\ /\ 2M_{ave} \qquad (4.19)$$

where D is the matrix density (mass per unit volume) of the matrix

and M_{ave} is the average kg mass of a matrix atom

Thus, from equation 4.17, the minimum fractional detectable impurity concentration $F_{x(min)}$ becomes;

$$F_{x(min)} = 2\ M_{ave}\ n_{x(min)}\ /\ Dm\delta z\tau_x\ d^2 \tan\Theta \qquad (4.20)$$

where $n_{x(min)}$ is the number of atoms of X that are required to be detected for a specific precision to be achieved. In an ideal case this is governed by the error in counting statistics, where $\sqrt{n}$ is the uncertainty. Thus for a precision of 33%,

10 ions must be detected; $n_{x(min)} = 10$. The minimum absolute impurity concentration detection level, $C_{x(min)}$, is therefore given by;

$$C_{x(min)} = 2\, n_{x(min)} / m\delta z \tau_x\, d^2 \tan\Theta$$

For the following easily achieved conditions; $\Theta = 0.08°$, $d = 40\ \mu m$, $\delta z = 10$ nm, $m = 200$, $\tau_x = 0.01$, $n_{x(min)} = 10$; a detection limit of 4.5×10^{14} atoms cm^{-3} may in principle be achieved. This will be coupled with a lateral resolution of approximately 50 nm.

4.10 INSTRUMENTAL REQUIREMENTS

In order to fully utilise the available material, the complete area of the square pad containing the structures must be within the gated area. As this is approximately 2 mm across, the scanned area needs to be a square of side at least 2.3 mm. This area must be covered by straight, accurately aligned, linescans with an even spacing and uniform scan rate. The instrument must, of course, be able to collect data in a gated linescan mode.

A task more demanding than scanning the primary beam is collecting the secondary ions from the sample surface. To permit the comparison of neighbouring linescans in the reconstruction algorithm, secondary ions must be collected from all over the sample with uniform efficiency.

In the EVA 2000 instrument these criteria are fulfilled by the use of a digital raster scanner and box style energy filter described in sections 3.5.2 and 3.5.4.

Provision must also be made for rotating the sample and for accurately assessing the probe conditions.

5.0 EXPERIMENTAL

5.1 INTRODUCTION

This chapter details the experimental work carried out during the development of the two dimensional profiling method, including sample fabrication and SIMS analysis. A full description is provided of the tests designed to assess the performance and limitations of the instrument and of the techniques used to align the sample with the linescan direction, as this is an important parameter limiting lateral resolution.

The development of the technique is broadly divided into three sections; these being representative of the three major generations of samples manufactured during its evolution.

5.2 Investigation of crater flatness

To realise the maximum possible depth resolution (limited only by mixing effects) it is necessary for the ion milled surface to be evenly eroded. The primary ion beam scanning, in the EVA 2000 instrument, is controlled by a high linearity digital raster scanner that has been shown to be capable of producing craters with a bottom flatness of better than 0.1%, across the typical depth profiling square of 400 μm side (Dowsett et. al. 1992). As the structures for two-dimensional analysis require scanning at least a 2 mm square, to permit the electronic gating to exclude edge effects yet still include the entire structure so as to collect maximum signal, it was felt prudent to investigate flatness over this area.

Initially, to test the flatness, a 2.5 mm side square crater was milled in a plain silicon sample and the crater measured with a surface profilometer. This

measurement showed the floor of the crater to be flat to better than 5 nm across the scanned region.

A more sensitive and realistic test was then made by depth profiling a thin boron "delta" structure with two crater sizes, 0.4 mm - normally used for depth profiling and 2 mm - that required for the special samples. Both were profiled with 4 keV primary ions. The results, shown in figure 5.1 display good agreement. If the erosion had been non-uniform across the larger crater, parts of the delta would have been exposed before others and the profile would have appeared broader.

This experiment confirms that there is no loss of depth resolution caused by the use of the larger scanned area; the depth resolution of the 2d data will thus be comparable with that obtained from a standard depth profile.

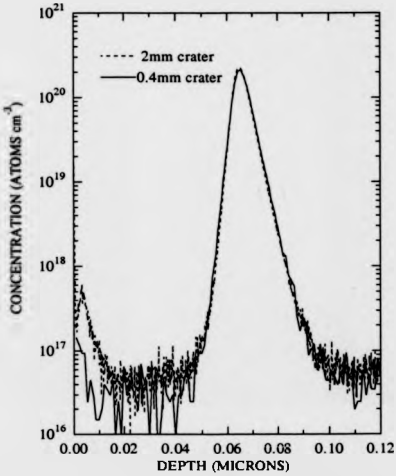

Boron delta 19/4, 1.6×10^{14} cm^{-2}. Profile conditions, 4keV O_2^+ primary ions normal incidence.

Figure 5.1 Comparison of depth profiles of a delta structure collected with different sized craters

5.3 INVESTIGATION OF SECONDARY ION EXTRACTION

5.3.1 Mapping the collection efficiency

The secondary ions are extracted from the sample surface by a modified Wittmaack "box" type energy filter (section 3.5.4). By varying the potential of the front screening electrode the field of view of the extraction optics may be changed, however, as the acceptance angle is increased the extraction efficiency falls (Longhurst, 1968). For normal depth profiling, where the crater is typically only 400 μm across, the energy filter is tuned to pass maximum signal at the centre of the scanned area and show little degradation towards the crater edges. Also, provided that the efficiency remains constant throughout the analysis, collection biased towards the centre of the crater does not affect the profiling of planar samples. In fact, it may even help in the reduction of background signals by providing some element of optical gating. Published extraction efficiency data, for this type of filter, are shown in figure 5.2 (Wittmaack et al 1982). Here, the increased extraction efficiency of the screened system, having a half width of approximately 0.75 mm, can be seen. Also shown is a plot of the unscreened case (screen at extraction plate potential), giving rise to a somewhat larger field of view.

The special samples to be used for two-dimensional analysis require ions to be extracted with similar efficiency over the complete 2 mm side square area. Variation of extraction efficiency in the direction parallel to the original implanted stripes leads to an apparent incomplete sampling and thus, with lower counts recorded, causes degradation in analytical precision. If collection efficiency varies along the length of the stripes, then adjacent linescans may not be compared, hence the profile reconstruction methods discussed in chapter 4 are invalid.

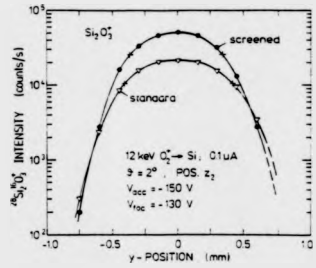

Figure 5.2 The extraction efficiency diagram determined by Wittmaack (1982) for the Wittmaack "box" style energy filter

To investigate variations in collection efficiency a large piece of silicon wafer was mounted and the $^{28}Si^{16}O^+$ secondary ion monitored using an analogue ratemeter. As a molecular ion has a smaller energy spread than an atomic ion, its signal is far more sensitive to variations in the extraction fields, and is therefore ideal for extraction efficiency investigations. Initially the energy filter was tuned to pass maximum signal, as in a depth profile. The primary beam (O_2^+, 8 keV, 200 nA) was then manually stepped across a region of approximately 2.5 mm square. At each step site, within the region, the beam was held stationary until equilibrium was achieved (approximately 15 seconds). The ratemeter reading was then recorded and the beam moved to the next site. In this way the collection efficiency could be mapped in two directions.

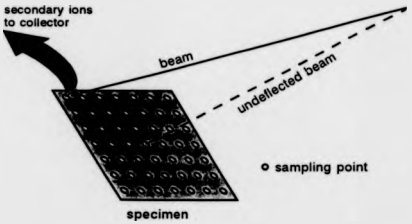

Figure 5.3 Method of collecting extraction efficiency maps

The two maps presented in this thesis show a 2.5 mm side square area. The X and Y axis are labelled from the bottom left hand corner of the analysed region. The position of the undeviated beam is at (1.25, 1.25). The Z axis represents the count rate at a particular position as a percentage of the maximum count rate found on the map.

Figure 5.4 shows the collection efficiency as a function of position for a standard depth profiling condition. Generally, a crater of side 400 μm is sputtered

when depth profiling with the EVA 2000 instrument. Ions are collected from a centrally positioned square gate of side 125 μm. Thus the peak of secondary ion collection efficiency adequately immerses the analysed region. In the case of an optically gated instrument this peak would be much thinner and more pronounced so as to extract ions from only the central region of the crater. The overall shape of the linescan through the peak is in good agreement with that determined by Wittmaack for a similar energy filter used on the A-DIDA instrument, shown in figure 5.2.

Figure 5.5 shows the collection efficiency map obtained for the case where the screening electrode voltage has been increased with respect to the negative extraction potential floating the whole energy filter (ie the extractor potential is now nearer that of the target). The Z-axis once again shows the collection efficiency as a percentage of the maximum count rate *for this map*. However, in reality, the maximum of this figure is *2.5 times less* than that of figure 5.4.

The effect of increasing the screen voltage has been to reduce the peak rather than raise the level of the surrounding area. The surface of the plateau is roughly square in shape, the corners lying along the direction of the axis. This shape is directly attributable to the two condenser plate sets making up the energy filter, with the diagonals of the plateau being in the same direction as the plates.

The efficiency is more linear in the direction of the Y-axis, consequently this will be used in the critical direction (the direction of the stripes) when analysing the 2d samples. For 2d sample analysis, the informative region of the sample should be positioned under the central 1.4 mm plateau so as to permit accurate comparison of the signals from adjacent scans.

Prior to the attempts to analyse the 2d samples, the collection of complete maps was unnecessary. To satisfactorily tune the secondary column, the optics

Secondary Ion Collection Efficiency
Tuned for depth profile analysis
Signal % of max.
25 50 75 100
2.5
2.0
1.5
1.0
0.5
0.0
Distance from bottom / mm
0.0
0.5
1.0
1.5
2.0
Distance from top / mm

Figure 5.4

Secondary Ion Collection Efficiency
Tuned for 2D analysis

Figure 5.5

were first set for the most efficient extraction of boron from the central region - the peaked condition normally used for depth profiling. The mass spectrometer was tuned to the silicon-30 peak (with the same target bias applied) and a 2.5 mm raster started. By observing the silicon-30 image, displayed on the instrument oscilloscope, and adjusting the extraction controls towards the settings known to provide a flat response, the central high efficiency region was extended. This is a successive approximation process owing to the multidimensional nature of the extraction optics. When the oscilloscope screen showed uniform brightness, a few linescans were made across the width of the region to obtain an objective view of the tuning. Finally, count-rate data were collected for 3 or 4 frames to ensure that the collection efficiency had not been over suppressed.

5.3.2 Recovery of extraction linearity

Although the previous investigation permitted a relatively flat extraction efficiency to be achieved over the 2 mm area to be analysed, a certain amount of non-linear response must be expected, especially at the edges of the area. Multiplication of the data by the inverse of a boron collection efficiency map, pixel for pixel, would fully correct for such effects; however, this would result in very poor statistical precision as regions with low count rates (and therefore high uncertainties) would be multiplied by points on the map determined themselves by relatively low count rates, thus compounding the errors. Using linescan data (integrating pixels along a complete linescan) collected from a sample containing a uniform concentration of the required species would also be impractical as significant deviations in collection efficiency are observed when the sample holder is moved. This is because the sample stage itself causes some shaping of the extraction field, thus a once and for all calibration is invalid. If the analysis is not

to be hampered by a time consuming and difficult pre-analysis mapping, another method of overcoming the non-linearities must be sought.

As standard procedure, a silicon matrix channel is always monitored together with the impurity channel. As the impurity is very dilute, the matrix channel should be of constant value.

An investigation was conducted to ascertain whether it was possible to overcome the non-linearity of the extraction efficiency by normalising the matrix channel to its maximum value. The factor by which each line of the matrix frame had to be multiplied to achieve this was then applied to the impurity signal of the same line from the subsequent frame. The extraction system was tuned to a set of conditions between those of figure 5.4 and 5.5, so as to introduce a non-linear response. A 3 mm square crater was sputtered in a 30 keV 10^{16} cm^{-2} implanted boron standard, and the secondary ions collected in linescan mode. Thus the count rate for both impurity and matrix should be constant, and any variations due to changes in collection efficiency.

Figure 5.6 shows the effect of the recovery process. The upper graph shows the variation of the signal about its mean value (100%) and the lower graph the absolute count rate data.

The raw boron channel shows a steady decline with increasing linescan number (moving towards the top of the sample holder), whereas the silicon signal shows rapid gradient changes. When the normalisation method is applied, there is a good recovery of the constant boron signal up to frame 100, after which a large positive error occurs at the same point as the rapid gradient change in the silicon signal. This is due the differences in extraction efficiency between the boron and silicon secondary ions. This variation is attributable to the fact that the peak emission energy of each species and the most probable take-off angle is different

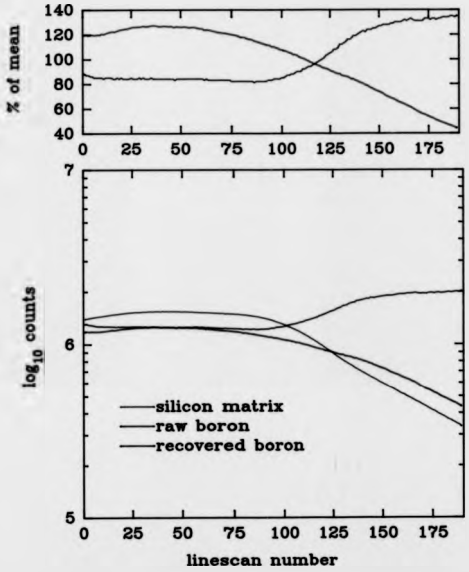

Study of data recovery by matrix channel normalization

Figure 5.6

and that the extraction optics is filtering in *both* these parameters. Despite this, the overall effect has been to reduce the *total* spread from 85% to less than 50%.

In an actual 2d analysis, data collection over 2 mm is required. This represents 125 frames on figure 5.6. Even with the rather peaky tuning used for this investigation a linearity of better than 20% may be achieved if it is arranged for the data to be collected from the region of the first 125 frames. This is possible as the two condenser plate pairs of the energy filter may be used to steer the collection area over the sample surface. If two constraints are placed on the data;

(i) the data is restricted to regions where the matrix channel varies by less than 20 %,

(ii) there are no sharp gradient changes,

then the recovered signal shows a spread of less than 5%. Thus, bearing these conditions in mind whilst tuning the instrument, the normalisation data recovery technique may be applied with reasonable confidence.

For actual 2d analysis, linearity may be better than anticipated as the region of greatest interest is somewhat smaller than half of the total sample area.

5.4 Assessment of probe quality

To permit accurate profile reconstruction the probe should have a gaussian current density evenly distributed about a central maximum. Before analysis of the structure could commence, the primary ion column was adjusted to provide a circular probe of approximately 50 μm FWHM at an accelerating potential of 6 keV and a current of 200 nA. The focus was verified by scanning the beam across a fine wire and monitoring the current on an oscilloscope, thus the current density profile of the probe could be observed and focussing corrections be objectively made with their results being apparent in real time. As no stigmator is fitted to the

Plate 5.1 Cu^+ secondary ion image of copper grid.

EVA 2000 instrument, any observed astigmatism must be corrected for by adjustments in beam steering.

This has the advantage of preventing stigmator controls from being used to correct for poor column alignment and allowing other aberrations to go unchecked. For example, current may be lost to a large, low current density, halo about the beam centre. This will give rise to a significant signal and reduce the signal-to-noise ratio.

Further confirmation of beam quality is obtained by imaging a copper grid with 100 μm holes and 30 μm bars (200 mesh). Plate 5.1 shows a Cu^+ ion image of the copper grid displayed on the analogue storage oscilloscope. The vertical bars in this image are somewhat weaker than those running horizontally, indicating astigmatism in the X-direction. The image also shows that the extraction is linear across the size of the scan (approximately 0.5 mm) as it is of even brightness.

A final assessment was made by milling a pit in silicon and observing the beam halo. This is a very sensitive technique with currents of below 0.1% of the peak quickly creating enough of an altered layer to be visible.

Post analysis, the beam width was determined by tracking the stylus of a surface profilometer across a sputtered line in the silicon surface. By creating this line using a repeatedly overscanned linescan, blurring due to sample vibration, where the effective wavelength traced on the sample is large compared with the stylus tip diameter, may be taken into account. Measurement was made before and after analysis to asses probe degradation during the long analysis time. The probe always becomes slightly enlarged as the focussing conditions are optimised before analysis and thus variation of any parameter with time causes defocussing.

Figures 5.7 and 5.8 demonstrate the measurement of effective beam diameter using surface profilometry.

The major cause of variation in probe quality with time is the aging of the Penning discharge. As oxide is deposited on the anode, and as the cathode pin is eroded, the running voltage increases, thereby causing a mismatch into the extraction optics. From experience, the most stable period lasts for approximately ten days, one week after the discharge components have been replaced. Where possible all extended running was completed within this period. The typical lifetime of the source is five weeks.

The source was redesigned by the author to permit easier refurbishment. This allowed the components to be replaced as soon as instability was noticed, thereby ensuring consistent data collection. These modifications are presented in chapter 7.

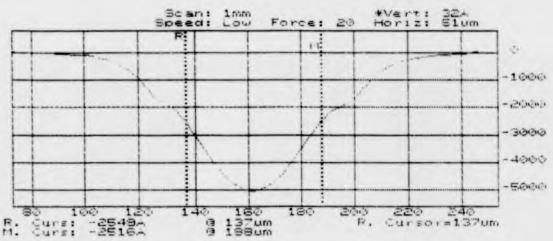

Figure 5.7 Surface profile across a sputtered line in silicon showing the presence of a halo about the probe. FWHM (between cursors = 51 μm.

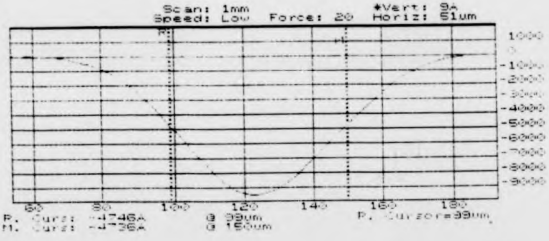

Figure 5.8 Surface profile across sputtered line in silicon showing "clean" probe (X-axis scale magnified in comparison to figure 5.7). FWHM = 51 μm.

5.5 INITIAL SAMPLE FABRICATION

An initial sample set was fabricated to allow evaluation of the data produced from a wide range of stripe angles, and to highlight constraints of both instrument and sample. In order to provide this in a cost effective way, a single electron beam drawn mask was designed. This allowed definition of both the implant stripes and the trenches to be cut across them. A diagram of the mask is shown in figure 5.9, the angles having been exaggerated for clarity. Each site is a 1.8 mm side square containing 300, 3 μm wide, stripes on a 6 μm pitch. The angles chosen were 0.2°, 0.08° and 0.03°, which would effectively permit a correctly aligned 50 μm diameter probe to produce lateral resolutions of 175 nm, 70 nm and 25 nm respectively.

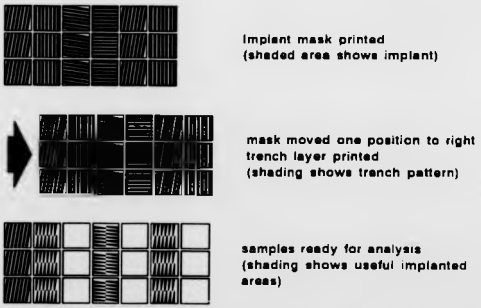

Figure 5.9 Diagram showing the use of a single mask to produce the structures

Both horizontal and vertical stripes were included in the design so that effects of implant angle and crystal direction could be included in future analysis.

The samples were fabricated on three inch diameter, [100] oriented, silicon substrates. Firstly a 1 μm thick thermal oxide was grown across the entire wafer and then coated with photoresist. Using a stepper type mask aligner the mask pattern was exposed at a number of locations across the wafer and the resist developed. This pattern was used to open windows in the oxide coating so as to define the striped regions to be implanted. The wafer was then implanted with 80 keV boron ions at a dose of 5×10^{15} ions cm^{-2}. A second implant, 30 keV arsenic at a dose of 2×10^{15} ions cm^{-2}, was also made in order to permit location of the mask edge in the reconstructed profile. The wafers were next subject to a variety of anneal schedules similar to those used in standard integrated circuit fabrication.

Boron-11 was chosen as the dopant species as not only is it the most widely used p-type dopant, and therefore of major interest, but it is also easily detected in the quadrupole mass spectrometer, as there is no molecular ion interference signal and it is associated with good dynamic range in SIMS depth profiling.

After implantation, the oxide masking layer was etched off and a fresh layer deposited at low temperature, so as not to disturb the profile shape. The mask pattern was once again transferred to the oxide layer, however, this time the exposure was made with the pattern offset one site width to the right, causing the angled stripes to fall across the previously implanted horizontal and vertical ones. After opening the windows in the layer, the substrate received an anisotropic plasma etch, producing vertically walled, flat bottomed, trenches approximately 1 μm deep. The oxide was removed, leaving the implanted stripes effectively sectioned at a small angle in the vertical plane.

The wafers were then diced by cleavage ready to be mounted in the SIMS instrument.

5.6 SAMPLE - LINESCAN ALIGNMENT

As discussed in chapter 4 it is necessary to accurately align the scan direction with the sample, otherwise degradation of lateral resolution will result. An effect of oxygen bombardment of silicon is the generation of an altered layer that has distinctly different optical properties. This allows even a relatively low ion dose, a lot less than that required to reach equilibrium, to be seen; thus a single linescan is highly visible. In the EVA 2000 instrument the sample may be viewed by an off axis telescope with a field of view of approximately 20 mm. The 2d samples were mounted as blocks of 21 pads (ie one complete mask field) onto a sample holder.

The primary beam was then scanned near to one of the sites inappropriate for 2d analysis and the sample manipulated until the visible scanned line accurately occluded one edge of the pad. The rotary axis of the manipulator was then disengaged and the sample traversed so that a relatively deep sputtered line could be placed about 200 μm from the edge of another site. Post analysis this feature permits an accurate angular measurement to be obtained by measuring the distance between the line and the site at both ends, by either surface profilometry or microscopy.

Once the rotary axis is disengaged and the alignment bar milled, any site on the sample may be analysed without further adjustment.

5.7 LOCATION AND SIZE OF THE GATED AREA

The digital raster scanner fitted to EVA 2000 provides a 256 line raster with a central sampled area (the electronic gate) of up to 198 lines, shown schematically in figure 5.10.

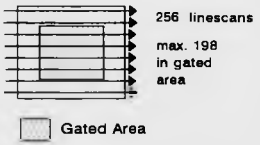

Figure 5.10 Diagram of the electronic gating of EVA 2000

To extract the maximum possible signal from the sample, the gate should be coincident with the striped region and an area of at least four beam widths be left around the gate to prevent material sputtered from the sloping edges of the crater from being collected.

To increase the lateral resolution, the use of a fine probe is desired. However to create a flat floored crater the adjacent linescans must overlap by at least 66% (Wittmaack, 1977) and to be safe an overlap of 75% is advisable. Thus to fulfil these requirements the probe should not be less than 40 μm in diameter (FWHM) if the full area of the sample is to be used.

5.8 PRELIMINARY ANALYSIS

The first set of samples delivered from Plessey Caswell had received processing as described in section 5.5. A sample that had received no anneal was chosen for the first analysis and mounted and aligned as previously described. Linescan data was collected using LINAC a basic linescan acquisition program written by Dowsett.

It is usual to count secondary ions from both the impurity and matrix during a SIMS analysis, and in this case the matrix signal was required for later processing. As the difference in concentration between the two materials may be greater than 10^4, the signal from the matrix must be suppressed to prevent saturation (and possible damage) to the detector. With silicon, it is usual to collect $^{30}Si^+$ ions, the minor isotope, and offset the target bias so that only ions from the high energy tail of the distribution are detected. This procedure results in a slight shifting of the primary beam position between channels. To prevent this shift, ions from both materials were collected at the same target potential. The matrix signal was reduced by tuning the mass spectrometer to give higher mass resolution (and a consequently lower signal) with increasing mass (see figure 3.3 scan b).

5.9 ANALYSIS OF TOPOGRAPHY

The original samples had a castillated cross section. Under ion bombardment modification of this shape may be expected, so observation of the structure in cross section was required.

The samples were cleaved across the stripe direction and mounted on 45° stubs for SEM analysis. By tilting the SEM stage a further 45°, the true cross sectional profile could be examined.

The sputtered surface consists of a layer of SiO_2 approximately 20 nm thick (the altered layer). Under electron irradiation this thin layer charges significantly and results in an over bright surface from which the features are obscured. This problem is compounded by glancing incidence electrons being reflected from the vertical surface and directed towards the detector.

The charging problem was only partly reduced by gold coating and to obtain sharp, even brightness, images it was found necessary to remove the altered layer by etching in HF for a few seconds immediately prior to coating. By moving the sample slightly off the vertical the problem of reflection was cured, permitting high magnification images to be obtained.

Plate 5.2(a) shows an SEM view of the cleaved cross section of an uneroded structure, displaying the vertical walls obtained from anisotropic plasma etching. Plate 5.2(b) shows a similar cross section after ion bombardment. The exposed corners of the castillated structure have suffered much greater erosion than the planar top surface. This is because the sputter yield is greatest at approximately 70° to the incident beam. Therefore an angled face develops at the corner and subsequent erosion of this face rapidly consumes the structure. The material ejected from this surface has a low ion yield (typically three orders of magnitude below that from the normally incident surface) and is therefore lost to the analysis. In this way, most of the implant was removed by sideways erosion.

The topographical evolution of the structure was investigated using 8 keV O_2^+ ions. By eroding a series of such samples, and imaging the cross section, the progression of the erosion was charted, as in plate 5.3. Plate 5.3(a) shows the cross section after a dose of 7×10^{17} ions cm^{-2}. The trough forming to the left of each projection is due to the fact that the analysing beam is slightly off normal incidence. Ions, coming from left of the surface normal, are reflected by glancing collisions with the vertical surface and thus loose most of their energy by collision

with the floor, adding to the sputtering effect of directly impinging ions; this process is shown diagrammatically in figure 5.11

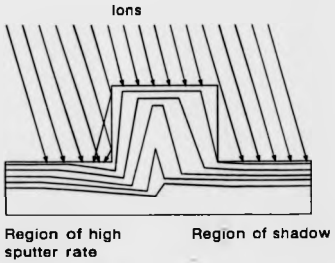

Figure 5.11 Diagram showing the [illegible] process causing trough formation

Plate 5.3(b) shows the effect of continued bombardment with the erosion in the vertical direction being negligible to that horizontally. The projecting surface has very nearly been removed. Plate 5.3(c) shows the near planar surface resulting after a total dose of 7×10^{18} ions cm^{-2} with the only topography being due to the reflection sputtering process.

The first experiments were conducted with linescans in the X direction and, as in plate 5.2(b), showed no trough formation. The topographical evolution study used linescans in the Y direction. Thus it was easily demonstrated that the beam was not normal in the Y direction only. Dismantling of the instrument revealed that the final neutral dump bend angle, ideally 4°, was in fact set too great, and on

re-assembly this was corrected. Thus by bombardment of a castillated structure, it is possible to determine the accuracy of normal incidence.

Plate 5.2(a) Cross section SEM of 1.5 μm wide castillation before bombardment.

Plate 5.2(b) Similar castillation after $1x10^{18}$ ions cm^{-2}

Plate 5.3(a) Structure after $7x10^{17}$ ions cm^{-2}

Plate 5.3(b) Structure after $2x10^{18}$ ions cm^{-2}.

Plate 5.3(c) Structure after 7×10^{18} ions cm^{-2}

5.10 SECOND GENERATION SAMPLES

5.10.1 Fabrication

Initial analysis of the samples described in section 5.5 suggested that if useful data was to be collected, the preferential sputtering occurring at the top of the trench walls should be prevented. An obvious remedy to this situation is to fill the trenches, leaving the whole area planar.

The material used to planarize the structure must have a sputter rate as close as possible to that of silicon so that the structure remains planar throughout analysis. A further property the filling material must posses is electrical conductivity. If an insulator was used, local charging effects would cause microscopic deflections in the primary ion trajectories leading to the creation of macroscopic topography. This effectively rules out SiO_2 for use as a filling.

At about the same time as the filling was required a selective silicon epitaxy process was being developed at Plessey Caswell. In this process selectivity of growth is achieved by opening windows in a masking oxide to expose the underlying crystal. The masked wafer is then introduced into a chemical vapour deposition (CVD) reactor with the substrate at a suitable temperature to permit a high atomic mobility on the oxide but allow growth to occur on the crystal.

A second batch of 2d samples was commissioned, this time on five inch diameter, [100] oriented, silicon substrates.

Unlike the structures described in 5.5 the oxide used to mask the trench etch was left in place, to permit selective epitaxial silicon to be grown in the trenches. As it was critical to ensure an even growth rising from the trench floor, the walls were required to be protected. This was accomplished by growing a 4 nm oxide,

the thinnest that would allow reliable growth selectivity, over the whole structure. The oxide covering the trench floor was removed by anisotropic plasma etching.

By carefully calibrating the growth rate, it was possible to fill the trenches to within 20 nm of the top of the walls. However, the growth rate was not uniform across the whole wafer. Where the growth exceeded the surface level, localised three dimensional growth took place. This resulted in the appearance of crystallites approximately 2 μm across decorating the top edges. The density of crystallites was greatest in the regions of high boron concentration, the reason for this is not understood but may be the result of lattice damage during implantation. This effect was so gross that only two sample groups were suitable for profiling on the single wafer subjected to this processing.

Figure 5.12 shows a diagram of the finished sample structure in cross section.

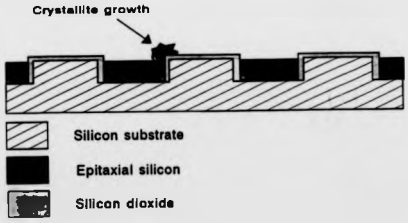

Figure 5.12 Diagram of epitaxially filled sample

5.10.2 Investigation of topography

The original cross section of the samples is shown in plate 5.4(a). The sidewall oxide has been etched out to show the interface more clearly.

Plate 5.4(b) shows a similar sample after bombardment with O_2^+ ions at a dose of 5×10^{17} ions cm^{-2}. The thin sidewall oxide has been more rapidly removed than the surrounding silicon, leading to the opening of a crack along the interface. The crack has not been uniformly eroded, but shows even exposure for 10 - 20 μm lengths separated by material bridging the gap (this is distorted in the photograph owing to the foreshortening effect of the angle).

After this topography was first observed, the density of the projecting microcrystallites was noted before bombardment and later compared with the density of the bridges. A good correlation was found between these quantities, and a mechanism for their formation has been proposed.

Figure 5.13 shows the stages in topographical evolution of the filled structures. Initially the structure is resistant to attack with the oxide protecting the corners and the planar structure eroding evenly over the whole area. The microcrystallites are rapidly planarized at this stage but a flatter projection remains, ultimately providing very good protection. As the erosion progresses, the higher sputter rate of the oxide begins to produce noticeable groove formation, thus exposing the corners of both the original structure and the filling material. The corners are then subject to the high erosion rates experienced with the first sample set, thus the grooves develop rapidly. The microcrystallites, being more resistant than the surrounding material cause the bridge structure to develop. Continued erosion results in a similar topography to that previously seen. However, as the structure is no longer effectively two dimensional, the bridge structures permitting

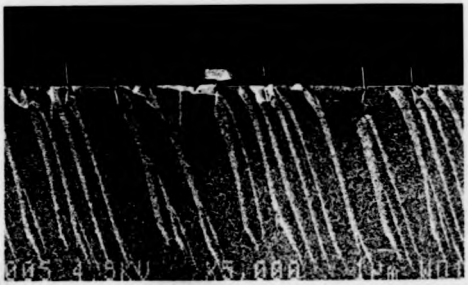

Plate 5.4(a) Cross section of filled structure

(striated area = cleaved surface - normal to view, uniform dark region = top surface - in direction of view)

Plate 5.4(b) Similar view after erosion

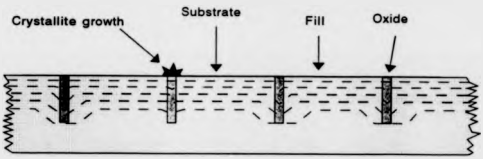

Figure 5.13 Evolution of filled topography

material removal along the direction of the stripes, the final surface is locally pitted and irregular, although the stripe pattern is visible on a macroscopic scale.

5.11 IMPROVED FILLING TECHNIQUES

5.11.1 Method of assessing filling techniques

As the selective epitaxial silicon fill was only partially successful a number of alternatives were tested on purely "mechanical" samples. Using an old mask consisting of hundreds of stripes 1 mm long and having widths between 1 μm and 15 μm, a trench pattern was created on a silicon substrate. Each filling technique could then be attempted on the structure. The filled sample was then subjected to ion bombardment followed by cross sectional SEM study.

The major failing of the selective fill was the thin sidewall oxide which, even at only 4 nm, had permitted the top corner to become exposed, resulting in excessive material removal. Thus, to overcome this problem, the filling material must be in intimate contact with the sidewall.

5.11.2 Polysilicon overfilling with post deposition polish

The plasma deposition of polycrystalline silicon (polysilicon) is a well characterized and routine fabrication step in integrated circuit production. When applied to a stepped structure, the deposit is not wholly conformal, tending to fill inside corners. An attempt was made to use this effect to planarize the trench structures. 5 μm of polysilicon was deposited over the structure (some 8 hours deposition time). The deposition of such a thick layer (typically layers are only a few hundred nanometres thick) permitted the growth of large crystallites resulting in a surface roughness of the order of one micron. The trench positions were just discernible through the thick layer indicating that the underlaying topography had not been totally removed. The structure is shown in cross section in plate 5.5.

As a remedy to the problem of large crystallite roughness it was proposed that a layer of about 2.5 μm would sufficiently fill the trenches and that the overfill could be mechanically polished off afterwards. However, it was found that adequate parallelicity to the original surface could not be achieved with such a thick layer. To maintain a depth resolution of 10 nm requires the polished surface to be at an angle of less than 5 μRadians to the original substrate surface. The resulting surface must also be scratch free. Because of these severe constraints it was felt that polishing could not be used to planarize the overfilled structure.

5.11.3 Amorphous silicon corner filling

Amorphous silicon deposited by CVD preferentially fills internal corners (Pearson, 1992). Trenches on test wafers were subject to a variety of deposition conditions, the plasma etch protecting oxide being retained across the top of the castillations. Cross sectional study confirmed that it was possible to place fillets in

the internal corners of the trenches such that, when the oxide layer was removed, a near horizontal surface would be presented to the analysing beam in the region immediately around peaks of the castillations. Figure 5.14 shows the ideal resulting topography.

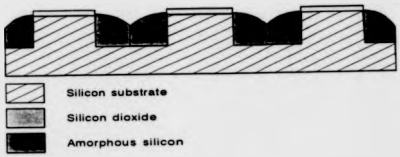

Figure 5.14 Ideal filling with amorphous silicon

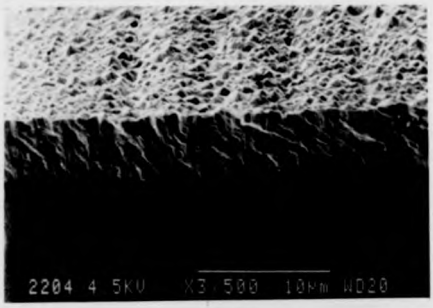

Plate 5.5 SEM micrograph showing the rough surface resulting from a 5 μm polysilicon deposition

5.12 THIRD GENERATION SAMPLES

5.12.1 Overview

The third generation of 2d samples were the last to be manufactured at the Caswell site. In close collaboration with the author a new multilayer mask was designed to incorporate many of the ideas formulated from the analysis of the previous 2d samples and the investigations of filling processes. Area on the mask was shared between structures used for the anodic carrier profiling work of Hill and Pearson (described in section 2.2.2.1) and the 2d SIMS work described in this thesis. The mask was shared in this way not only to permit more economic use of mask area to be made, but as the samples would be fabricated simultaneously, to allow direct comparison between the carrier and dopant profiles.

The major differences between the patterning of this generation of samples and that of the first two sets, are the inclusion of structures permitting more accurate alignment and the use of only one trench angle.

5.12.2 Alignment method

Inaccurate alignment of the structures and the linescan direction poses a serious problem, as it effectively increases the probe size and therefore restricts the lateral resolution.

An initial study was made to verify the practicality of the method proposed in chapter 4. A set of accurately drawn lines were photographed onto 35 mm high contrast film. The film was used to contact print the line pattern onto a photoresist coated aluminised silicon wafer. Using this crude method, lines 45 μm wide, on a 100 μm pitch, and 3 mm long were written.

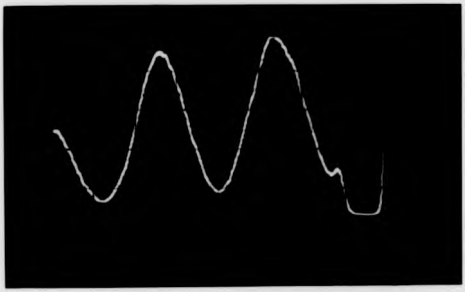

Plate 5.6 Al+ signal from alignment stripes (distance between peaks = 960 μm

Using a 50 μm FWHM spot full 2.5 mm long linescans were made of the structure. Alignment was readily achieved to 0.2° (10 μm in 2500 μm). Plate 5.6 shows the signal resulting from a misalignment of 5° (P=90 μm, λ=960 μm). Further improvement could be obtained by permitting the now near parallel linescan to partially overlap the stripe. Under these conditions the alignment procedure is to aim for a constant signal along the length of the stripe; indicating that the probe is overlapping the stripe by the same amount along its whole length..

The centre of rotation of the manipulator fitted to EVA 2000 is approximately 100 mm from the analysis position. The disadvantage of this arrangement is that rotary movement causes severe lateral shifting of the sample. Thus during angular alignment it is not usually possible to observe the signal peaks parting as the angle reduces. However, on returning to the stripes, a quick measurement may be taken and a further correction made. As the aligned state is reached, backlash in the drive system prevents calculated adjustments and a trial and error approach must be taken Despite this seemingly inefficient final step, the optimum position is reached surprisingly quickly.

Once aligned, the rotary drive is disengaged ensuring only translational motion may be applied.

5.12.3 Alignment structures on the mask

Owing to both the expense of mask design and the imminent closure of the Plessey silicon fabrication facility at Caswell, it was decided that the third generation of samples should anticipate future developments such as the availability of micron spot size reactive ion guns. To this end, the alignment stripes were designed with widths varying from 50 μm down to 2 μm with a similar change in pitch. As space was at a premium, the thicker bars were made up by grouping

thinner ones. This provides for very efficient alignment as the same area of the sample may be used for successfully fine adjustments without having to relocate to find thinner stripes.

5.12.4 Mask layout

Three mask layers were available for fabrication. This meant that it was now unnecessary to step the mask, hence all sites could be made useful. The first layer was used to define the implanted stripes, the second the trenches and the third the alignment stripes. A standard mask was used prior to processing to define alignment marks for the Cannon stepper used for printing the patterns. The alignment accuracy of this machine is better than 0.5 μm over 30 mm (Pearson 1992), leading to the possibility of up to 0.001° angular misalignment.

As only one depth profile need be done to calibrate a two dimensional profile it is unnecessary to include large areas of planar implants and a 1 mm side square region was placed at the centre of the field, as in figure 5.15. The 2 mm long alignment stripes were positioned radiating out from the sides of the central planar region, with the 2 mm side square 2d sample pads placed in the space remaining in each quadrant. The design is deliberately compact to ensure that angular alignment errors and secondary ion collection efficiency variations, resulting from translation of the sample holder, are kept to a minimum.

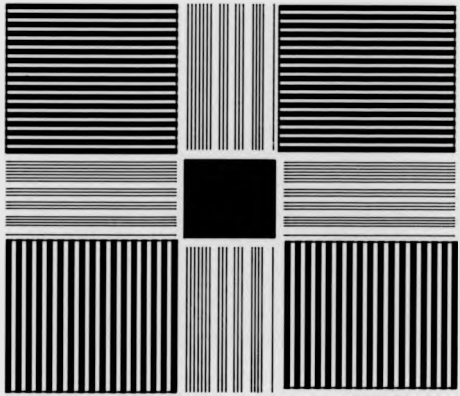

Mask layout for third generation 2d samples

Figure 5.15

5.12.5 Geometry of the sample

Analyses of the early samples had shown the optimum sectioning angle to be around 0.08°. An angle of 0.1° was therefore standardized upon for all of the pads in the new sample set.

A very important aspect of the analysis is location of the data minimum. The largest probe expected to be used on the samples was 50 μm, thus it must be ensured that a large enough gap exists between the edges of the implanted region, under conditions of maximum likely lateral spread, to permit a linescan of undoped silicon to be recorded. This parameter is controlled by the width of the implant window and the pitch of the structure. However, making an oversize gap leads to a need for increasing the pitch distance, lowering the total number of stripes, with consequent loss of sensitivity. Also, for calibration, a linescan including the planar region must be included.

As it is usual to implant at an angle to the wafer, so as to reduce channelling effects, orthogonal implant stripe directions must be included on the mask. Also, to obtain the fullest information, both sides of the implanted profile should be accessible either side of the minimum.

The final geometry, shown in figure 5.16, includes a region of background signal, a region of planar implant, and both sides of the implant.

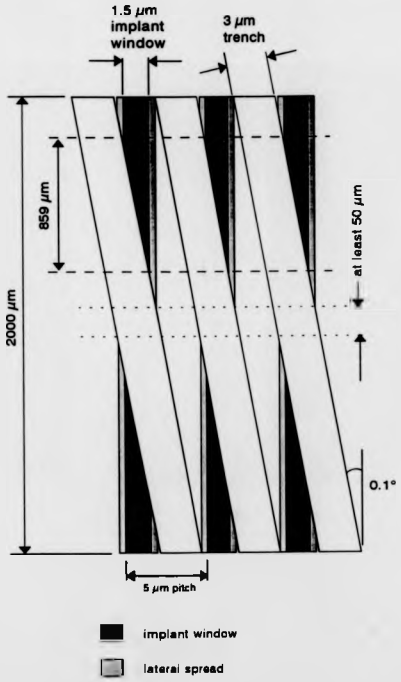

Figure 5.16 Sample geometry of the third generation of 2d samples

5.12.6 Trench filling

5.12.6.1 Overview

Two methods of trench filling were applied to these samples. Half of the set were treated with a variation of the amorphous filling technique of section 5.11.3, and the other half with a modified selective epitaxial method. Due to the imminent closure of the fabrication facility it was not possible to fully characterize both filling methods before manufacture. Thus, because of the resulting planar structure, it was felt that the epitaxially filled samples would be more likely to survive analysis than those filled with amorphous silicon. This was reflected in the implant and anneal conditions with the wider range of dopants contained in the epitaxially filled samples. Table 5.1 shows the conditions used for this batch of samples.

	Wafer number											
Process	1	2	3	4	5	6	7	8	9	10	11	12
Amorphous Filling												
Expitaxial Filling												
Boron 5E14 20 keV												
Boron 5E15 20 keV												
Arsenic 1E16 120 keV												
No anneal												
950 C 30 seconds												
950 C 300 seconds												

Table 5.1 The processing received by the twelve wafers making up the third generation of 2d samples.

5.12.6.2 Epitaxial filling

The failing of the first selective epitaxial fillings, section 5.10, was the thin oxide left on the trench sidewalls to prevent uneven growth. A well characterized step in the fabrication of many integrated circuits is the filling of deep narrow trenches. It was therefore proposed that if a thicker oxide was used on the sidewalls, and etched out after epitaxy, the resulting trench could be filled with amorphous silicon in a similar way.

The processing stages are shown in figure 5.8. The castillated cross section, with the trench mask oxide in place, was coated with a 40 nm deposited oxide. An anisotropic plasma etch was used to remove the oxide from the horizontal surfaces. Next, selective epitaxial silicon was grown from the trench floor. Some amount of overfilling was encountered, attributable to higher growth rates caused by an increase in nucleation on the plasma damaged trench floor. The overfill was corrected for by polishing with Syton on soft felt pads. Finally the oxide was stripped from the wafers and 50 nm of amorphous silicon deposited. The resulting topography was both planar and uniform.

When observed in cross section, by SEM, the fill appeared to be complete, showing no voids or overspill.

Samples with high doses of both boron and arsenic were introduced into the SIMS instrument and analysed. Inspection of the topography after analysis showed the same deep cracks opening along the interface between the fill and the substrate.

An uneroded sample was later etched to highlight crystal defects and then subject to SEM examination. This showed that the epitaxial silicon was highly defective. The etch also removed some of the amorphous backfilling, suggesting that it was spongelike in places.

Castillated surface with original trench mask oxide

Deposit 40 nm oxide - plasma etch to expose trench floor
Grow 1.4 μm selective epitaxial silicon

Syton polish, strip oxide and deposit 50 nm of amorphous silicon

Figure 5.17 Revised epitaxial filling technique

Thus the interface and regions of the fill were not as resistant as the single crystal material, thereby permitting exposure of the corners after a relatively short period of bombardment.

5.12.6.3 Amorphous silicon filling

The amorphous silicon filling technique (based on a technique first proposed by the author in his first year report to the University on this work) requires standard processing equipment and is exempt from the critical growth rate calibrations necessary for the selective epitaxial filling. Instead of striving to achieve a planar surface, the technique is based on extending the lifetime of the trench wall by sacrificial erosion. Thus this method is not applicable for very deep implants.

Figure 5.18 shows the process schematically. Starting from the original castillated topography with a thick masking oxide still in place, a 2.5 μm amorphous silicon deposition was made. This was then plasma etched back to expose the oxide mask, this can easily be done by approximation or by detection of oxygen in the plasma. The general form after this process is of filleted corners, similar to that of the amorphous silicon fill test structures. A second amorphous silicon deposition of 50 nm was then made, preferentially filling the central trench. The structures were delivered to the author in this condition.

Once at Warwick, careful mechanical polishing was used to remove most of the 0.5 μm masking material and the silicon overlayer. The samples were cleaved so as to produce squares of side 20 mm with the structure of interest at the centre. By making such oversize pieces, the 2d structure was eliminated from the effects of the preferential removal of material that occurs at the edges, during polishing.

The cleaved samples were mounted, using wax, onto a stainless steel disc before being placed a simple polishing jig. A ball bearing was positioned between the sample disc and the mass used to apply pressure, so that the sample maintained its own level and hence bevelling of the surface was reduced.

Castillated surface with original trench mask oxide

Deposit 2.5 μm amorphous silicon

Etch back to oxide and deposit 50 nm amorphous silicon

Polish back to within 100 nm of original surface

and etch off oxide

Silicon substrate

Silicon dioxide

Amorphous silicon

Figure 5.18 Diagram showing processing of the amorphous filled samples

Polishing was carried out on a commercial perforated fibre-board pad using 0.1 μm diamond paste. The pad was mounted on a square of window glass. The polishing pad itself permits large particles to become embedded, reducing their ability to cause severe scratching. However, as damage to the striped area would render later analyses invalid, elaborate precautions were taken to exclude particles from the polishing area. Thus this stage in the preparation was undertaken in a class 100 clean station after *all* items of equipment (including the author's hands) had been thoroughly washed in de-ionised water. Gloves were worn at all times and the equipment stored after use in clean self sealing plastic containers (these were washed immediately prior to opening). A major source of particulate contamination, when polishing silicon wafer samples, is fragmentation of the specimen corners. To prevent this occurring samples were subjected to ultrasonic cleaning (to release loose material) then, after wax mounting, a surround of PVC insulation tape was built up to just under the sample thickness. The tape prevents tilting of the specimen, hence reducing the chance of a corner "biting" into the pad.

Polishing by hand, although time consuming and laborious, allows a *feel* to be built up. Thus changes in the drag of the jig can be used to fine tune the amount of lubrication required and sudden biting can be investigated before damage is caused to the specimen. Strict adherence to these precautions ensured that even after three hours polishing, the amount required by these samples, the surface was specular and free from scratches, even to microscopic examination.

The samples were polished until the oxide thickness was approximately just under 100 nm. Monitoring the thickness was achieved by comparison with a colour-thickness chart.

When polishing was complete, the sample was removed from the jig and carefully cleaned. A wax protection could then be applied to the aluminium alignment stripes and the remaining oxide removed by etching in HF. The wax was

later dissolved in xylene and the specimen cleaned ready for introduction to the SIMS instrument.

The remaining projections of the amorphous fill are rapidly eroded under ion bombardment, in a similar way to the castillated profile of the original sample set, affecting ion collection from only the upper 20 nm of the analysis.

A major advantage of this technique is that the true surface of the structure is protected until the oxide is stripped after polishing. Thus damage from the polishing compound is kept to a minimum. The retention of the original surface also prevents non-uniformities in the polishing process affecting the final result, hence a sample with virtually no oxide on one side and 130 nm on the other is valid to be analysed. If this situation were to occur on an unprotected surface, the loss of depth resolution during subsequent SIMS analysis would render the profile of little value.

A polishing machine was later used to prepare the samples. It was first thoroughly cleaned, to remove any traces of previous polishing grit, then all surfaces within the perspex hood were coated with a thin layer of lubricant. This not only prevents particulate emission from the surface but also acts as an efficient particle trap. As the hand jig had been so successful, this was mounted on the oscillating arm of the machine. Figure 5.19 shows the arrangement used. The hand jig is suspended a few millimetres above the polishing surface (when hand operated the jig rests on the surface). Thus the sample holder is pushed by the jig, the downward force being transmitted via the ball bearing through the centre of the sample to permit self levelling. The ball bearing is confined only at the sample holder, being free to move at the weight end.

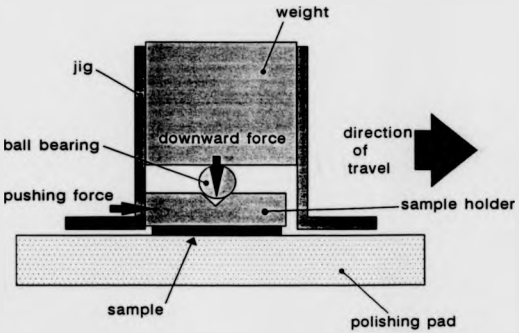

Figure 5.19 Diagram of polishing jig used for automatic polishing (for hand operation the body of the jig rests on the polishing surface)

5.12.6.4 Topographical evolution

The amorphous filled and polished samples were mounted in the instrument and bombarded with an 8 keV, 200 nA, oxygen beam. The principle behind the fill was that it should be sacrificial, being removed slowly enough so as to allow the original surface to be protected for long enough for the data collection to be made. The limited number samples prevented a full evolution study from being made, so cross sections were taken of an uneroded structure and of a sample from the same field after an estimated 500 nm vertical erosion.

Plate 5.7(a) shows the original cross section. Despite severe charging, the shape predicted in diagram 5.18 is evident, with the flat region being bounded by raised corners of the amorphous fill.

After bombardment, as in plate 5.7(b), the informative, flat, region is of similar width, however, the convex profile of the fill has become concave. Further bombardment will rapidly erode the informative region, hence the amorphous fill provides protection for only about 500 nm. Thus this enables implants shallower than this depth to be profiled. .

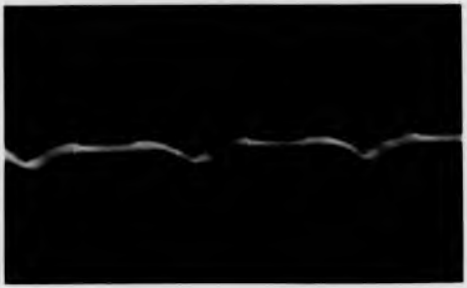

Plate 5.7(a) Cross section SEM of uneroded polished and etched structure

Plate 5.7(b) Cross section after 500 nm vertical erosion

6.0 RESULTS AND DISCUSSION

6.1 INTRODUCTION

This chapter presents the experimental results obtained from the special structures described in chapters four and five.

The chapter begins with the presentation of raw data. The stages of profile reconstruction are then illustrated and a complete profile determined. The first profiles were distorted by the topographical changes of the sample. The implications of these changes are discussed and the reason for the shape of the observed profiles is given.

The chapter concludes with the first profile from the amorphous filled samples and a comparison of a directly measured depth profile with that derived from a two dimensional analysis, showing that the effects seen in the early analyses have been overcome.

6.2 CALIBRATION PROFILE

To permit calibration of the reconstructed profile a depth profile through a similar implant must be taken. The sample used was implanted at the same time, and under the same conditions, as the special samples and should therefore provide accurate calibration.

The profile, shown in figure 6.1 was itself calibrated by equating the area under the peak (to about 0.6 μm) with the implant dose of 5×10^{15} ions cm^{-2}. The depth calibration was obtained by measurement of the crater by surface profilometer, providing an accuracy of $\pm$ 5 nm.

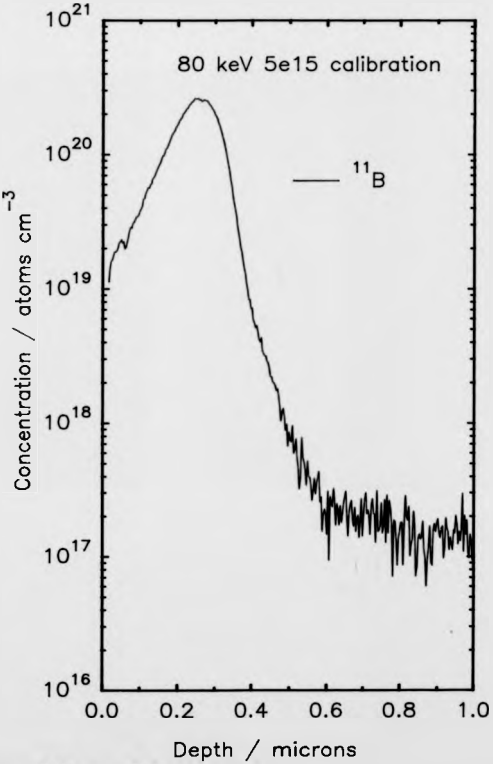

Figure 6.1 Calibration profile for the first session

(implant conditions ^{11}B 80 keV $5x10^{15}$ ions cm^{-2})

As the implant was the same in both of the first two generations of samples, only one calibration profile was required.

6.3 ANALYSIS OF THE ORIGINAL SAMPLES

6.3.1 Data collection

The first samples to be analysed were those possessing a trench angle of 0.2°. This was because they should include all of the regions predicted in chapter 4 and thus would provide a useful initial check of the quality of the data.

The instrument was set up to record 189 linescans from a 256 line frame, and this gate was sized to fully cover the 1.8 mm square site. The time for each frame to be collected was 500 s, with the primary ions impacting with an energy of 6 keV at a current of 200 nA.

Figure 6.2 shows ten frames of data collected, early in the analysis from a 0.08 ° sample scanned by a 60 μm probe. The data for the boron (impurity) and silicon (matrix) channels are collected alternately, thus in later processing, the effects of the energy filter during a particular impurity frame may be compensated for by comparison with the average of the matrix channel both before *and* after that frame. The matrix channel fulfils the conditions set in chapter 5 for both overall spread and lack of sharp gradient changes.

This data was collected after equilibrium was obtained - ie. the matrix channel had stabilized. However, there was some boron contamination at the surface; this is evident as the minimum in the data continues to decrease for the first three frames, as the contamination is removed.

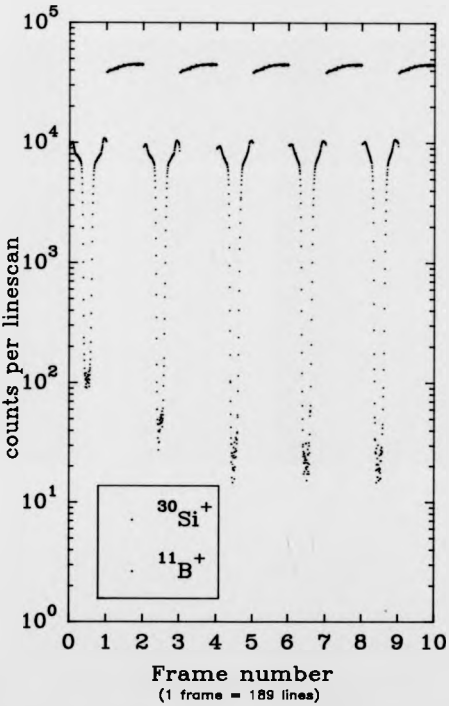

Figure 6.2 Ten frames of data collected immediately after equilibrium was reached

The peak of the implant, from figure 6.1, occurs at 0.25 μm. The maxima of the recorded data represent the centre of the implant and should therefore follow the measured depth profile. As the expected erosion rate for the analysis conditions is approximately 1.4 nm per frame, the peak should therefore appear after 178 frames. However, the maximum count rate occurred after 70 frames, equivalent to only 98 nm.

The reason for this anomaly was apparent when the sample was sectioned and the topography examined. The high sputter rate at the top corners of the structure, coupled with low ion yield from the angled faces, permitted material to be removed *without* being recorded.

6.3.2 Topography and the shape of the data

Using the topographical evolution determined in chapter 5 the data collection was modelled. Initially, a vertical implant profile was chosen. A linear diffusion was then determined, considering the vertical profile as an infinite impurity source. The resulting distribution was then superimposed upon a diagram of the topographical evolution.

Figure 6.3 shows schematically how the model was operated. The data collection from an ideal sectioning and that from the topographically changing sample was then modelled by integrating the pixel intensities from the respective regions. Thus, to obtain the ideal data collection, the structure was sectioned in horizontal slices. For the topographical effects, only pixels in the darker region were counted; ie only those normal to the analysing beam. The results of this modelling are shown in figure 6.4. The topographically altered data shows a peak much nearer the surface than the data for the ideal collection. This is the

same as was seen in the actual analysis; the implant peak was apparently shifted towards the surface.

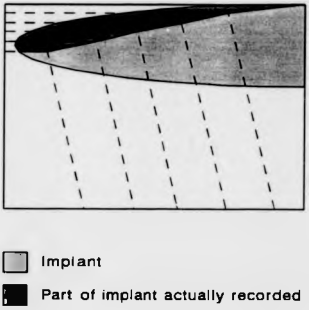

Figure 6.3 Schematic of modelled data collection

Also, the peak value is at least an order of magnitude lower in the altered case.

Although a partial reconstruction of the two dimensional profile from the experimental data would be possible large errors would be expected owing to the amount of "missing" information. Very accurate modelling of the topographical changes would also be required as, in a "real" profile, the diffusion would be exponential. Thus, relatively small errors in determining the number of pixels to be counted in each horizontal line could have a great influence on the sum of the counted pixels.

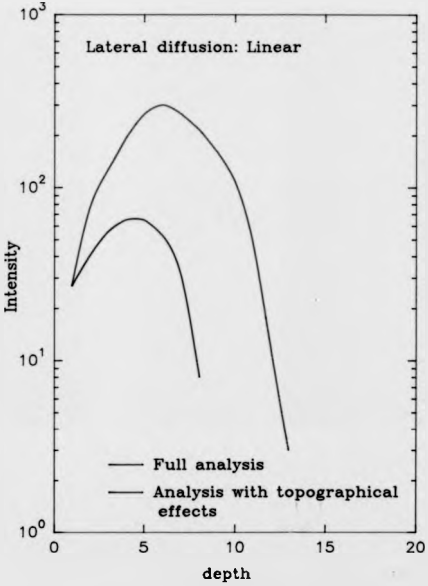

Figure 6.4 Theoretical reconstructed depth profiles from samples with and without preferential corner erosion

6.3.3 Reconstruction of the lateral distribution

Figures 6.3 and 6.4 show that the only time there is agreement between the ideal and actual data is in the near surface region. Thus the lateral distribution may be determined from a layer of data acquired soon after equilibrium has been achieved. Frame 9 of figure 6.2 is suitable as it occurs only 27 nm from the sample surface and *after* the majority of surface boron contamination has been removed.

Figure 6.5 shows this frame after being adjusted for extraction efficiency variations, as described in chapter 5, the validity of this method being demonstrated by the similarity in intensity either side of the central minimum. It can be seen that the shape of the data is the same as that predicted from the model in section 4.4.1, the various regions being well defined and labelled I to III, as in that chapter. By comparison with figure 4.7 it can be seen that the lateral distribution is contained within the region marked I and III, and that region II should yield a region of constant concentration in a reconstruction. As the lateral spread data in regions III represent the same part of the profile as those of regions I on the opposite side of the minimum, but with a greater uncertainty owing to the constant count rate superimposed upon them, they may be neglected. By application of the basic triangle method of reconstruction (section 4.7) the lateral spread was determined for this layer. Both sides of the distribution were reconstructed and are presented in figure 6.6.

The concentrations were calibrated by comparison of the part of the distribution representing the planar section of the implant with the concentration at a similar depth found on the calibration implant (figure 6.1). The point at which the lateral distance equals zero was positioned at the edge of the planar region and *does not* necessarily coincide with the mask edge.

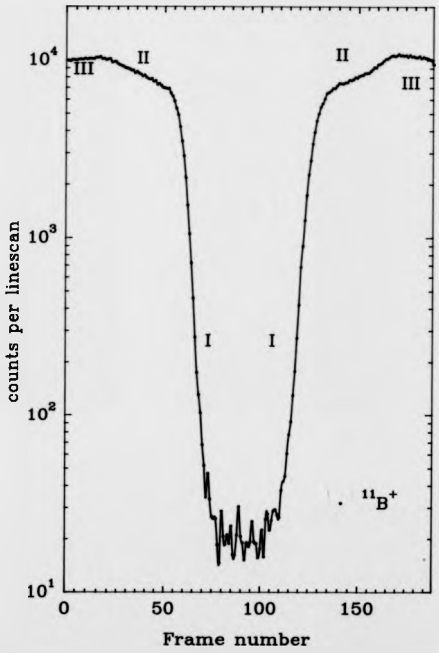

Figure 6.5 Boron signal for a frame 27 nm from the surface

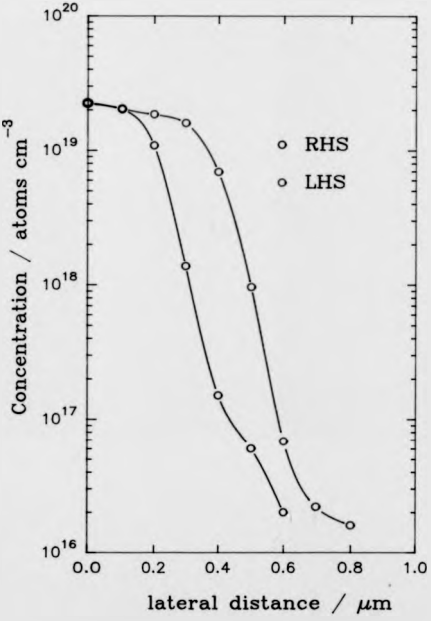

Figure 6.6 Reconstructed lateral dopant distributions from data of figure 6.5

When compared with a model (TITAN V, CNET/CNS), the measured lateral spread shows good agreement. with the $1x10^{17}$ atoms cm^{-3} level falling approximately 0.5 μm from the edge of the planar region. The RHS curve intersects this level at around 0.4 μm and the LHS curve just before 0.6 μm. The asymmetry of the curves is caused by the original implant being at 7° to the surface normal and directed toward the LHS of the structure. The lateral resolution is approximately 100 nm.

6.3.4 Summary

The first results were very promising, demonstrating that analysis of the sample was possible using the EVA 2000 instrument and that the data produced were of the correct shape and of sufficient dynamic range to be useful. The lateral spread could also be recovered from the data with a reasonable degree of accuracy, however, the variation in topography as the analysis proceeded prevented the full distribution from being recovered. Confidence in the accuracy of the technique was reenforced by the asymmetry shown in lateral spread; this was on the correct side of the window.

The reconstruction demonstrated that a sensitivity of almost $1x10^{16}$ atoms cm^{-3} could be achieved with a lateral resolution of 100 nm. This is an order of magnitude better in sensitivity than the tomography work of Goodwin-Johansson for a similar resolution (Goodwin-Johansson, 1992).

Overall, the 0.08° samples were found to be the most informative as they provided a compromise between the extremely coarse data from the 0.2° samples and the data from the 0.02° samples which lacked enough of region II to provide accurate calibration.

6.4 THE SECOND GENERATION OF SAMPLES

6.4.1 Data collection

The second generation of samples had the trenches filled with epitaxial silicon to provide a planar topography. In places, the edges of the trenches were decorated by small crystallites, of up to 1 μm diameter, where three dimensional growth had occurred. This severely restricted the number of sites available for analysis and, in fact, only two site groups were clean enough to attempt work on.

Because the erosion rate was typically 1.5 nm per frame, to fully analyse the sample takes some three hundred and fifty frames, collected over fifty hours. This generates over 60,000 data points. The 380Z microcomputer is capable of storing only 3000 data points before downloading to disk, for which a human operator must be present. To overcome the restriction of tending to the computer every two or so hours, data are averaged over a number of frames. The collection sequence first involves collecting up to ten frames from the impurity channel and continually summing them line by line to effectively produce a single frame up to ten times as deep (this unit is called a cycle). The same procedure is then applied to the matrix channel, before once again recording impurity ions. Thus one hundred and fifty frames, collected at the rate of ten frames per cycle, produce only fifteen frames of stored data and require human intervention every twenty hours. The depth resolution is of course degraded by this procedure, and, for this case, becomes 15 nm; this is still in excess of the lateral resolution. The summing of a number of frames increases the statistical precision of the data, especially in the important

minimum region and would be done anyway, for this reason, before profile reconstruction.

In general, only five frames were integrated in each cycle as, if twelve five frame cycles are collected before downloading of data, the time between downloadings is approximately eight hours; this may be easily fitted around a working day.

As analyses of the original structures had suggested that the best data was collected from the structures of intermediate angle, thus these structures were reserved for data collection. The extremely course and fine structures were employed for topographical evolution studies.

The data collected from these samples showed the expected shape and did not show the early drop to background noticed in the original set. The fact that the onset of excessive material removal was delayed was confirmed by the topographical study (section 5.10.2). This suggested that data from the upper layers was reliable, as the filling and original surface were evenly eroded. However, the slightly weaker oxide, at the interface, permitted exposure of the upper corners of both components. This eventually led to a similar condition as that experienced with the unfilled structures.

A feature to note about the data from these structures was that the overall dynamic range was poorer than that achieved previously. The likely reason for this is contamination of the epitaxial silicon fill.

6.4.2 Reconstruction of the first full profile

The quality of the data produced from the epitaxially filled samples was such that a reconstruction of a full two dimensional profile could be attempted.

A full data set was acquired from the 0.08° pad displaying the lowest amount of decoration by crystallites using a 50 μm probe. The scanned area was 2.3 mm across and the 189 linescans comprising the gate covered 1.7 mm of the 1.8 mm sample. Thus the spacing between adjacent scans was 9 μm. Before application of the triangle method, the data were integrated in groups of six so as to be representative of that which would be collected by a single pass of a 50 μm probe.

The lateral spread information for each layer of data was determined and then compiled to form a complete profile. Calibration was performed by comparing the peak concentration of the 2D data with that of the calibration profile.

Figure 6.7 shows the final result presented a contour plot, together with the profile of a similar implant generated by the TITAN V process simulator (CNET/CNS, 1991). Comparison of the two shows the experimentally determined profile to have a greater lateral spread than that proposed by the model. This probably caused by the collective effects of surface contamination by crystallites early in the analysis, uneven erosion as time progressed and uncertainty in positioning the mask edge. The uneven erosion, caused by the weakness of the sidewall oxide, is also responsible for the apparent shallowness of the measured profile. If a depth profile is extracted from the experimental result and compared with the known depth profile in the planar region, the serious nature of the effect can be demonstrated. Figure 6.8 shows just such a profile, and the amount of missing information can easily be seen.

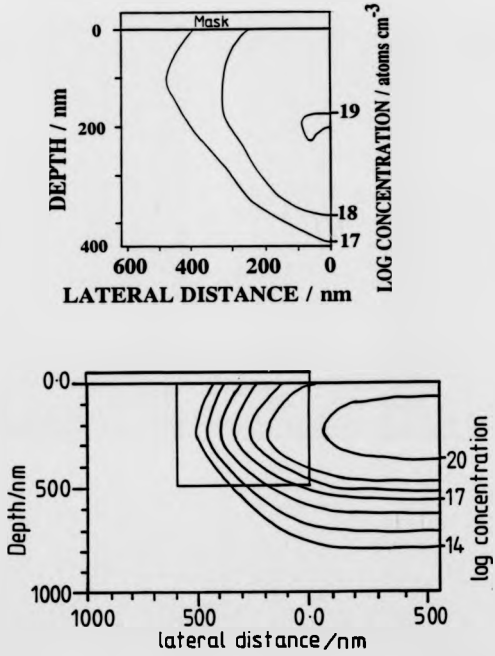

Figure 6.7 Reconstructed two dimensional profile (top) together with TITAN V simulation (lower) [rectangle shows extent of experimental profile]

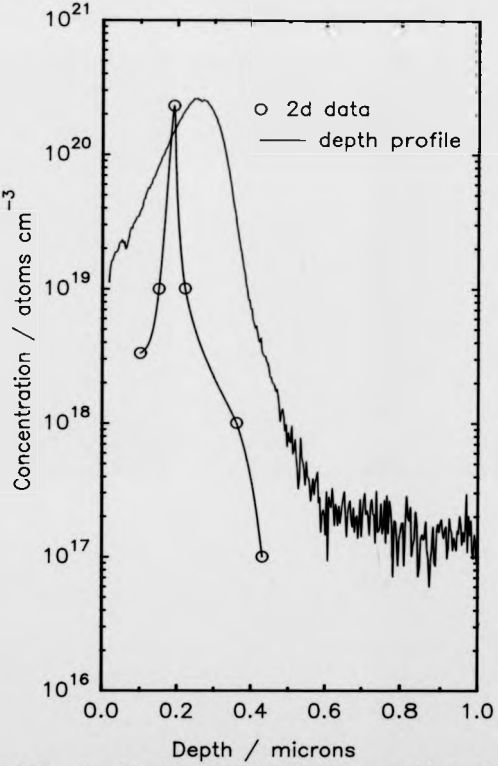

Figure 6.8 Comparison of directly measured depth profile and reconstructed depth profile from the 2d data

The experimental profile is highly distorted and much shallower. This is typical of the exclusion of material from the analysis caused by the low ion yield and high sputter rate occurring at an exposed corner. A similarity with the model of this process for an unfilled structure, figure 6.4 can also be seen.

A further profile was reconstructed, this time both sides were included. Calibration was made by comparison with a point near the surface and with the TITAN V model. Figure 6.9 shows this profile as a surface plot. This type of plot permits the observer to see the more subtle variations in the data as it is not hampered by the way that the contours are found. (The contour search routine may become confused in regions of high noise or local extremes and thus produce an unfair representation, although it does make the reading of absolute values easier.)

The profile shown in figure 6.9, viewed from the silicon bulk looking towards the surface, shows the distribution as it would appear in two adjacent implants; ie the LHS of the implant is shown on the right and the RHS on the left. Thus the diagram is *congruent with the data collection sequence.* The asymmetry caused by the angled implant is easily visible. However, a general pattern of noise is evident crossing the whole graph, parallel to the surface, and periodic with depth. Careful comparison with the raw data shows that the peaks occur directly after data have been downloaded. Although data transfer takes only a matter of minutes, there is a period of time during which the instrument stands idle waiting for human intervention, this may last a couple of hours if data collection ceases during unsociable hours. Thus, material from the residual gas may be adsorbed leading to a significantly higher count rate when data collection resumes.

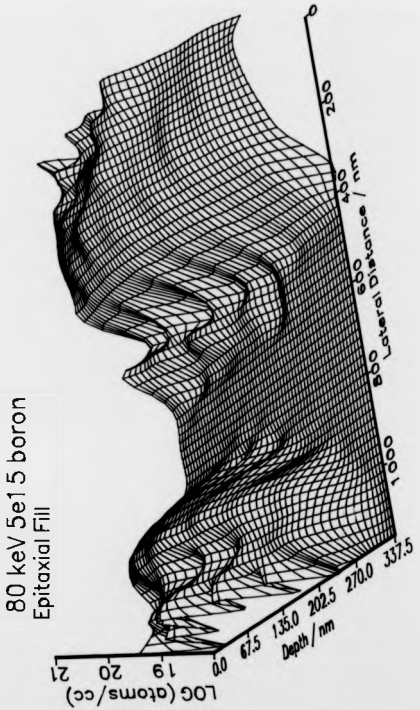

Figure 6.9 Reconstructed profile showing both sides of the implant window

A significant feature of the graph is the peak at around 500 nm lateral distance. This was traced to a group of crystallites that occurred in an ordered pattern across the sample, as in figure 6.10. A number of such patterns were observed on the more heavily decorated samples. They always showed sharply defined boundaries but, as yet, no explanation has been found for the formations although implant damage and, or, dopant concentration appear to play some role in their formation.

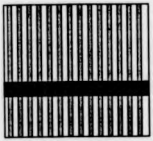

Figure 6.10 The crystallites showed a high degree of order on the sample surface.

Figure 6.11 shows a contour plot of another reconstructed profile, again showing the asymmetry caused by the implant angle.

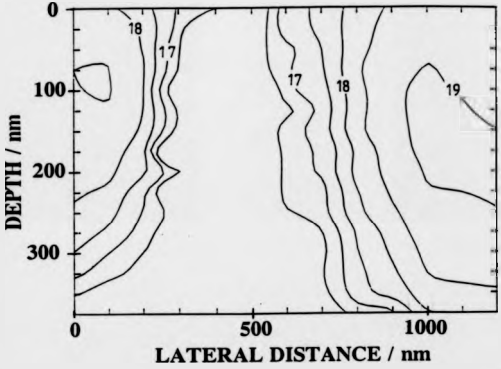

Figure 6.11 Contour plot of 80 keV implant showing asymmetry due to implant angle

6.4.3 Summary

The epitaxial fill provided only limited protection for the top corners of the trenches and introduced a source of background doping at about the 10^{17} atoms cm^{-3} level. This protection was enough to permit reconstruction of the full 2D profile. However, these results could not be deemed to be reliable owing to the removal of undetected material. The presence of overgrowth material also introduced distortion into the result and, consequently, the use of this particular process was ceased.

6.5 AMORPHOUS FILLED SAMPLES

6.5.1 Data collection

The previous samples were aligned by eye, and uncertainty about the angular alignment persisted until a measurement could be made after the analysis. However, the new samples contained the angular alignment structures described in section 4.5. These provided a means of assessing the angular alignment *before* analysis.

Data from the amorphous filled samples showed the same increase in background signal experienced with the epitaxially filled samples. The topographical evolution studies showed that reliable protection could be achieved for a true vertical erosion of at least 0.5 μm, therefore a reduced implant energy, 20 keV, was chosen as the doped region is well contained within this region.

6.5.2 Profile reconstruction

Whilst the amorphous filled samples were being fabricated at Caswell, the relaxation technique for extracting the 2d profile (section 4.8) was developed. The data from the new samples were processed using this technique, reducing the need for any smoothing prior to reconstruction.

The first sample to be analysed had received a 300 s anneal at 950 C. Figure 6.12 shows a surface plot of the reconstructed data and figure 6.13 a contour plot. The lateral resolution of both is better than 70 nm. No mask edge is shown as a co-implant for this purpose was not made. The overall distribution is smooth with a high concentration peak of approximately 10^{21} atoms cm^{-3} at a depth of 0.1 μm. This represents a region of boron precipitation that acted as a source of diffusion. As diffusion could only occur below the solid solubility limit (approximately 10^{20} atoms cm^{-3}) impurity material at higher concentrations remained immobile. As with the epitaxially filled structures, there is a noticeable periodicity with depth (more evident in the contour plot), however, distortions due to crystallite formation are absent.

Figure 6.14 compares the depth profile used for calibration with that extracted from the 2d data. The precipitate sourced diffusion is clearly visible, and the agreement between the curves demonstrates that the problem of corner erosion has been overcome with these samples.

Figure 6.12 Reconstructed profile of boron implanted amorphous filled sample

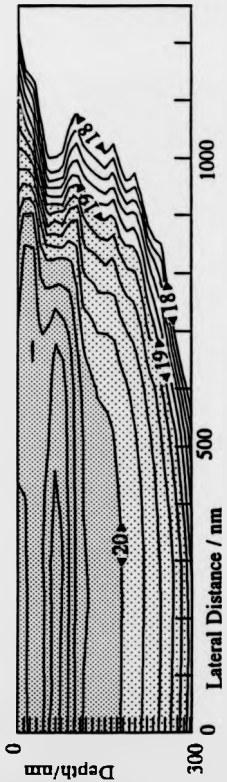

Figure 6.13 Contour plot of reconstructed profile

(Boron 20 keV 5E15 anneal: 300s 950 °C)

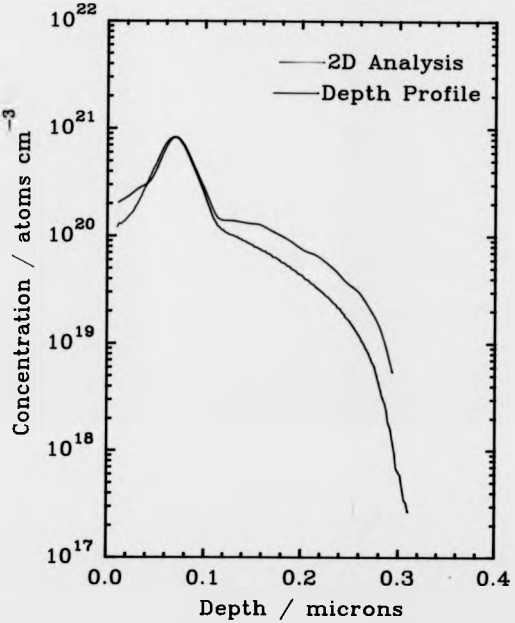

Figure 6.14

Depth Profile comparison with 2D derived 1D profile for 20keV 5x10^{15}atoms cm^{-2} B.

Sample MS0129A/TP6-22

6.5.3 Summary

The amorphous filling provides adequate protection of the upper trench corners. This, together with the accurate alignment possible with the included structures, has permitted the reconstruction of complete two dimensional profiles with a sensitivity of 10^{17} atoms cm^{-3} and a lateral resolution of 70 nm. The major problem remaining is the need to halt analysis whilst data is downloaded. This is discussed further in section 8.2 under Future Work.

7.0 A NEW PENNING SOURCE FOR EVA 2000

7.1 THE PENNING SOURCE

In 1937 Penning described a vacuum gauge that worked by monitoring characteristics of an electric discharge immersed in a magnetic field (Penning, 1937).

In other ionisation gauges, a hot filament is used as an electron emitter. This is required as, at the low pressures being measured, the mean free path is very long, hence many electrons are required to ensure that enough of the residual gas is ionised to permit measurement. The Penning gauge contains no hot components and overcomes the constraint of a long mean free path by increasing the distance travelled by the electrons.

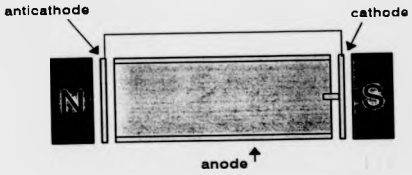

Figure 7.1 Diagram of the layout of a Penning discharge

Figure 7.1 shows the basic layout of a Penning discharge. Operating with a pressure of 1 Pa to 10^{-2} Pa, a potential of up to a few thousand volts is applied between the tubular anode and the cathodes. Electrons are drawn from the cathode, which may be fitted with a projecting pin to concentrate the field and enhance emission, and accelerate towards the anode. However, the magnetic field causes them to describe a helical path along the direction of the

axis. As they approach the anti-cathode they are reflected, consequently they oscillate between the two cathodic surfaces. This improves their chance of collision with a gas molecule many-fold. Ionised gas molecules are themselves accelerated and drawn towards one or other electrode surfaces (though because of their much greater mass the effect of the magnetic field is negligible). On impacting the electrode, further secondary particles may be released, thus enriching the charged particle flux within the cavity. Eventually, with a constant current being passed, a stable plasma is produced. Ions may be extracted from the plasma through a hole in the anticathode or a slot in the anode. For the production of noble gas ions the running voltage may be very high, in excess of 3000 V. To overcome this a hot filament may be substituted for the cathode, reducing the running voltage to less than 100 V (Nielson, 1957).

7.2 THE EVA 2000 SOURCE

The EVA 2000 source components are manufactured from high purity aluminium and the gas used is oxygen (Dowsett and Parker, 1983). The plasma produced is rich in positive ions; these are drawn to the cathodic surfaces and cause significant sputtering. The sputtered aluminium combines with oxygen and is deposited as alumina on the other components in the plasma cavity.

As the anode becomes coated, the voltage required to maintain a constant current rises. Ultimately the plasma becomes unstable and the anode must be replaced. Simultaneously with the deposition of material on the anode, the cathodic components become eroded and also require replacement. The typical lifetime of the source is four to six weeks.

The ideal source should thus contain components that are simple to manufacture and install.

7.3 THE ORIGINAL SOURCE AND EARLY MODIFICATIONS BY THE AUTHOR

The source originally fitted to the instrument was designed by Dowsett some 12 years ago and based on an earlier design by Wittmaack. The anode was manufactured from aluminium alloy tube, held in place with a bayonet type fitting. The cathode plate and pin were made from high purity (99.999%) aluminium and the anticathode was a 2 mm pure aluminium disc with a central machined well and 0.5 mm diameter hole, through which ions could be extracted. Removal of this component was hampered by deposition of material around the edges. To overcome this, the anticathode and its mount were modified by the author shortly after commencement of the project.

Figure 7.2 shows the modified source. To replace the anode and cathode, the end seal (a standard UHV copper gasket) is broken and the assembly removed together with the gas bottle (1 litre, 12 bar) and leak valve. The components mounted on the flange are then relatively easy to change. This operation does however risk damaging the gas handling system, especially a ceramic isolator.

Replacement of the anticathode is somewhat more difficult as it necessitates working some 150 mm down the 40 mm bore of the source. Initially three M1.6 screws must be removed. The anticathode can then be loosened and finally ripped out with a modified screwdriver. This procedure completely destroys the anticathode and also risks damaging the extraction

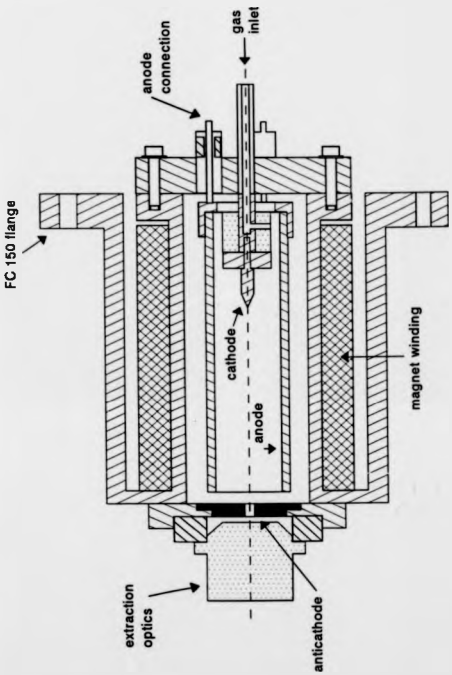

Figure 7.2 Cross sectional diagram of the original source fitted to EVA 2000

optics. The new anticathode must then be carefully aligned and, owing to the tight tolerance to ensure concentricity, drifted into position. The three screws are then replaced, the end flange reassembled and the source pumped.

The most stable period of operation was found to last for approximately ten days, one week after refurbishment.

Figure 7.3 shows a silicon-30 positive ion signal collected over a period of one hour, one week and five weeks after source refurbishment. The lower trace (1 week) shows variations consistent with counting statistics (ie $\sqrt{N}$). This demonstrates that a beam of constant current is being transferred from the source to the sample, ie the source is stable. This is completely opposed to the trace collected 4 weeks later. Here, the source has become unstable and large changes in the extracted current are occurring. Although the current passing between anode and cathode is the same in both cases (20 mA), the build-up of deposits on the anode, in the latter case, is causing the plasma to move in the cavity. As sites of relatively good conductivity become covered, the plasma shifts to more preferable areas. This shifting is somewhat periodic - in this case approximately 0.2 hours - and the frequency increases more rapidly with source age. At six weeks it has reduced to a few minutes.

During normal depth profiling, where the data are collected in an hour or two, the gradual changes in source performance go unnoticed. Because of the time and risks associated with changing the electrodes, the source is often run until instabilities become apparent on the scale of a few hours. However, for two dimensional profiling, taking anything up to 50 hours, it is necessary to collect data in the more stable period.

Thus the source was redesigned to permit quick, easy and risk free, refurbishment with the intention that the components may changed before each run.

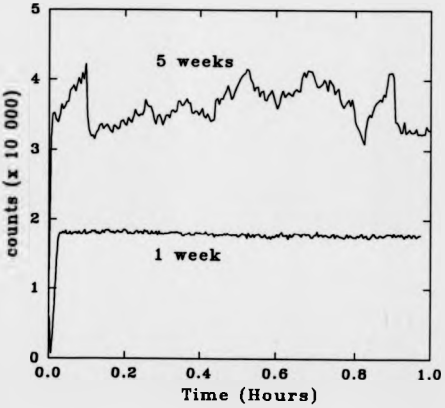

Figure 7.3 Silicon positive ion signals collected from a bulk sample 1 week and 5 weeks after source refurbishment.

7.4 DESIGN OF THE NEW SOURCE

The *main* aim of redesigning the source was to permit easier changing of the anticathode. The other main consideration was to allow the gas handling system to remain in position during refurbishment.

Figure 7.4 and plates 7.1 and 7.2 show the new design. The 30 mm diameter anticathode is manufactured by pressing from 0.5 mm thick pure aluminium sheet. The exit canal is then drilled in an accurate jig and the resulting component clamped in a stainless steel ring by three M2 screws. The ring is mounted into the flange with another three screws (visible in plate 7.1). The anode is simply an aluminium tube that fits into the housing and is retained by a ring at the anticathode end. The cathode, comprising a pure aluminium pin and plate, is mounted on a viton sealed flange and may be removed through the rear of the source (plate 7.2).

The gas is leaked in through a leak valve mounted on the main flange and travels through a buried bore to the discharge cavity. The main body of the source, at anode potential, is isolated from the cathodic flange by a peek spacer and vacuum sealed by a large "O" ring (these components are in place in plate 7.1).

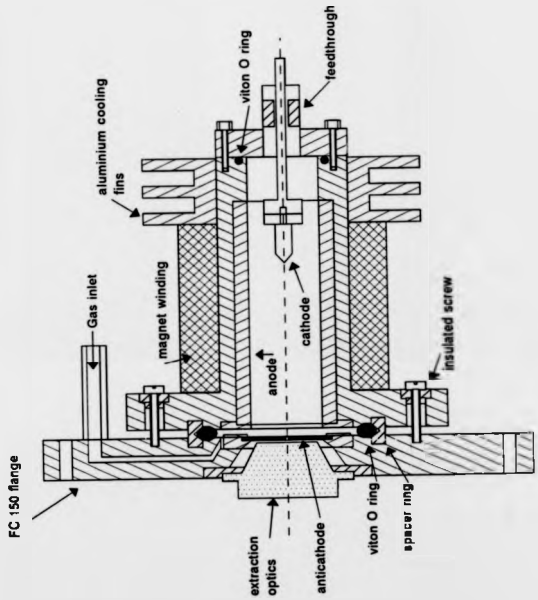

Figure 7.4 Cross sectional diagram of the new source

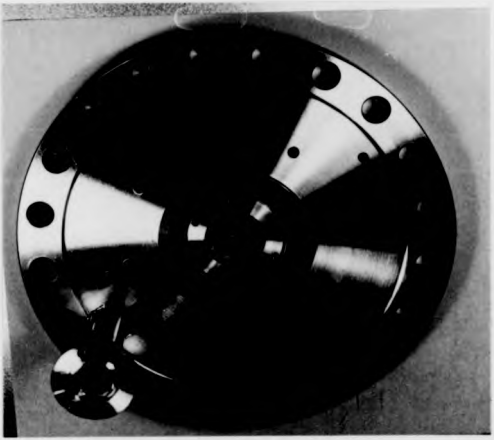

Plate 7.1 Photograph of the main flange, showing the anticathode, isolating spacer ring, and viton "O" ring vacuum seal

Plate 7.2 Photograph of the main body of the source, showing the anode (installed) and the cathode (side)

As an appreciable amount of heat is generated, both by the plasma (10 W) and in the magnet windings ($\approx$40 W), a finned aluminium heatsink is fitted to the end of the source and cooled by forced air ventilation.

In use, the source required a higher voltage than the original one, 500 V as opposed to 400 V, and permitted slightly less current to be extracted. It was proposed that this was due to a lower plasma density at the anticathode end. When dismantled, heavy sputtering and deposition at the cathode confirmed that most of the discharge was taking place at that end. The reason for this was the low magnetic field at the anticathode, as the winding finished some 10 mm from the anticathode plane. Electrons emitted from the cathode pin travel in a helical path towards the anticathode. However, those emitted at a large angle to the axis describe larger diameter paths, thus when the field decays beyond a certain level further increase in the path diameter results in collision with the anode.

7.5 REFINEMENT OF THE DESIGN

To overcome the low current problem, the anticathode mount was refined to permit fuller immersion in the magnetic field. As shown in figure 7.5, it is now mounted in a stacking "top hat" structure, with the extraction optics modified to allow greater penetration.

The anode retaining method was also modified, as there is no room in this design for the retaining ring. Instead, the anode is held by a wire clip.

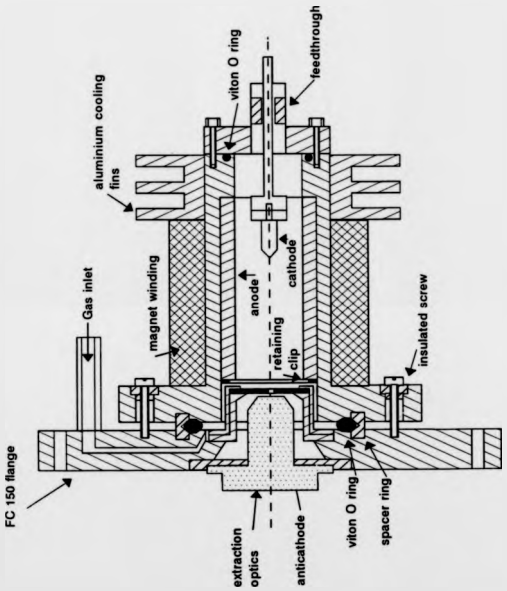

Figure 7.5 Cross sectional diagram of the refined new source

7.6 PERFORMANCE

The performance of this source was found to be very similar to that of the original one. The running voltage is approximately 400 V at the start of its life, rising gradually to 650 V when instability begins. The maximum current that may be transferred to the sample is approximately 20% lower than the original source, however, the actual usable current during profiling is approximately the same, 250 nA (R D Barlow, 1992). The stable lifetime is also similar.

The great advantage of this design is that the source may be easily dismantled and the components changed in a matter of minutes, rather than taking half a day. This is assisted by the design of the components which are somewhat simpler, the anode being a straight tube and the anticathode being manufactured by pressing; this means that replacement components require no tight tolerance machining.

7.7 POWER SUPPLIES FOR PENNING SOURCE

Power for the Penning discharge is supplied from a commercial unit (ATOMIKA). This provides a constant current source of up to 20 mA for a cold cathode discharge and 60 mA for a Nielson type source. The supplies are isolated from ground and may be floated by up to 15 kV supplied from an external unit. This float voltage is responsible accelerating the ions to the required energy. Originally, the potential was applied between the cathode and ground. The plasma is at a potential very close to that of the anode, therefore the ions emerging from the extraction optics have an energy that is the sum of both the extraction voltage and potential between the plasma and the cathode

(the cathode fall). Typically the discharge runs at 500 V; thus, for a 4 kV extraction potential the actual ion impact energy at the sample is around 4.5 keV. Although this may be taken into account when a particular impact energy is required, a potentially more serious problem may arise as the discharge ages. As deposits build up on the anode the discharge voltage rises; this in turn leads to an increase in the ion energy. During tuning, the optics in the column are optimised for a particular ion energy - any change in energy therefore degrades the probe.

To overcome this problem, the float potential of the new source is connected to the anode. Thus the ions emerge with constant energy, no matter how the discharge voltage varies. Figure 7.5 compares the two systems.

A change has also been made to the way the potential to the first lens is supplied. Originally it was provided by a power supply directly from ground. In the new design it is subtracted from the accelerating potential. This has two advantages. Firstly, any variation in accelerating voltage causes a similar change in that supplied to the lens, hence the change in focal length is minimised. Secondly, the ripple in a 2.5 kV supply is usually less, in absolute terms, than that in a 10 kV or 15 kV supply which, combined with the former point, results in a lower overall noise level on the first lens.

The magnet current is supplied from within the ATOMIKA unit and is connected to the cathode. In the original source the body was cathodic, however, the new source has an anodic body and thus a potential of up to 1 kV may arise between the components. To prevent damage to the insulation of magnet, the coil was wound on a PEEK bobbin.

A new set of power supplies was designed and built in the electronics workshop at Warwick. These provide the extraction potential for the source and the potentials for the electrostatic elements of the column. The EHT supplies

are provided from voltage programmable units. The programming voltages for the units are derived via simple analogue networks that track linearly with the accelerating potential applied to the anode (the potential for the Wien filter tracks as the square root). In this way, once the column is tuned for a particular energy, changing the ion energy merely requires the potential to the anode to be changed; the electrodes follow the change and only small adjustments are then required to optimise the column for the new energy.

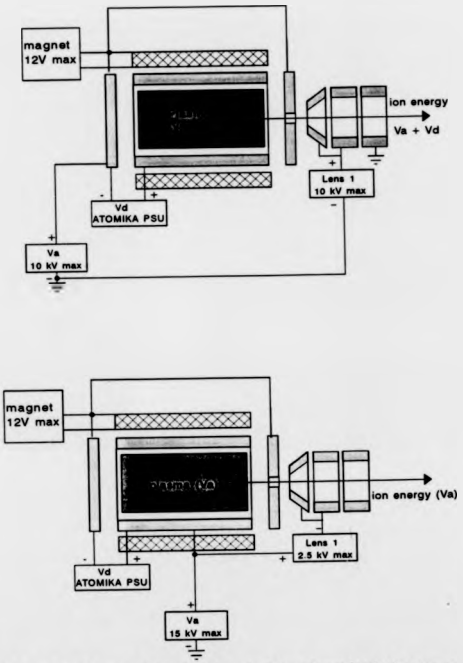

Figure 7.6 The original (upper) and revised (lower) wiring schemes for the ion source.

8.0 CONCLUSION

8.1 DEVELOPMENT OF THE TECHNIQUE

This project was initiated in an attempt to develop a technique capable of determining the cross sectional dopant distribution, in the region of the mask edge, suitable for comparison with process simulators. This application requires a combination of high spatial resolution, better than 100 nm, together with the detection of impurity material at concentrations below 10^{18} atoms cm^{-3}. SIMS is currently used to measure the depth profile of dopant species with both high resolution and sensitivity. To employ SIMS directly to determine the impurity distribution, at the required spatial resolution, would not permit a large enough analyte volume at each pixel to maintain a suitable statistical precision; hence the sensitivity would suffer. The technique described in this thesis overcomes this constraint by means of a special sample. By arranging for an implanted stripe to be sectioned in the vertical plane, and collecting data in a linescan mode, it has been possible to increase the volume available for sampling and, simultaneously, to use a reactive ion probe to increase the secondary ion yield. As this structure is reproduced a few hundred times across the sample, the resulting multiplication of the signal again improves the sensitivity.

The initial problem of excessive material erosion at the top corners has been solved by means of a sacrificial amorphous fill. By observing the sputter shadow effects, in the unfilled structures, it was possible to check the angle of incidence of the probe in the x and y directions independently. This is an otherwise difficult parameter to measure and structures like these may be of use in future work.

A criticism of the technique, early in its development, was the effect on the lateral resolution of angular misalignment. The aluminium alignment structures have overcome this problem and, in their present form, (as narrow as 2 μm) permit an alignment of better than 0.05°.

The research has been highly successful, with the technique already producing two dimensional maps with both spatial resolution and sensitivity within the required limits. This is the only technique that has satisfactorily solved the problem of limited analytical volume and thus has the potential to measure very low doping concentrations. The fact that the data analysis procedures permit sensitivity and lateral and depth resolutions to be mutually traded, *post acquisition*, is a particular strength - as profiles may be optimised for different requirements *from the same data set*. Furthermore, there is still much room for future development (see section 8.2). This should result in an improvement in sensitivity of at least an order of magnitude *coupled with* the possibility of an ultimate lateral resolution of around 10 nm.

8.2 FUTURE WORK

Development of the technique is continuing. The major problems yet to be overcome are the need to stop the analysis, whilst data is downloaded, and the 500 nm depth limit.

By sending data from the 380Z control computer, via a serial interface, to a separate microcomputer dedicated to data storage, it is hoped to dispense with regular halts in analysis.

Because of the expectations held for the epitaxially filled samples, the current trench width was optimised for that process. It is unlikely that this is

also the optimum for the amorphous fill, therefore a fuller study of the topographical evolution, of samples with varying trench width, should enable a better fill to be obtained. This should extend the maximum depth that the technique can analyse from 500 nm to at least 1 μm. This is enough to characterize most current implants.

The data recovery method of section 5.3.2 is only partially successful and fulfilling the criteria leads to a loss in collection efficiency. This may be overcome by dynamic emmittance matching the extraction system and the primary beam position. By applying a proportion of the scan voltage to the energy filter plates, the peak of the extraction efficiency characteristic may be made to follow the probe. Thus the highest possible extraction efficiency may be used. This may increase the sensitivity by up to an order of magnitude.

A simpler method of sample alignment may be used with imaging instruments by wrapping an image of the sample around the screen so that the two vertical edges appear down the centre of the screen. Angular misalignment is thus easily visible as a step in the image.

The later samples were made without a means of determining the position of the mask edge. In future batches it is hoped to include a low energy, germanium implant for this purpose. The germanium, being relatively immobile, would tend to remain below the implant window during thermal processing whilst more mobile impurities diffuse.

The data processing methods currently used are inherently noisy, requiring the differential of the measured data to be taken. If the profile could be determined without this stage, more precise results may be obtained. One way of doing this would be to use a forward processing method beginning with an approximate distribution from a process simulator. The simulated distribution would firstly be dissected using a model of the SIMS analysis

procedure to give a theoretical data set that could be directly compared with that obtained experimentally. The simulated distribution could then be adjusted, and the new theoretical data set compared. Using a maximum entropy technique to achieve an unbiased convergence, this process would be continued until suitable agreement was reached (Skilling and Gull, 1989)(Collins et. al. 1992).

To be of use, this method requires a good model of the "SIMS" effects to be produced so that an accurate theoretical data set may be found. This may be achieved by first determining how a sharp change in doping concentration is affected by the analysis and then applying the resulting function to the modelled distribution on a point by point basis. By convolving the data with an experimentally determined function in this manner, the highly complex interactions of the SIMS process may be included *without* excessive mathematical modelling and *without* making unrealistic assumptions.

Measurement of the response function may be made by using the implant mask oxide to define trenches to be produced by anisotropic plasma etching. The trenches could be filled with doped material, poly or amorphous silicon, and then a further set of trenches cut at an angle. The sample may then be planarized by polishing. As the information is the same throughout the structure there is no requirement for extreme parallelicity. Thus a sample with a very sharp doping edge is produced. Analysis of this structure will yield the convolution function for the forward model.

The lateral resolution is currently limited by the number of linescans in the frame (currently 256) as adjacent linescans must overlap by at least 25% to produce a flat crater (section 5.7). This prevents the use of probes of less than 40 μm FWHM. A 14 bit raster scanner, theoretically capable of 16 384 lines per frame, will be used in future, lifting this restriction.

Although already providing data of an unsurpassed quality, these future developments should enable the technique to provide the much needed experimental data to fine-tune process simulators and thereby permit further reduction in device size and increase in performance.

REFERENCES

Akasaka Y, Horie K and Kawazu S, Appl. Phys. Lett **21**, 128 (1972)

Ashworth D G, Oven R, Hill C, Clark E A, Dowsett M G and Thornton J, Proceedings UK IT 88, University of Swansea, July 1988.

Augustus P D, Spiller G D T, Dowsett M G, Kightley P, Thomas G R, Webb R and Clark E A, Proceedings SIMS VI, 485-488 (1988)

Bacon F M, Rev. Sci. Instr. **49**, 427 (1978)

Bardeen and Brattain, Phys Rev **74** 230 (1948)

Barlow R D, Dowsett M G and Fox H S, to be published in Nuclear Instruments and Methods (1992)

Benninghoven A, Rüdenauer F G and Werner H W, Secondary Ion Mass Spectrometry, page 429, John Wiley and Sons (1987).

Binnig G, Rohrer H, Gerber C, and Weibel E, Appl. Phys. Lett. **40**, 178 (1982)

Blood P, Semicond.Sci. and Technol **1** 7-27 (1986)

Bradley R C, J. Appl. Phys., **30**, 1 (1959).

Bryan S.R, Woodward W.S, Linton R.W, and Griffs D.P, J. Vac. Sci. Technol. **A3**, 2102 (1985)

Cerva H, J. Vac. Sci Technol **B10** 491 (1992).

CNET/CNS Process Simulator TITAN-V

Collins R, Dowsett M G and Allen P N, *Proceedings of SIMS VIII*, pages 111-114, John Wiley and Sons (1992).

Dowsett M G Ph.D Thesis, CNAA 1978

Dowsett M G, Parker E H C and King R M, Nucl. Instr. and Methods **B4**, 167 (1982)

Dowsett M G, Heal J W, Fox H and Parker E H C, *Proceedings of SIMS V*, Springer-Verlag, pages 176-178 (1986)

Dowsett M G, Parker E H C, King R M, Mole P J, J. Appl. Phys. **54** 6740

Dowsett M G, Barlow R D, Fox H S, Kubiak R A A, Collins R, J. Vac. Sci. Technol. **B10** 353 (1992)

Gong L, Barthel A, Lorenz J and Ryssel H, Simulation of the lateral spread of implanted ions: experiments, Proceedings of the 19th European Solid State Device conference, ESSDERC 89, edited by A.Heuberger, H.Ryssel and P.Lange, pages 198-201, Berlin Springer Verlag 1989.

Gong L, Lorenz J and Ryssel H, Direct observation of the mask edge effect in boron implantation, Proceedings of the 20th European Solid State Devices conference, ESSDERC 90, Bristol, edited by W.Eccleston and P.J.Rosser, pages 93-96, Adam Hilger (1990).

Goodwin-Johansson S.H, Subrahmanyan R, Floyd C E and H.Z.Massoud, IEEE Trans. on Computer Aided Design, **8**, 323 (1989)

Goodwin-Johansson S, Ray M, Kim Y and Massoud H.Z, J. Vac. Sci. Technol. **B10** 369 (1992).

Heywood G,*The effects of oxide growth on distribution of implants in silicon*, Ph.D thesis, Polytechnic of Newcastle upon Tyne, March 1979.

Hill C and Butler A.L, Integrated circuit process modelling, in *Inst. of Phys. Conf. series. No. 69, (Solid State Devices 1983)*, edited by E.H.Rhoderick, Institute of Physics London, (1984).

Hill C, Augustus P D and Ward A, Determination of arsenic distribution in silicon by a termal oxidation technique, *Institute of Physics conference series No. 76: Section 11*, Institute of Physics, London (1985)

Hill C, Pearson P J, Lewis B, Holden A.J and Allen R.W, A 2-D carrier profiling technique for VLSI planar structures, in *Proceedings of the*

17th European Solid State Device Research Conference, ESSDERC 87, edited by G.Soncini and P.U.Calzoiari, pages 923-926, Bologna, Technoprint (1987).

Hill C, Pearson P.J, Lewis B, Holden A.J and Allen R.W, A 2-D carrier profiling technique for VLSI planar structures, in *Solid State Devices*, edited by G.Soncini and P.U.Calzolari, pages 147-150, Amsterdam, North Holland, (1988a).

Hill C and Pearson P.J, 2-d boron distributions after ion implant and transient anneal, in UK IT 88 Conference Publication, pages 470-473, Swansea, UK, July 4-7, (1988b).

Hill C, Compositional analysis of submicron silicon in one, two and three dimensions, *Proceedings of the 20th European solid state device research conference, ESSDERC 90*, edited by W.Eccleston and P.J.Rosser, pages 53-60, Bristol, Adam Hilger (1990).

Honig R E, J. Appl. Phys., **29**, 549 (1958).

Hosaka S, Hosoki S, Takata K, Horiuchi K, and Natsuaki N, Appl. Phys. Lett. **53** 487 (1988)

Johnson W.C and Panousis P.T, IEEE Trans. on Electron Devices **ED-18**, 965 (1971)

Kordic S, van Loenen E.J, Dijkkamp D, Hoeven A.J and Moraal H.K, International Electron Devices Meeting, Washington, D.C., USA, 277 (1989)

Kordic S, van Loenen E.J and Walker A.J, J. Vac. Sci. Technol. **B10** 496 (1992).

Kyung C.M, Electron. Lett. **21**, 587 (1985).

Lang J M and Degrève F, Surf. and Interface anal., **7**, 53 (1985)

Lange K and Carson R, Journal of Computer Assisted Tomography, **8**, 306 (1984)

Leamy H.J, J.Appl. Phys. **53**, R51 (1982)

Levi-Setti R, Crow G, Wang Y.L, Scanning Electron Microscopy II, 535, (1985)

Longhurst R S, *Geometrical and Physical Optics*, Longmans, 1968.

Magee C W, Harrington W L and Honig R, Rev. Sci. Instrum. **49**, 477 (1978)

Magee C.W and Honig R.E, Surf. and Interface Anal. **4**, 35 (1982)

Martin Y, Abraham D.W and Wickramasinghe H.K, Appl. Phys. Lett. **52**, (1988)

Maul J L and Wittmaack K, Surf. Sci., **47**, 358 (1975)

Muralt P, Meier H, Pohl D.W and Salemink H.W.M Appl. Phys. Lett. 50, 1352 (1987)

O'Boyle M.P, Abraham D.W, Wickramasinghe H.K, Slinkman J and Williams C.C, Proceedings of the *First International Workshop on the Measurement and Charaterization of Ultra-Shallow Doping Profiles in Semiconductors*, pages 363 - 370, edited by C.Osburn and G.McGuire, MCNC 1991.

Okada T.K et. al. Non-equilibrium diffusion process modelling based on three-dimensional simulator and a regulated point-defect injection experiment, Proceedings of the International Electron Devices Meeting, pages 733-736, San Francisco 1990.

Ouwerling G.J.L, J. Appl. Phys. **66**, 6144 (1989)

Ouwerling G.J.L, Solid State Electronics **33**, 757 (1990)

Oven R, Ashworth D.G and Hill C, Simulation and measurement of the lateral spreading of ions into amorphous targets, *Proceedings of the Third International Conference on the Simulation of Semiconductor Devices*

and Processes (SISDEP-88), edited by G.Baccarani and M.Rudan, 429-440, Bologna (1988)

Paul W and Steinwedel H, Zeitschrift Für Naturforschung, **8a**, 448 (1953)

Pawlik M, J. Vac. Sci. Technol. **B10** 388 (1992).

Pearson P.J and Hill C, J. de Physique **49**, C4 515 (1988), proceedings of ESSDERC 88.

Pearson (1992) Private Communication

Renteln P, Ast D.G, Mele T.C and Krusius J.P, J. Electrochem. Soc. **136**, 3828 (1989)

Roberts M.C, Booker G.R, Davidson S.M and Yallop K.J, Inst. of Phys. Conf. Series No. 67:section 10, London, Institute of Physics (1983).

Roberts M.C, Yallup K.J and Booker G.R, A new TEM technique for evaluating 2-D dopant distributions in silicon with high spatial resolution, *Inst. of Phys. Conf Series No. 76: section 11*, Institute of Physics London, (1985)

Roitman P, Albers J and Meyers D.R, J. Appl. Phys. 55, 4436 (1984).

Sakurai T, Kawata H, Sato T, Hisatsugu T and Furuya T, J. Appl. Phys. **50**, 1287 (1979)

Schwettmann F.N, J. Appl. Phys., 45, 1918 (1974)

Sheng T.T and Marcus R.B, J.Electrochem. Soc. **128**, 881 (1981)

Sigmund P, Physical review, **184**, 383 (1969)

Sigmund P, Appl. Phys. Lett., **25**, 169 (1974)

Skilling J and Gull S F, in *Maximum Entropy and Bayesian Methods*, ed. J Skilling, Dordrecht, Kluwer (1989)

Subrahmanyan R, Massoud H.Z and Fair R.B, Accurate junction-depth measurements using chemical staining, in *Semiconductor Fabrication:*

Technology and Metrology, ASTM STP 990, edited by D.C.Gupta, American Society for Testing and Materials, Philadelphia, PA. (1988)a

Subrahmanyan R, Massoud H.Z and Fair R.B, Appl. Phys. Lett **52** 2145 (1988)b.

Subrahmanyan R, Massoud H.Z and Fair R.B, J. Electrochem. Soc. **137**, 1573 (1990)

Subrahmanyan R, J. Vac. Sci. Technol. **B10** 358 (1992)

Sze S M, *Physics of semiconductor devices*, appendix H page 850, John Wiley and Sons (1981)

Sze S.M, C-V Technique, in *VLSI Technology*, pages 186-188, McGraw-Hill (1984a).

Sze S.M, Spreading resistance technique, in *VLSI Technology*, pages 188-190, McGraw-Hill (1984b).

Sze S.M, EBIC, in *VLSI Technology*, pages 543-546, McGraw-Hill (1984c).

Tannenbaum E, Solid State Electronics **3**, 123 (1961)

Thomson J J, Philosophical Magazine **20**, 752 (1910)

Townes C H, Phys. Rev., **65**, 319 (1944)

Tsong I S T, Monkowski J R, Hoffman D W, Nucl. Instr. Methods, **182/183**, 237 (1981)

Vandervorst W, Maes H E, DeKeersmaecker R F, J. Appl. Phys., **56**, 1425 (1984)

Vandervorst W, Clarysse T, Vanhellemont J and Romano-Rodriguez A, J. Vac. Sci. Technol. **B10** 449 (1992)

von Ardenne M, in *Tabellen der Elektronenphysik, Ionphysik and Ubermikroskopie*, Deutscher Verlag der Wissenschaften, Berlin (1956)

von Hippel A, Ann. Phys. **81**, 1043 (1926)

Wach W and Wittmaack K, Nucl. Instr. Methods, 191, 327 (1981)

Werner H W, Vacuum, **24,** 493 (1974)

Williams P, Surf. Sci. **90,** 588 (1979)

Williams C.C, Slinkman J, Hough W.P and Wickramasinghe H.K, Appl. Phys. Lett. **55,** 1662 (1989).

Williams C.C, Slinkman J, Hough W.P and Wickramasinghe H.K, J. Vac. Sci. Technol.A, 8(2), 895 (1990).

Wilson I H, Chereckdjian S, Webb R P, Nucl. Instr. and Methods **B7/8,** 735 (1985)

Wittmaack K, Appl. Phys. Lett., **29,** 552 (1976)

Wittmaack K, Advances in Mass Spectrometry, **VII,** 758 (1977a)

Wittmaack K, J. Appl. Phys., 12, 149 (1977b)

Wittmaack K, Nucl. Instr. Methods, **168,** 343 (1980)

Wittmaack K, Appl. Surf. Sci., **9,** 315 (1981)

Wittmaack K, Dowsett M G and Clegg J B, Int. J. of Mass Spec. and Ion Phys, **43,** 31 (1982)Wittmaack K, Vacuum, **34,** 119 (1984)

Wu C.P, Douglas E.C and Mueller C.W, IEEE trans. Electron Devices, **ED-22,** 319 (1975)

Wu C.P, Douglas E.C, Mueller C.W and Williams R, J. Electrochem. Soc **126,** 1982 (1979).References Chapter 3

Ziegler J F, Biersack J P and Littmark U, *The stopping and range of ions in solids vol 1,* Pergamon Press London (1985)

NUMEROUS ORIGINALS IN COLOUR

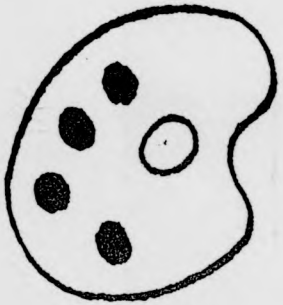

VARIABLE PRINT QUALITY